# CLAY-COATED POLYUREA MICROCAPSULES FOR CONTROLLED RELEASE

**To my parents, Elke and Leonard Hickey**

# CLAY-COATED POLYUREA MICROCAPSULES FOR CONTROLLED RELEASE

By

JANICE N. HICKEY, B.Sc.

A Thesis

Submitted to the School of Graduate Studies

in Partial Fulfillment of the Requirements

for the Degree

Masters of Science

McMaster University

**MASTER OF SCIENCE (2009)** **McMaster University**

**(Chemistry)** **Hamilton, Ontario**

**TITLE:** **Clay-coated Polyurea Microcapsules for Controlled Release**

**AUTHOR:** **Janice Hickey, B.Sc. (McGill University)**

**SUPERVISOR:** **Dr. Harald D. H. Stöver**

**NUMBER OF PAGES: 114**

## ABSTRACT

Polyurea microcapsules are micron-scale, hollow polymer spheres commonly used in agriculture to encapsulate pesticides for controlled diffusive release onto target crops. Diffusion of these active materials through a protective polymer wall offers a safer and more effective method of delivery compared to the direct spraying of crops with toxicants. The approach we are taking to control the release rate is to coat pre-formed porous polyurea capsules with a separate release-controlling outer layer. This allows us to separately optimize the load-bearing capsule wall and the release control layer, an approach commonly used in other membrane diffusion systems.

Montmorillonite clay incorporation into polymer matrices can reduce membrane permeability by forcing diffusants to take a tortuous path around the stacked silicate sheets. Effective formation of clay-polyurea composites requires the delamination of clay particles into thin sheets with high aspect ratios, and their incorporation into polyurea microcapsules either during interfacial polymerization, or post-polymerization. The net negative surface charge of the silicate sheets should facilitate their initial binding to the cationic polyurea surfaces, as well as subsequent binding of polycations to the clay-coated polyurea capsules to create layer-by-layer (LbL) capsule assemblies with decreasing release rates of internal materials.

The main focus of this project is to gain a fundamental understanding of montmorillonite clay and polyurea microcapsules, and the development of a model polyurea composite capsule for release rate analysis. Emphasis will be placed on the reduced permeability of microcapsules coated with clay by LbL assembly post-polymerization, followed by an exploration of further layering with polycations.

## ACKNOWLEDGEMENTS

First and foremost, I would like to thank my thesis supervisor, Dr. Harald D. H. Stöver. His knowledge and support is what guided me through this project, and I feel I have learnt so much from him on so many levels. The respect he shows towards his students is undeniable, and I truly appreciated the freedom and trust he placed in me to pursue independent thinking. Words can not express my sincere gratitude.

I would like to thank my committee member, Dr. Michael Thompson from the Faculty of Chemical Engineering. His knowledge and understanding of clay chemistry proved invaluable to this project, and his contributions help to guide it in the right direction.

I am grateful for all the support from LANXESS Inc. in Sarnia, Ontario over the past few years. Thank you for believing in me.

I would also like to thank the following people for their impact on this project:

- Dr. Nick Burke, I do not think this document could have been written without your help and support. Thank you for everything.
- My research group: Jian (Jeffrey) Li, Jafar Mazumder, and Casey Mills for keeping me sane.
- Dr. Jim Britten (XRD), Frank Gibbs (TGA), Ernie Spitzer, Marcia Reid, and Marnie Timleck from Electron Microscopy in the Faculty of Heath Sciences.
- My friends, both past and present, for all of your support and faith in me.
- My family for always being there for me, no matter what.
- Michael John Gaspar for your unconditional love and support. You are my rock.

## TABLE OF CONTENTS

PAGE

Abstract....iii
Acknowledgements....iv
Table of Contents....v
List of Figures....viii

CHAPTER 1.0 INTRODUCTION....1
1.1 Pesticide Delivery Systems (PDSs)....1
1.2 Polyurea Microcapsules....4
1.3 Release of Encapsulated Materials....6
1.4 Montmorillonite Clay....9
1.5 Layer-by-Layer (LbL)....13
1.6 Thesis Objectives....17

CHAPTER 2.0 MONTMORILLONITE CLAY INCORPORATION DURING POLYMERIZATION....19
2.1 Experimental....21
2.1.1 Materials....21
2.1.2 Instruments....22
2.1.3 Procedures....24
2.1.3.1 Preparation of Cloisite® $Na^+$ dispersions....24
2.1.3.2 Preparation of polyurea microcapsules by interfacial polycondensation....25
2.1.3.3 Preparation of fluorescent labeled clay....25
2.2 Results and discussion....26
2.2.1 Incorporation of Cloisite® $Na^+$ from the continuous aqueous phase....26
2.2.1.1 Characterization of clay delamination....26
2.2.1.1.1 Particle size distributions by light scattering....28

2.2.1.1.2 X-ray diffraction (XRD)..... 30
2.2.1.1.3 Transmission electron microscopy (TEM)..... 35
2.2.1.2 Characterization of polyurea-clay composite microcapsules..... 37
2.2.1.2.1 Optical microscopy..... 38
2.2.1.2.2 TEM..... 39
2.2.1.3 Fluorescent labeling of Cloisite® $Na^+$ with rhodamine..... 41
2.2.1.3.1 Fluorescent labeling of clay with rhodamine 6G (R6G)..... 42
2.2.1.3.2 Fluorescent labeling of clay with rhodamine B (RhB)..... 45
2.2.2 Incorporation of organically-modified clay from the dispersed organic phase.....48
2.2.2.1 Characterization of clay delamination..... 49
2.2.2.1.1 Cloisite® 30B..... 50
2.2.2.1.2 Cloisite® 10A..... 50
2.2.2.1.3 Cloisite® 15A..... 51
2.2.2.2 Characterization of polyurea-clay composite microcapsules ..... 51
2.3 Conclusions..... 53

CHAPTER 3.0 MONTMORILLONITE CLAY INCORPORATION POST-POLYMERIZATION.....56
3.1 Experimental..... 59
3.1.1 Materials..... 59
3.1.2 Instruments..... 59
3.1.3 Procedures..... 61
3.1.3.1 Preparation of Cloisite $Na^+$ dispersions..... 61
3.1.3.2 Preparation of polyurea microcapsules by interfacial polycondensation.....61
3.1.3.3 Coating of microcapsules with clay..... 62
3.1.3.4 Gravimetric analysis..... 62

3.1.3.5 Synthesis of poly ([3-(amino propyl)]-methacrylamide), PAPM..... 63
3.1.3.6 Labeling of PAPM with fluorescein isothiocyanate, FITC (PAPM-FITC).....63
3.1.3.7 Coating clay-coated microcapsules with PAPM-FITC..... 64
3.2 Results and Discussion..... 64
3.2.1 Selection of the appropriate model polyurea capsule system..... 64
3.2.1.1 Microcapsule strength..... 65
3.2.1.2 Microcapsule permeability..... 67
3.2.1.2.1 Temperature accelerated release..... 68
3.2.1.2.2 Internal co-solvent accelerated release..... 70
3.2.2 Coating microcapsules with montmorillonite clay..... 73
3.2.2.1 Characterization of composite microcapsules..... 74
3.2.2.1.1 Optical microscopy and TEM..... 74
3.2.2.1.2 Thermogravimetric analysis (TGA)..... 76
3.2.2.2 Optimization of clay deposition..... 78
3.2.2.2.1 Concentration of clay in solution..... 78
3.2.2.2.1.1 Effect of pH.....81
3.2.2.2.2 Immersion time..... 84
3.2.3 Gravimetric analysis of clay-coated polyurea microcapsules..... 86
3.2.3.1 Mechanism of encapsulate release..... 89
3.2.3.2 Monitoring of individual encapsulate release from PMPPI/DETA polyurea microcapsules.....91
3.2.4 Layer-by-layer assembly of polyelectrolytes..... 94
3.2.4.1 Polycation adsorption onto clay-coated capsules..... 95
3.3 Conclusions..... 103

CHAPTER 4.0 FUTURE WORK..... 106

REFERENCES.....108

## LIST OF FIGURES

**PAGE**

Fig. 1.1. Reservoir and monolithic diffusion controlled PDSs..... 3
Fig. 1.2. Polycondensation between a diisocyanate and a diamine to form polyurea.... 5
Fig. 1.3. Fickian release through a spherical membrane.....8
Fig. 1.4. Crystal structure of a single montmorillonite clay sheet..... 10
Fig. 1.5. Model for the tortuous path of diffusion of a permeate through an exfoliated polymer-clay composite..... 12
Fig. 1.6. (A) Simplified schematic of the layer-by-layer method using slides and beakers. Step 1: polyanion adsorption; Step 2: washing; Step 3: polycation adsorption; Step 4: washing...(B) Blow-up of slide surface outlining adsorption steps onto a cationic substrate..... 15
Fig. 2.1. The two mechanisms of montmorillonite clay incorporation during polyurea microcapsule formation: (a) clay dispersed in the aqueous phase; (b) clay dispersed in the organic phase..... 20
Fig. 2.2. Custom made XRD sample holder for aqueous clay dispersions.....23
Fig. 2.3. Schematic representation of the three stages involved in breaking apart clay particles into individual sheets in solution.....26
Fig. 2.4. Particle size distribution of 1.0 wt % aqueous clay dispersions following mechanical agitation (♦) and ultrasonication (♦)..... 29
Fig. 2.5. Particle size distribution of 1.0 wt % aqueous clay dispersions following 1 minute (♦), 10 minutes (◊) and 20 minutes (♦) ultrasonication..... 30
Fig. 2.6. X-ray diffraction curve of pristine Cloisite® $Na^+$ (—) and dried Cloisite® $Na^+$ (—)..... 33
Fig. 2.7. X-ray diffraction curve of powder pristine Cloisite® $Na^+$ (—) and 10.0 wt % Cloisite® $Na^+$ dispersed in water (—).....34
Fig. 2.8. TEM images of the formvar coated grid with (a) no sample, (b) the non-agitated clay solution, and (c) the ultrasonicated clay solution..... 36

Fig. 2.9. Optical microscope images of polyurea-clay composite microcapsules synthesized (a) without PVA and (b) with PVA.....38
Fig. 2.10. TEM images of polyurea-clay composite microcapsules synthesized (a) without PVA and (b) with PVA.....40
Fig. 2.11. The chemical structures of the fluorescent labels (a) rhodamine 6G (R6G) and (b) rhodamine B (RhB).....43
Fig. 2.12. The (a) UV-vis absorbance and (b) fluorimeter fluorescence emission spectra of free R6G (♦) and R6G-labeled Cloisite® $Na^+$ (◊).....44
Fig. 2.13. The (a) UV-vis absorbance and (b) fluorimeter fluorescence emission spectra of dissociated R6G in the aqueous phase (♦), free R6G (♦) and R6G-labeled Cloisite® $Na^+$ (◊).....45
Fig. 2.14. The (a) UV-vis absorbance and (b) fluorimeter fluorescence emission spectra of free RhB (♦) and RhB-labeled Cloisite® $Na^+$ (◊).....46
Fig. 2.15. The (a) UV-vis absorbance and (b) fluorimeter fluorescence emission spectra of dissociated RhB in the aqueous phase (♦), free RhB (♦) and RhB-labeled Cloisite® $Na^+$ (◊).....47
Fig. 2.16. Structures of the interlayer cations of three commercially available organically-modified clays. T = tallow (~ 65 % C18; ~ 30 % C16; ~ 5 % C14); HT = hydrogenated tallow.....50
Fig. 2.17. Schematic representation of the method of clay incorporation from the organic phase to form a composite polyurea wall.....52
Fig. 2.18. Optical microscope image of polyurea-clay composite microcapsules synthesized with Cloisite® 30B in the dispersed organic phase.....52
Fig. 2.19. Transmission electron microscope image of the cross-section of a polyurea microcapsule formed with Cloisite® 30B dispersed in the organic phase.....53
Fig. 3.1. Schematic of the layer-by-layer assembly at the microcapsule surface.....57
Fig. 3.2. Post-polymerization deposition of Cloisite® $Na^+$ onto the microcapsule surface.....58

Fig. 3.3. (a) Optical microscope and (b) TEM cross-sectional images of PMPPI-based polyurea microcapsules.....66
Fig. 3.4. The gravimetric release rate profile of PMPPI/DETA polyurea microcapsules at room temperature (♦), 65 °C (◊), and 75 °C (♦).....69
Fig. 3.5. (a) Optical microscope and (b) TEM cross-sectional images of PMPPI/DETA polyurea microcapsules prepared with a 10:90 butyl acetate:xylene organic phase.....71
Fig. 3.6. Gravimetric release profile at 75 °C of PMPPI/DETA microcapsules prepared with 100 % xylene (♦) and 10:90 butyl acetate:xylene (♦) organic phases.....72
Fig. 3.7. Gravimetric release rate profile at 75 °C of PMPPI/DETA microcapsules prepared with 10 % (♦), 15 % (◊) and 20 % (♦) butyl acetate in the organic phase.....73
Fig. 3.8. TEM cross-sectional images of clay-coated PMPPI/DETA polyurea microcapsules with a 15-minute immersion time.....75
Fig. 3.9. Thermogravimetric analysis of pristine Cloisite® $Na^+$ (---), PMPPI/DETA (—), and MMT-PMPPI/DETA polyurea microcapsules (—).....77
Fig. 3.10. Thermogravimetric analysis of MMT-PMPPI/DETA polyurea microcapsules immersed in a 1.0 wt % (—), 0.5 wt % (—), and 0.1 wt % (---) aqueous Cloisite® $Na^+$ solution.....79
Fig. 3.11. TEM cross-sectional images of MMT-PMPPI/DETA polyurea microcapsules immersed in a 0.5 wt % clay solution.....80
Fig. 3.12. TEM cross-sectional images of MMT-PMPPI/DETA polyurea microcapsules immersed in a 0.1 wt % clay solution.....81
Fig. 3.13. Dependence of the shear stress on the dispersion pH for a sodium montmorillonite dispersion.....82
Fig. 3.14. TEM cross-sectional images of MMT-PMPPI/DETA polyurea microcapsules immersed in a 0.1 wt % clay solution at a pH of 9.8.....84

Fig. 3.15. Thermogravimetric analysis of MMT-PMPPI/DETA polyurea microcapsules immersed in a 1.0 wt % clay solution for 15 minutes (—), 1 hour (—), and 48 hours (---)..... 85
Fig. 3.16. TEM images of MMT-PMPPI/DETA polyurea microcapsules coated with 1.0 wt % Cloisite® $Na^+$ at (a) 15 minute, (b) 1 hour, and (c) 48 hour immersion time..... 86
Fig. 3.17. The gravimetric release rate profile at 75 °C of PMPPI/DETA (♦) and MMT-PMPPI/DETA (♦) polyurea microcapsules..... 87
Fig. 3.18. The gravimetric release rate profile at ~ 80 °C in a convection oven of PMPPI/DETA (♦) and MMT-PMPPI/DETA (♦) polyurea microcapsules..... 88
Fig. 3.19. The regions of release in the gravimetric release rate profile at ~ 80 °C of PMPPI/DETA (♦) and MMT-PMPPI/DETA (♦) polyurea microcapsules..... 89
Fig. 3.20. $^1$H-NMR spectrum of the microcapsule extract at t = 0. Characteristic xylene peaks (containing ethyl benzene) = 1.18 (t), 2.21 (s), 2.24 (q), 7.05 (s), 3.99 (t); butyl acetate = 0.89 (t), 1.32 (m), 1.54 (m), 1.99 (s), 3.99 (t)..... 92
Fig. 3.21. Normalized amounts of xylene (♦, —) and butyl acetate (♦, —) plotted alongside the corresponding normalized mass loss of PMPPI/DETA polyurea microcapsules (◊, —) over several days of gravimetric analysis..... 93
Fig. 3.22. The polycation for LbL assembly, poly(aminopropyl methacrylamide) (PAPM)..... 96
Fig. 3.23. Fluorescence microscopy images of (a) native PMPPI/DETA, (b) PAPM-coated PMPPI/DETA, and (c) PAPM-coated MMT- PMPPI/DETA polyurea microcapsules..... 97
Fig. 3.24. UV-Vis absorbance spectrum of the supernatant of the PAPM-immersed PMPPI/DETA (♦) and MMT- PMPPI/DETA (♦) polyurea microcapsules.... 99
Fig. 3.25. TEM cross-sectional images of MMT- PMPPI/DETA polyurea microcapsules synthesized under a solution pH of (a) 9.6 ± 0.1 and (b) 7.4 ± 0.1..... 101

Fig. 3.26. Optical microscope images under the fluorescent filter of the PAPM-coated (a) PMPPI/DETA, (b) MMT- PMPPI/DETA, and (c) lower solution pH MMT- PMPPI/DETA polyurea microcapsules..... 102
Fig. 3.27. UV-Vis absorbance spectrum of the supernatant of the PAPM-immersed PMPPI/DETA (♦), MMT- PMPPI/DETA (♦), and MMT- PMPPI/DETA at low pH (◊) polyurea microcapsules..... 103

# 1.0 Introduction

## 1.1 Pesticide Delivery Systems (PDSs)

Over the past century, crop protection technology has progressed significantly from directly spraying crops with active ingredients such as pesticides and insecticides. These original methods consisted of spraying a dispersion of active materials in water, otherwise known as an emulsifiable concentrate formulation (EC).[1] While easy to implement, direct spraying demonstrated poor control over active concentrations and effective lifetimes, requiring shorter application intervals that resulted in additional annual costs of between $10 and 30 billion.[2] Of even greater concern were the harmful effects of direct exposure to toxic materials of both workers and the environment.[3,4] The often high acute mammalian toxicities resulted in such harmful effects as eye and skin irritation, skin sensitization, paraesthesia, and inhalation toxicity.[5] Subsequent crop protection research hence focused on the development of pesticide delivery systems (PDSs) incorporating controlled release technology and reduced toxin exposure.

PDSs allow the transport of active ingredients to a specific target at a concentration and duration designed to achieve high biological efficacy while reducing harmful side effects.[6] Most current PDSs are based on controlled-release approaches, involving a biologically active ingredient and excipient, usually a polymer, arranged to allow delivery of the ingredient to the target at controlled rates over a specific period.[7] The resulting rate of release should primarily depend on the properties of the storage material for the active ingredients, rather than on environmental conditions. The PDS may be designed to exhibit one of several types of controlled release mechanisms,

including: membrane erosion, retrograde chemical reaction, and diffusion through a rate-controlling membrane. It is also common for more than one method of release control to be active simultaneously, an example being the starch xanthate capsules described by Shasha and coworkers.[8] Microencapsulated solid and liquid pesticides are released by both membrane diffusion and by erosion of the starch xanthate wall. An alternative to passive, controlled release is active, triggered release where labile components incorporated in the encapsulating membrane enable very rapid increases in release rates.[9] One example are polyurea microcapsules comprising pH-sensitive thioester crosslinkers designed by Syngenta Inc.. These capsules are stored in suspension at neutral pH, and activation of release occurs by increasing the pH just prior to application, leading to alkaline hydrolysis of the thioester 'gate keepers'.[10] The benefits of both passive and active controlled release mechanisms for PDSs include a reduction in toxicity and improved release control, resulting in a more efficient method of crop protection. Of the three mechanisms described, diffusive release through a membrane relies largely on the solubility of the pesticide in the wall. Therefore, fine-tuning of release can be accomplished by varying the properties of the membrane, such as chemical composition,[11] wall thickness,[12] surface area or capsule size,[13] external coatings,[14] etc.[15]

The two main types of diffusive release PDSs are called monolithic and reservoir devices, respectively (Fig. 1.1).[16] The former system involves the dispersion, or dissolution of a pesticide in a matrix, while the latter involves encapsulation of the active ingredient within a distinct membrane. Reservoir PDSs typically contain a larger proportion of pesticide, and give zero-order release controlled by diffusion through the

capsule wall membrane. Matrix-type (monolithic) devices are sometimes easier to prepare, for example by the spray-drying of mixtures containing active and a matrix forming resin. However, the resulting release rates can vary dramatically during the course of release, due to non-linear erosion of a degradable matrix, or due to depletion of the active ingredient. The most common reservoir-type systems are polymer microcapsules, composed of a rate-controlling spherical polymer membrane encapsulating active ingredients for controlled release.

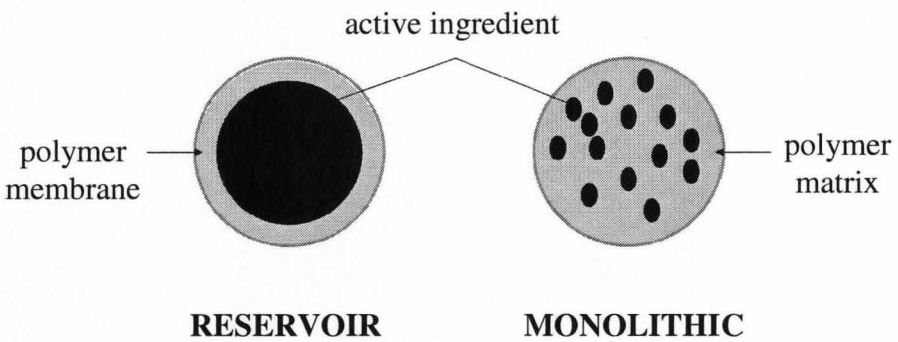


**Fig. 1.1.** Reservoir and monolithic diffusion controlled PDSs

Interestingly, the most significant commercial microcapsule-based product is not found in agriculture, but in paper technology as carbonless copy paper.[17] In the early 1950s, Green and Schleicher[18] described the undercoating of paper with pressure-sensitive microencapsulated pre-dyes, which experience rupture release from pressure produced by a pen or pencil. The released pre-dye reacts with acidic clay on the surface of a second sheet of paper to produce an actual dye, resulting in a printed carbonless copy. The

commercial application of this microcapsule technology is certainly wide-spread; including in standard multi-ply forms for credit-cards, cheques, packing slips, etc.

Application of microcapsule technology to agriculture requires the selection of an appropriate encapsulating material, in this case a polymer that satisfies several fundamental conditions. These include: suitable molecular weight, glass transition temperature and molecular structure for release, inertness to the encapsulated materials, biodegradability of capsule materials and their degradation products, storage and usage stability, and manufacturing at acceptable costs.[19] Based on these fundamental requirements, the most common polymeric wall materials for microencapsulation include polyamides,[20] polyesters,[21] polyureas,[22] polyurethanes,[23] cellulose,[24] and gelatin.[25] Although various polymer systems have been used successfully to form microcapsules for agricultural applications,[26] polyurea membranes were chosen for the present project.

**1.2 Polyurea Microcapsules**

Polyurea microcapsules are hollow spheres of 1-200 μm in diameter that are formed by interfacial step-growth copolymerization of isocyanates and amines in oil-in-water emulsions. The first such interfacial polycondensations were reported by Carothers at Dupont Company,[27] and involved the synthesis of polyamides. Since then, this method rapidly expanded to include the production of polyesters, polyphthalamides, polysulphonamides, and of course, polyureas.[28,29,30]

The general reaction is shown below:

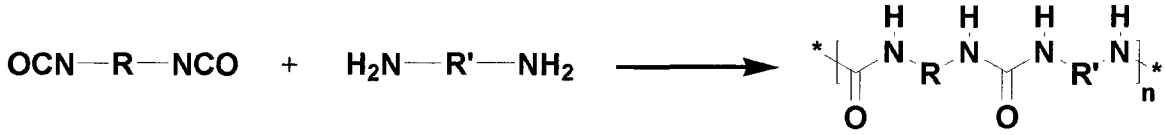

**Fig. 1.2.** Polycondensation between a diisocyanate and a diamine to form polyurea

Polyurea microcapsule synthesis involves the migration of an amphiphilic amine from the continuous aqueous phase into the dispersed organic phase containing an oil-soluble isocyanate. The resulting polyurea wall starts to forms at the interface, with subsequent wall growth occurring in the organic phase where the two monomers react. Wall formation stops once all the monomers have reacted, or when the amine can no longer penetrate the polyurea shell. The resulting polyurea microcapsule encapsulates the active ingredient and its surface carries a net positive charge due to protonated amines.

Encapsulation by interfacial polycondensation enables high pesticide loadings, variable size distributions, and the ability to vary wall permeability through monomer loading and process conditions such as temperature and mixing speed.[31] For example, Mathiowitz and Cohen[32,33] studied the effects of reaction time, monomer type, and capsule size on membrane permeability. Furthermore, an extensive description of interfacial polycondensation, along with the effects of variations in microcapsule parameters was reported by Morgan in 1965.[34]

Once polymerization is complete, the resulting aqueous dispersion of polyurea microcapsules is often directly applicable to host crops. The aqueous capsule slurry is a useful controlled release formulation for agriculture because:[35,36]

1. It is composed of discrete microcapsules as opposed to aggregates.
2. It can be diluted and sprayed with conventional equipment for uniform field coverage of pesticide.
3. Additives such as film forming agents can be added directly to the formulation to improve adhesion of microcapsules to foliage.
4. The suspension in water itself provides a supplementary barrier to retain pesticides during storage and application.

All that remains after the complete release of the encapsulated pesticide are empty polyurea shells that slowly degrade[37] by photolysis, hydrolysis, oxidation, and biological degradation.[38]

**1.3 Release of Encapsulated Materials**

In general, most polymer capsules are designed to exhibit diffusive release of active materials over periods of several weeks, to cover breeding or feeding seasons of certain insect pests. For example, Sjogren[39] developed a proteinatious reservoir to encapsulate protein-compatible pesticides, such as triazole and arsenic based insecticides, for control of pest populations over a period of 10-30 days. This microcapsule lifetime ensured: protection of the pesticide from substantial degradation, effective penetration of dense vegetation, multiple and uniform placement of controlling particles throughout the treated environment, and a controlled, continuous rate of release that maintains a sufficiently high concentration of pesticide in the environment. Hence the release profile of polyurea capsules is strongly dependant on the specific fill composition, as well as

environmental factors such as temperature and humidity. Empirical optimization of every microcapsule formulation is then required to ensure consistent release rates of the encapsulated materials for a given application.

The fine-tuning of microcapsule permeability for controlled release of a specific encapsulated material relies on a variety of material properties, capsular parameters, and environmental conditions, as described by Fanger.[40] Many studies have explored the correlation between microcapsule permeability and wall structure, including: the degree of polyurea crystallinity,[41] the distribution of microcapsule sizes, and the rates of polymerization.[42] Furthermore, many release models were developed to describe and predict the diffusion of active ingredients through the microcapsule membrane.[43,44,45] For example, Yadav et al[46] developed a theoretical model to relate the kinetics of polyurea microcapsule wall formation with the rate of encapsulate release. Therefore, in order to gain insight into methods to control release, an appreciation for the theory behind diffusive release must be gained.

Microcapsules hold active ingredients in a protective shell during storage and delivery to a target site, at which point dehydration occurs and release commences. Provided that the concentration of the encapsulate within the capsule remains constant, the resulting steady state diffusion can be described by Fick's law of zero-order release. The equation governing Fickian release from microcapsules is as follows:

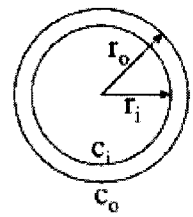


$$\text{Release Rate} = \frac{(4\pi r_o r_i) P (C_i - C_o)}{r_o - r_i}$$

$$P = KD$$

r = radius
P = Permeability
K = Solubility Coefficient
D = Diffusion Coefficient
C = Concentration

**Fig. 1.3.** Fickian release through a spherical membrane[47]

Therefore, the release rate of diffusion-based polymer microcapsules is directly proportional to surface area, permeability and concentration difference across the wall, and is inversely proportional to wall thickness. Several of these parameters are interrelated, and require experimental optimization. For example, increasing the membrane permeability by reducing the thickness of the polyurea shell may in fact weaken the microcapsule. While the high-density outer wall layer is typically responsible for the release rate,[48] the low-density inner wall lining contributes to the mechanical integrity of the reservoir.[49] Therefore, permeability, thickness and strength become interdependent factors in achieving a desired diffusive release profile, given that catastrophic rupture release via collapse is not desired. As a result, release profiles are

often difficult to control due to the heterogeneous structure of such capsule walls, in addition to ensuring fill composition compatibility.

Considerable effort has been invested in the development of universal controlled delivery systems, with minimal success. Consequently, new approaches to control release are needed, particularly methods that permit fine-tuning of release independent of the inherent properties of the polymer membrane itself. For example, Mathiowitz and Cohen[50] synthesized double layer membranes, where a second external wall could hinder the release of encapsulated materials. Alternatively, release may be controlled by the incorporation of nano-scale colloids with a high aspect ratio, such as montmorillonite clay, into the polyurea shell. Therefore, controlled release microcapsule technology and composite capsule formation are two aspects central to this thesis.

**1.4 Montmorillonite Clay**

Montmorillonite (MMT) particles consist of stacks of individual clay sheets that are classified as inorganic dioctahedral smectites, of the ideal chemical composition $[(Al_{3.50-2.80}\,Mg_{0.50-1.20})(Si_8)O_{20}(OH)_4]Na_{0.50-1.20}$. The MMT sheets, or platelets, are composed of 2:1 TOT sheets of an octahedral $AlO_6$ (or Al(OH)) layer sandwiched between two tetrahedral $SiO_4$ layers. The crystal structure of each clay sheet is shown in Fig. 1.4.

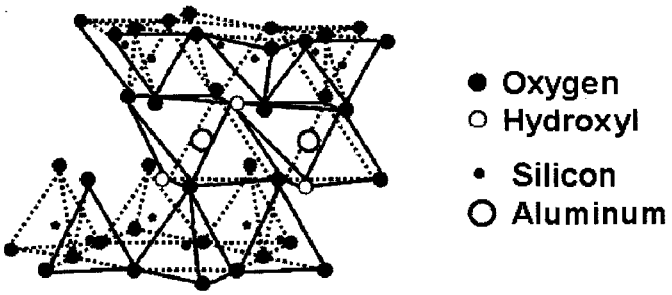


**Fig. 1.4.** Crystal structure of a single montmorillonite clay sheet[51]

Given the natural occurrence of isomorphic substitution between $Si^{4+}$ and $Al^{3+}$, each platelet possesses a net negative surface charge. Interlayer cations, such as $Na^{+}$, counterbalance the negative charge and hold the platelets together in the form of stacks, or clay particles. MMT clays are of particular interest due to their ability to swell (intercalate) and break apart (delaminate) in water with mechanical agitation. Extensive delamination in water can result in partially exfoliated dispersions, consisting of both individual platelets and smaller stacks of 2-20 layers of clay,[52] called tactoids. In aqueous solutions, the single clay layers and small tactoids are surrounded by a diffuse layer of Na cations that repel each other by electrostatic forces.[53] The hydrated counterions in the diffuse double layer result in long-range repulsion, which assists in maintaining the degree of particle delamination in solution.[54] Further delamination is preserved by short-range repulsion of partially hydrated Na cations, which are in close proximity to the Stern layer at the clay surface.[55]

Although platelet surfaces exhibit a net negative charge, clay is inherently amphoteric, and hence possesses sites of positive charge. These may originate from

hydrous oxides of iron, aluminum, and manganese, or more predominantly from exposed octahedral groups, which react as bases by accepting protons from water and acquiring a positive charge.[56] The exposed octahedral groups are located at the edge of clay sheets, known as the broken bond surface, which is primarily alumina-like with minimal contribution from broken Si-O bonds.[57] At pH values below 9, the broken bond surfaces gain a positive charge that further increases with decreasing pH. This allows for the formation of a potential 'house of cards' structure, where the cationic edges and the anionic faces randomly bond edge-to-face (EF).[58] At neutral pH however, the strength of the EF attraction is considerably less than face-to-face (FF) repulsions, owing to the small area of the broken bond surface.[59] Therefore, the spillover of negative charge from the platelet face increases with the aspect ratio,[60] preventing EF interactions from occurring in solution. Provided that the clay dispersion is highly delaminated at near-neutral pH, the individual clay sheets and tactoids will remain separate in an aqueous dispersion.

An extensive degree of particle exfoliation in solution is required prior to microcapsule incorporation in order to maximize surface interactions between clay sheets and the polymer, and to fully benefit from the high aspect ratio of the inorganic additive. Nano-scale dispersions of clay platelets can be combined into pre-polymer solutions or polymer melts to improve thermal and solvent resistance,[61,62] barrier control,[63] and mechanical strength.[64,65,66] In the absence of high degrees of delamination, non-uniform aggregation of clay particles can occur and result in defect sites that weaken the properties of the composite. The first synthetic description of a clay-polymer hybrid material was provided in 1987 by Fukushima and Inagaki at Toyota.[67] The group

incorporated clay modified with an organic compatibilizer into a nylon 6 matrix, aiming to maximize the degree of exfoliation of the organophilic additive. The hybrid material displayed improvements in all aspects of mechanical performance, including material rigidity, strength, elongation and toughness.

The incorporation of low loadings of montmorillonite clay sheets into polymer systems can result in nanocomposites with improved barrier properties,[68] due to the high aspect ratio (1000:1) of the inorganic additive. Upon uniform dispersion of clay sheets in a polymer matrix, the impermeable clay layers mandate a tortuous pathway for a permeant to transverse the composite material (Fig. 1.5.).

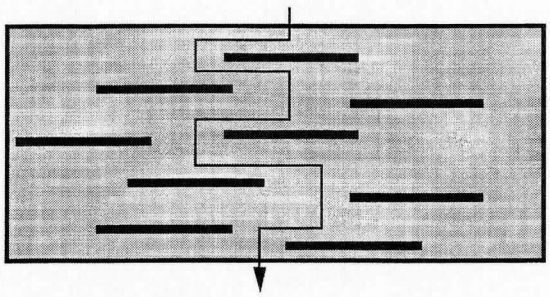

**Fig. 1.5.** Model for the tortuous path of diffusion of a permeate through an exfoliated polymer- clay composite[69]

The tortuousity factor in a model polymer system was extensively described by Yano et al.,[70] in which the permeability coefficients were related to the total path length traveled. Many studies have revealed a significant decrease in permeability upon incorporation of clay into such polymers as polyimides, rubbers,[71] and poly(ε-caprolactones)[72]. For example, $Na^+$ montmorillonite was dispersed in a protonated butadiene-acrylonitrile copolymer, and then mixed with nitrile rubber under crosslinking conditions. The

resulting vulcanizate experienced a 30 percent reduction in the permeabilities of hydrogen and water vapor relative to pristine nitrile rubber.[73] Therefore, the incorporation of highly delaminated MMT clay into the polyurea microcapsule wall may prove beneficial in controlling, and decreasing the rate of pesticide release from an otherwise permeable polyurea capsule.

In addition to composite polyurea shell formation, a second method of clay incorporation involves the adsorption of MMT clay to the external surface of the microcapsule. The external clay layer can behave as a release barrier, and provide a generic route to control release rates without having to modify the nature of the polyurea membrane. Permeability can thus be controlled by the addition of multiple layers onto the microcapsules, regardless of fill composition or application. Layering of clay onto the external spherical shell can be easily achieved via the layer-by-layer technique.

**1.5 Layer-by-Layer (LbL)**

The rising interest in organic/inorganic composite materials stems from the ability to combine desirable properties of the individual components into a finely-tuned hybrid material. Specifically, the layering of inorganic particles with an organic polymer can result in the improvement of several macro-scale properties at the nano-scale.[74] Research into composite polymer materials is quite extensive, with examples including the layering of polyelectrolytes and such particles as silica ($SiO_2$),[75,76] cadmium sulfide (CdS),[77] titanium dioxide ($TiO_2$),[78,79] molybdenum oxide,[80] gold,[81,82] iron,[83] etc. An example of such a hybrid material was described by Aliev et al.,[84] with the layering of silica and magnetite nanoparticles. The non-magnetic insulating properties of silica, combined with

the magnetic behaviour of magnetite, enabled the formation of low-noise high-density magnetic media. Further applications for hybrid materials are numerous, and include such systems as light-emitting diodes,[85] sensors,[86] conductive films,[87] optical devices,[88] and gas separation membranes.[89] In the case of polyurea microcapsules, the layering of alternating organic and inorganic polyelectrolytes may result in an electrostatically bound composite structure with tunable barrier properties.

Flat, layered hybrid materials are easily formed by Langmuir-Blodgett (LB) techniques, spin coating or vapour deposition. In contrast, spherical capsules are best coated by the layer-by-layer (LbL) technique, which involves the deposition of alternating layers of oppositely charged materials by electrostatic adsorption from solution. Introduced by Decher in 1991,[90,91] LbL sequential assembly is driven by the charge neutralization and re-saturation upon adsorption of charged materials on oppositely charged surfaces, resulting in an alternating change in the surface charge.[92] A simplified schematic of the LbL method is shown in Fig. 1.6.[93]

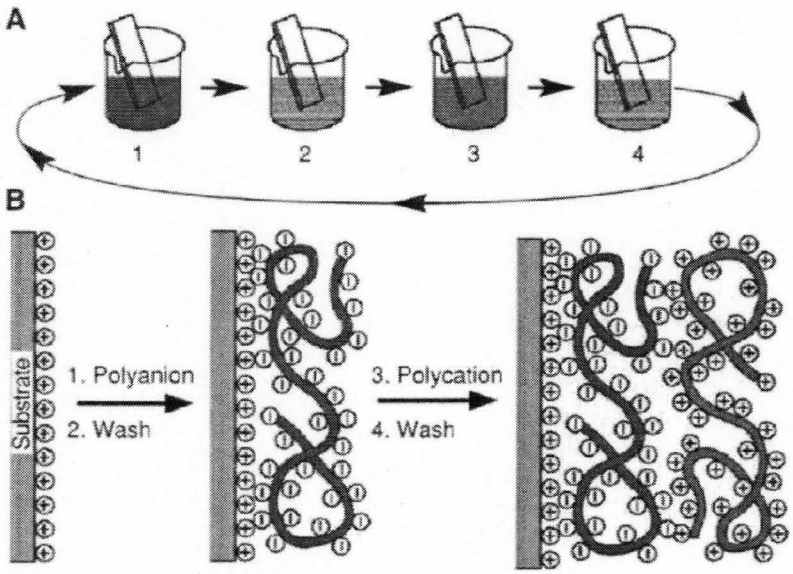


**Fig. 1.6.** (**A**) Simplified schematic of the layer-by-layer method using slides and beakers. Step 1: polyanion adsorption; Step 2: washing; Step 3: polycation adsorption; Step 4: washing...(**B**) Blow-up of slide surface outlining adsorption steps onto a cationic substrate

The charge reversal at the substrate surface enables control over the average thickness of each layer, given that the surplus of charge repels further layer growth. Therefore, the main incentives for applying LbL to coat polyurea microcapsules lie in the simplicity of deposition and in its independence of the nature, size and topology of the substrate.

Application of layer-by-layer deposition to polyurea microcapsules is facilitated by the overall positive charge of the external capsule surface, owing to protonated, unreacted amines. The spherical substrate is therefore weakly charged, enabling the direct layering of negatively charged species via electrostatic bonding. Determination of the first anionic layer involves considering the barrier properties of the material for potential fine-tuning of pesticide release. Although many negatively charged colloids are available

for surface adsorption, such as $SiO_2$ and $TiO_2$, incorporation of inorganic montmorillonite clay is of particular interest due to its ability to significantly decrease polymer membrane permeability at low loadings.[94] Nano-scale montmorillonite clay sheets exhibit several properties that are ideal for layering onto polyurea microcapsules, such as: a strong negative surface charge, extensive particle delamination in water,[95] and a high aspect ratio of up to 1000:1. The anionic clay sheets align themselves parallel to cationic surfaces, to form strong interfacial interactions over a large surface area.[96] Upon charge reversal, further adsorption of positively charged molecules would allow for a subsequent clay coating, in a classic LbL fashion.

The first example of a LbL assembly of polycations and clay to produce ultrathin multilayers was reported by Kleinfeld and Ferguson,[97] with the layering of poly(diallyldimethyl)ammonium chloride (PDDA) and hectorite clay. Subsequently, this work was extended to montmorillonite clay and linear polycations by Lvov et al.,[98] in an extensive description of precisely controlled architectures for enzyme incorporation. Of specific interest, however, are the research efforts that have concentrated on the transport and barrier properties of MMT-polycation multilayer films.[99,100] Recently, Lutkenhaus et al. described the trilayer assembly of poly(ethylene imine), montmorillonite clay and poly(ethylene oxide) to study ion transport structures for electrochemical devices.[101] Therefore, by the layer-by-layer assembly of montmorillonite clay sheets and a cationic polymer 'glue', the diffusive release rate of pesticides from polyurea microcapsules may be controlled and fine-tuned independent of the shell membrane.

## 1.6 Thesis Objectives

The goal of this research was to control the rate of release of volatile fills from a model polyurea microcapsule by the incorporation of montmorillonite clays into the polymer membrane. Control over the diffusive release of core materials by a method separate from the chemical nature of the wall broadens its applicability to a wide range of polyurea capsule formulations, regardless of the internal materials they contain. To accomplish this task, two approaches of clay incorporation were investigated:

1. Clay dispersed in the continuous aqueous phase, or the dispersed organic phase of an oil-in-water emulsion during interfacial polycondensation of an isocyanate and amine
2. Clay deposited post-polymerization onto the polyurea microcapsule surface by layer-by-layer assembly

The first approach involved extensive investigations into the nature of montmorillonite clays in order to gain an understanding of delamination, and in order to characterize the degree of exfoliation through measurement of particle size distribution, transmission electron microscopy (TEM), and X-ray diffraction (XRD). The solvent compatibilities, cation exchange mechanisms, emulsion stabilizing abilities, and fluorescent labeling of pristine and organically-modified clays were explored prior to microcapsule inclusion. Upon polyurea incorporation, methods of characterization include optical and transmission electron microscopy.

The second approach involved developing an understanding of polyurea microcapsules, in order to determine a model system of appropriate strength and release properties for permeability testing. Fine-tuning the choice of co-monomers, reaction parameters, and encapsulated fills resulted in polyurea formation by polycondensation of polymethylene polyphenyl isocyanate (PMPPI) and diethylenetriamine (DETA), using an organic phase that doubled as a model fill material consisting of a 90:10 mixture of xylene:butyl acetate. The parameters for layer-by-layer deposition of clay were optimized through the consideration of such variables as: adsorption time, clay loading, and pH. Clay-coated polyurea microcapsules were characterized by optical microscopy, TEM and thermogravimetric analysis (TGA). Further layer-by-layer assembly of alternating clay-polyelectrolyte coatings onto the microcapsules involved a weak polycation, poly(aminopropyl)methacrylamide (PAPM), fluorescently labeled with fluorescein isothiocyanate (FITC).

Fill release from the polyurea microcapsules was measured by temperature-accelerated gravimetric analysis, and monitored by proton nuclear magnetic resonance ($^1$H-NMR).

## 2.0. Montmorillonite Clay Incorporation during Polymerization

The application of polyurea microcapsules as vessels for pesticide delivery enables the controlled release of active ingredients to target crops. It must be emphasized, however, that each pesticide usually requires a delivery system designed specifically for the active ingredient and the intended application.[102] Consequently, fine-tuning of the polyurea membrane permeability is required to ensure a consistent release rate for a target application. Given the interdependence of fill and wall material parameters,[103] variations in the structure of the microcapsule membrane are often unpredictable and result in undesirable release profiles. Therefore, the ability to control the permeability of the polyurea wall by methods separate from the nature of the wall itself is highly desirable for application to a wider range of microcapsules. One such method is the incorporation of high aspect ratio colloids into the polymer matrix, which act as diffusion barriers to reduce release rates. Of the many inorganic colloids available,[104,105] nano-scale montmorillonite clay sheets are ideal materials for barrier control, given their high aspect ratios of ~ 1000:1. In fact, many research efforts reveal a significant decrease in permeability upon the incorporation of clay in various polymer matrices.[106,107,108] As an additional benefit, dispersions of clay platelets can be added to pre-polymer solutions or polymer melts to improve such material properties as thermal resistance, solvent resistance,[109,110] and mechanical strength.[111,112,113]

The synthesis of polyurea microcapsules involves the polycondensation of an amine and an organophilic isocyanate at the interfaces of an oil-in-water emulsion. Incorporation of clay into the polyurea wall during polymerization would then require

that the inorganic material be dispersed in one of two immiscible phases prior to polyurea capsule formation. Therefore, the synthesis of composite capsules was separated into two possible mechanisms: interfacial migration of natural $Na^+$ montmorillonite clay from the continuous aqueous phase (Fig. 2.1(a)) and the introduction of organically modified montmorillonite clay (O-MMT) in the dispersed organic phase (Fig. 2.1(b)). This chapter explores the development of both methods of clay incorporation into the polyurea microcapsule wall, with greater emphasis placed on the dispersion of MMT in the aqueous continuous phase (method (a)).

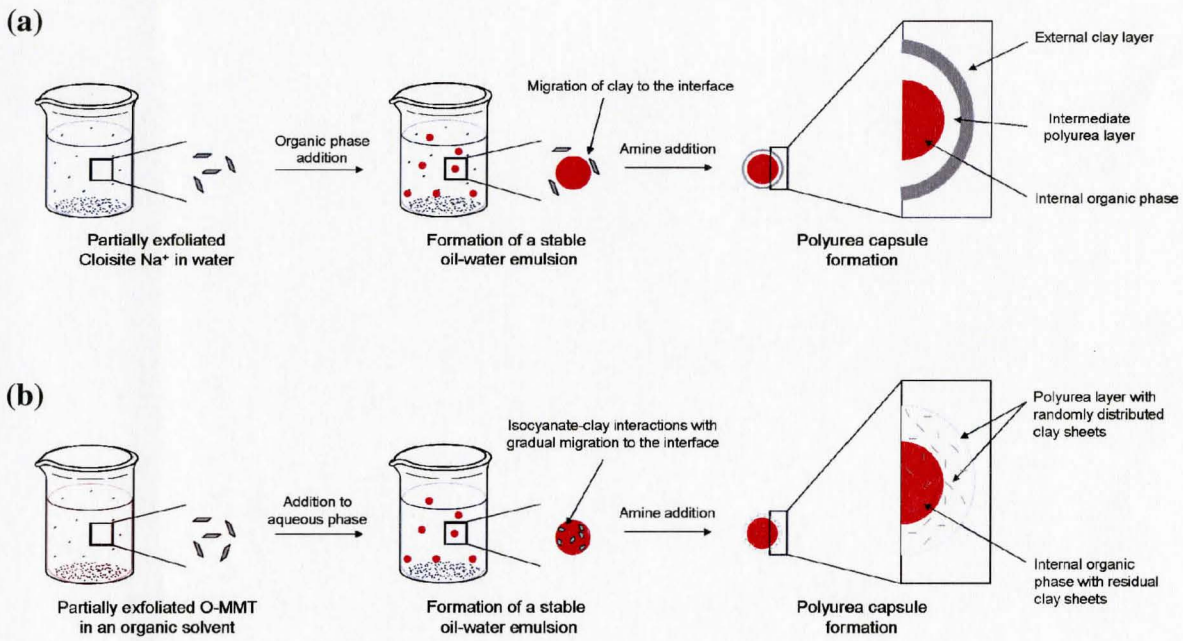


**Fig. 2.1.** The two mechanisms of montmorillonite clay incorporation during polyurea microcapsule formation: **(a)** clay dispersed in the aqueous phase; **(b)** clay dispersed in the organic phase

Initial investigations explore the fundamentals of montmorillonite clay chemistry, in hopes of determining the experimental conditions necessary to maximize the barrier properties of clay in the polyurea microcapsule system. Specifically, preliminary work involved solvent dispersions and emulsion stabilization, key factors to efficient incorporation of clay by interfacial polymerization. This was followed by determining the most effective method of particle delamination in solution, which is of utmost importance to maximize the aspect ratio of clay sheets. Characterization of the extent of exfoliation of clay-solvent dispersions was not a straightforward task, and required the combination of TEM and XRD. Finally, the incorporation of montmorillonite clay into polyurea microcapsule walls was achieved, as revealed by TEM imaging. Furthermore, fluorescent labeling methods were explored to simplify the identification of clay distributions via fluorescence microscopy.

## 2.1 Experimental

### 2.1.1 Materials

**Cloisite® $Na^+$,** cation exchange capacity (CEC) of 92.6 meq/100 g clay (from supplier), $d_{001}$ layer spacing of 11.7 Å, Southern Clay Products, Texas, USA.

**Cloisite® 10A,** alkyl quaternary ammonium bentonite with a 2MBHT (dimethyl, benzyl, hydrogenated tallow) organic modifier at a CEC of 125 meq/100 g clay, and a $d_{001}$ layer spacing of 19.2 Å, Southern Clay Products, Texas, USA.

**Cloisite® 15A,** alkyl quaternary ammonium bentonite with a 2M2HT (dimethyl, dihydrogenated tallow) organic modifier at a CEC of 125 meq/100 g clay, $d_{001}$ layer spacing of 31.5 Å, Southern Clay Products, Texas, USA.

**Cloisite® 30B,** alkyl quaternary ammonium bentonite with a MT2EtOH (methyl, tallow, bis-2-hydroxyethyl) organic modifier at a CEC of 90 meq/100 g clay, $d_{001}$ layer spacing of 18.5 Å, Southern Clay Products, Texas, USA.

Isopherone diisocyanate (IPDI, 98 %), polymethylene polyphenyl isocyanate (PMPPI, $M_n$ 340), poly(vinyl alcohol) (PVA, 80% hydrolyzed, M.W. 9000-10000), rhodamine 6G (R6G, ~ 95 %), rhodamine B (RhB, 90 %), diethylenetriamine (DETA, 99 %), ethyl benzoate (99+ %), methyl benzoate (99 %), propylene carbonate (99 %), all purchased from Aldrich Chemical Company, Inc.

Cyclohexane, 99.0 %, N,N-dimethylformamide (DMF), 99.8 %, and tetrahydrofuran (THF), 99.0 %, purchased from Caledon Laboratory Chemicals.

Xylene (o-, m-, p-isomers, contains up to 25 % ethyl benzene, 99.9 %), Fisher Scientific.

### 2.1.2 Instruments

**Safe Pressure Reactor,** Büchiglasuster polyclave reactor equipped with a Cyclone 075 80W stirrer drive, a propeller type mixer, and a Büchi Miniclave Drive 100 mL glass reactor.

**Mechanical Agitator,** LAB-LINE Multi-wrist Shaker, model 3589, 50/60 Hz, shaker speed setting 10 (750 rpms).

**Ultrasonicator,** Branson Sonifier 150 Digital, 60 Hz, sonication level set to 7 (~ 15 watt rms).

**Ultrasonication bath,** Branson Ultrasonic Cleaner 1210R-MT, 1.9 L capacity, 50-60 Hz.

**Optical Microscope,** Olympus BH-2, equipped with a Kodak DC 120 Zoom Digital Camera for taking optical microscope pictures.

**Particle Size Distribution by Light Scattering,** Coulter LS230 Series with Fluid Module, 50/60 Hz, Coulter Corporation, measures particles sizes from 0.04 μm to 2000 μm. Equipped with a 4 mW laser at a wavelength of 750 nm.

**XRD,** X-ray diffraction, 2D diffractometer equipped with a Rigaku RU200 Generator, a Cu Kα ($\lambda$ = 0.154184 nm) rotating anode, a Göbel monochromator with cross-coupled mirrors, a Bruker AXS SMART 6000 CCD camera detector, and a Bruker D8 3-circle goniometer at fixed $\chi$ (54.78°). The sample was placed at a distance of 29.69 cm from the detector. The data was collected using Bruker SMART software, processed from 2D to 1D using GADDS, and viewed in 1D using TOPAS. The liquid dispersion sample holder (Fig. 2.2.) was constructed by drilling a hole (d ~ 0.5 cm) into a standard 1 mm thick glass slide, and permanently sealing one side of the opening with a 0.12 mm thick piece of Mylar®. The hole was then filled with liquid sample, and held in place by a second piece of Mylar®.

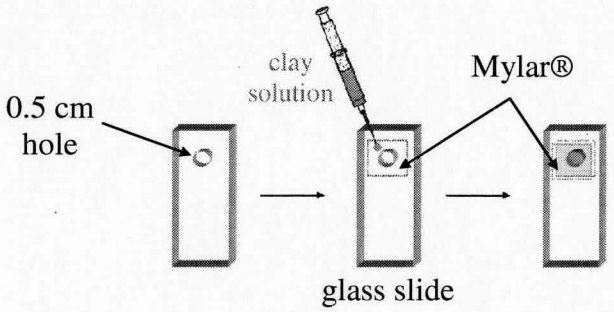


**Fig. 2.2.** Custom made XRD sample holder for aqueous clay dispersions

**TEM,** Transmission Electron Microscope, JEOL 1230 equipped with a 4 megapixel AMT digital camera. All aqueous clay solutions were deposited onto 100 mesh, formvar (polyvinyl formal) coated copper TEM grids and left to dry prior to analysis. All microcapsules for TEM analysis were swollen in tetrahydrofuran to extract residual solvents and unreacted isocyanates. The extracted capsules were dried under vacuum at 70 °C, embedded in Spurr epoxy resin, and ultramicrotomed to about 100 nm thickness.

**Fluorimeter,** Spex® Fluorolog® - 3 equipped with a 450-W xenon light source, and a room-temperature R928P detector. The data was processed using the DATAMAX computer program. The excitation wavelength was set to 500 nm for both rhodamine 6G and rhodamine B chromophores.

**UV-Vis Absorbance,** Varian Cary 50 Bio UV-Visible Spectrophotometer equipped with a Xenon lamp. The data was processed with Varian Cary WinUV software.

### 2.1.3 Procedures

#### 2.1.3.1 Preparation of Cloisite® $Na^+$ dispersions

Pristine sodium montmorillonite clay (Cloisite® $Na^+$) was dried in a vacuum oven at 70 °C for a minimum of 24 hours. A 20 mL aqueous dispersion of 1.0 weight % (wt %) dried Cloisite® $Na^+$ was prepared by ultrasonicating the dispersion for 10 minutes in a 50 mL polypropylene conical tube. The solution warmed to 70 °C during sonication, and was left to cool to room temperature prior to use.

### 2.1.3.2 Preparation of polyurea microcapsules by interfacial polycondensation

The multifunctional isocyanate (IPDI or PMPPI, 1 g) was added to xylene to make up 10 mL of organic phase. The aqueous phase consisted of 1.0 wt % PVA dissolved in distilled water. The aqueous phase (30 mL) was placed into a 100 mL reaction vessel fitted with 3-bladed overhead stirrer set to 800 rpm. The organic phase (10 mL) was added to the reaction vessel through an inlet at the top of the reactor, and dispersed for 15 minutes under stirring at room temperature. Finally, the difunctional amine (DETA, 1.5 g), dissolved in another 5 mL of aqueous phase, was added to the reactor to start the isocyanate – amine polycondensation at the interfaces. The reaction vessel was submerged into a water bath heated to 70 °C, and left to react overnight under stirring at 600 rpm. The resulting polyurea microcapsules were washed three times with distilled water in a separatory funnel, and stored as an aqueous slurry of capsules.

### 2.1.3.3 Preparation of fluorescent labeled clay

The fluorescent probe, rhodamine 6G (R6G) or rhodamine B (RhB), was added to a 1.0 wt % aqueous Cloisite® $Na^+$ solution at a concentration of 1 mol % of the CEC of the clay. The solution was placed in an ultrasonication bath for about 90 minutes. The extent of adsorption onto clay was monitored by UV-vis absorbance and fluorescence emission of the diluted labeled clay solution.

## 2.2 Results and Discussion

### 2.2.1 Incorporation of Cloisite® $Na^+$ from the continuous aqueous phase (Fig. 2.1. (a))

#### 2.2.1.1 Characterization of clay delamination

The introduction of highly delaminated clay sheets into the continuous aqueous phase during interfacial polymerization to form polyurea requires an understanding of clay chemistry, including methods to both maximize and measure clay particle delamination in aqueous dispersions. Fundamentally, there are three stages involved in breaking apart pristine clay particles into individual sheets and small tactoids: intercalation, delamination, and exfoliation (Fig. 2.3.).

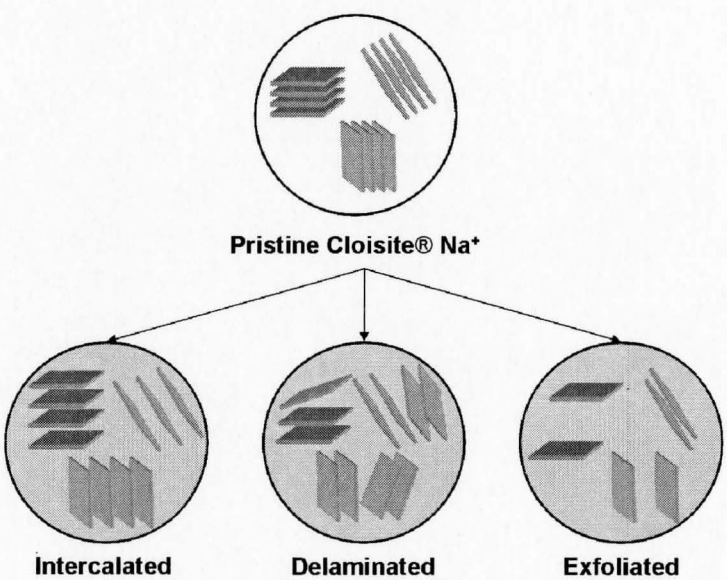


**Fig. 2.3.** Schematic representation of the three stages involved in breaking apart clay particles into individual sheets in solution

Intercalation of sodium montmorillonite in an aqueous solution involves the penetration of water molecules into the intergallery spacings between sheets, known as the osmotic swelling of clay particles.[114] The interpenetrating water molecules hydrate the counter cations that neutralize the negative platelet surface charge.[115] Intercalation pushes the individual clay sheets further apart, while strengthening the long-range repulsion in the diffuse double layer. The platelets begin to separate from the particle into free-standing individual sheets or smaller particles, which remain isolated by osmotic repulsion.[116] This process of separation is referred to as delamination. Further delamination of small particles by applied shear, such as agitation, leads to an increase in individual sheets and small tactoids in solution. This highly separated system is described as an exfoliated, aqueous clay dispersion. Complete delamination, however, to an exfoliated state comprising only single clay sheets is not possible and only a fraction of the clay mineral is truly exfoliated in solution.[117]

In its natural state, $Na^+$ montmorillonite (Cloisite® $Na^+$) disperses and partially delaminates in aqueous solutions with mechanical agitation. In fact, natural smectite clay minerals are among the materials that are most easily delaminated; depending on the counterion they undergo immediate particle breakdown upon mere contact with some aqueous solutions.[118] Delamination of Cloisite® $Na^+$ in aqueous systems results in an exfoliated clay dispersion, defined by the presence of small tactoids and individual platelets of varying morphologies. Consequently, characterization of the degree of delamination in disordered systems becomes a great challenge, particularly due to the mobility of clay in solution. Therefore, several complementary methods are required to

gage the degree of delamination.[119] It is reported[120] that the extent of exfoliation/delamination of clay nanolayers must be determined by TEM and other methods which supplement the use of XRD.[121,122] Therefore, the three methods explored to characterize exfoliated Cloisite® $Na^+$ solutions prior to polymer incorporation are light scattering, TEM and XRD.

**2.2.1.1.1 Particle size distributions by light scattering**

Light scattering provides distribution curves of diffracting volume (% of total volume) versus particle size, which can be used to measure the degree of delamination in solution. Specifically, exfoliated solutions result in distribution curves with the most particles at the smallest sizes. Unfortunately, given that the instrument evaluates particle size based on a spherical model system, rather than based on planar clay sheets, the method is restricted to qualitative comparisons only. The 1.0 wt % Cloisite® $Na^+$ samples were dispersed in water by two methods of applied shear, and at time periods deemed appropriate for the given method: 30 minutes of mechanical shaking on a wrist-shaker set to 750 rpm and 5 minutes of ultrasonication.

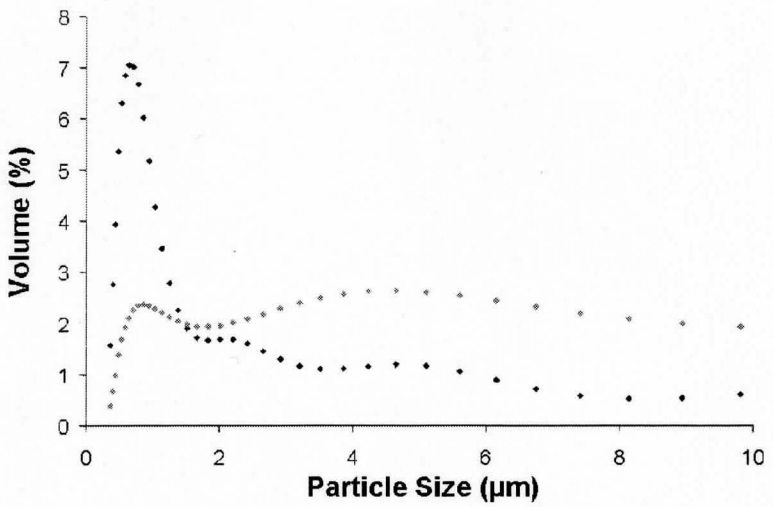


**Fig. 2.4.** Particle size distribution of 1.0 wt % aqueous clay dispersions following mechanical agitation (♦) and ultrasonication (♦)

Upon sample analysis (Fig. 2.4.), over 50 % of the ultrasonicated particles were of a size ≤ ~ 1.0 µm, compared to a mere ~ 15 % for the mechanically shaken particles. Subsequently, the length of the solution ultrasonication time was varied from 1 to 20 minutes. Although the resulting size distributions were similar (Fig. 2.5.), it appeared as though the most favourable results were achieved with 10 minutes ultrasonication. All three sonication times delaminated well over 50 % of their particles to sizes below ~ 1.0 µm, and therefore the median value of 10 minutes was chosen as the standard for subsequent testing. Furthermore, testing of samples stored for one week showed no re-aggregation of clay sheets during this time, validating the theory of osmotic repulsion. Therefore, light scattering techniques indicated that the highest degree of clay particle separation in water occurs after 10 minutes of ultrasonication.

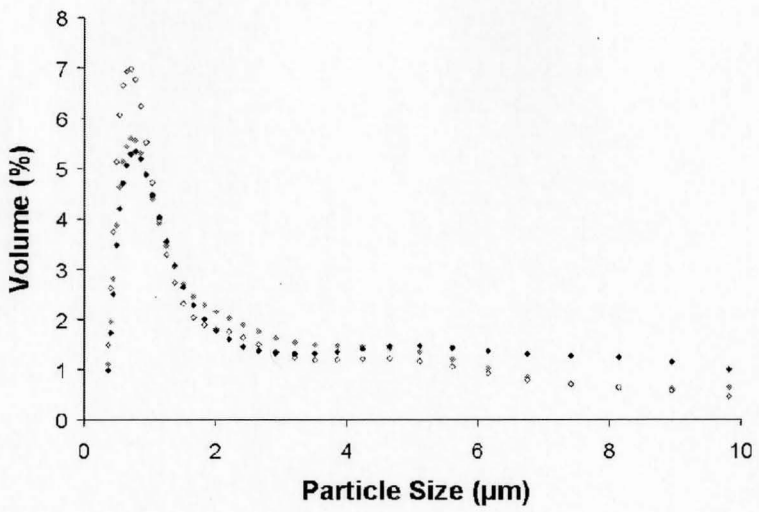


**Fig. 2.5.** Particle size distribution of 1.0 wt % aqueous clay dispersions following 1 minute (◈), 10 minutes (◊) and 20 minutes (♦) ultrasonication.

#### 2.2.1.1.2 X-ray diffraction (XRD)

X-ray diffraction is the most widely used technique for determining the degree of intercalation, delamination and exfoliation in clay dispersions. The application of XRD to clay characterization is enabled by the repeat spacing of the crystal structure of individual sheets that make up pristine clay mineral particles. In powder form, each type of montmorillonite clay possesses a characteristic d-spacing value, $d_{001}$, corresponding to the distance between individual platelets, or the intergallery spacing. Specifically, the d-spacing value is evaluated from the 2θ diffraction spectrum obtained by XRD, using Bragg's law of constructive interference:

$$n\lambda = 2d\sin\theta \qquad (1)$$

where $n$ is the order of the diffraction beam, $\lambda$ is the x-ray wavelength, $d$ is the distance between crystal planes, and $\theta$ is the angle of the diffracted wave.

Upon dispersion of pristine clay in a good solvent, the solvent penetrates the clay layers and increases the gallery spacings, pushing the individual platelets further apart. The resulting increase in the $c$ axis of the unit cell (d-spacing) can be monitored by XRD,[123] revealing the extent of particle intercalation in the clay dispersion. Subsequently, the introduction of shear results in the breaking apart, or delamination, of swollen particles to a disordered, exfoliated state of individual sheets and small tactoids in solution. The progression to this exfoliated state is accompanied by a gradual loss of order, which is reflected in the diffraction spectrum by a decrease and broadening of the 2θ peak. Therefore, highly exfoliated clay solutions are too disordered to give coherent scattering,[124] and are characterized by the disappearance, and absence of peaks in the diffraction spectrum.[125]

Sodium montmorillonite clay, with a d-spacing of ~ 11.7 Å,[126] expands the interlayer spaces when immersed in a hydrophilic solvent such as water. The osmotic swelling pushes the clay platelets further apart to increased d-spacings, as reported by Norrish.[127] Although clay structure analysis by XRD is more common for solid, polymer-clay composites, solution state samples have been tested by a variety of methods specific to certain diffractometers and applications.[128,129,130] For example, Bongiovanni et al.[131] performed XRD on clay suspensions in a concave hemispherical glass sample holder, with the liquid surface at a level above the rim of the container. Sample analysis involved

aligning the exposed portion of the liquid into the diffraction plane by parafocalization geometry prior to measurement. In the present work, initial analyses of Cloisite® $Na^+$ dispersions were conducted in thin-walled glass capillary tubes with an average diameter of 0.5 mm. Although mainly amorphous, the capillary glass walls contained crystalline regions that contributed significantly to the background scatter of the instrument. Given that low concentrations of clay dispersions ($\leq$ 5.0 wt %) emit low scattering intensities,[132] the diffraction spectra of 1.0 wt % Cloisite® $Na^+$ in water could not be resolved. An increase in clay concentration was thus necessary, which resulted in a significant increase in solution viscosity. This prevented the use of capillary tubes and led to construction of a sample holder incorporating completely amorphous Mylar® sample windows (Fig. 2.2.).

The clay loading was increased from 1.0 wt % to 10.0 wt % in water for XRD analysis only, with subsequent testing and polymer incorporation to be done using the less concentrated dispersion of lower viscosity. Therefore, the diffraction data collected for the 10.0 wt % solution will represent the minimum amount of clay delamination possible for the standard solution of much lower clay loading. The assumption made, is that the degree of clay particle delamination observed for the 1.0 wt % solution would be as great, or greater, than the 10.0 wt % solution tested. A further increase in the scattering intensity was achieved by using the as-purchased material rather than oven-dried Cloisite® $Na^+$. The characteristic diffraction peak of oven-dried Cloisite® $Na^+$ is of much lower intensity, and at a greater $2\theta$ value than that of the as-purchased clay (Fig. 2.6.). As the clay dries under vacuum at ~ 70 °C, the absorbed water at the surface of clay platelets is released, while intercalated water molecules begin to evolve. The movement of water

molecules causes a compression of clay particles, which can result in either a symmetric decrease in the intergallery spacings or an asymmetric structural collapse of platelets. The first instance accounts for the downshifting of the 2θ diffraction peak of dried clay, while the latter accounts for the decreased intensity due to undetectable, disordered stacks of clay sheets.

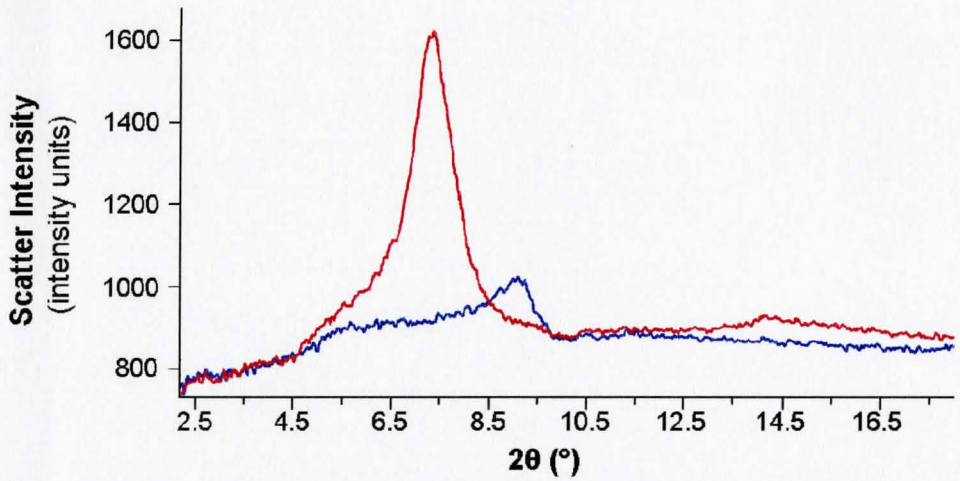


**Fig. 2.6.** X-ray diffraction curve of pristine Cloisite® $Na^+$ (—) and dried Cloisite® $Na^+$ (—)

Initial XRD analysis was performed on a pristine Cloisite® $Na^+$ powder sample, in order to obtain the reference curve shown in Figure 2.7. The resulting 2θ curve is characteristic of powder $Na^+$ montmorillonite,[133] and consists of two ordered regions: the basal reflections (d-spacings) at higher 2θ values, and the general diffractions of the structure of the smectite layers themselves at very low 2θ values.[134] The first region is concerned with the extent of hydration of the intergallery voids, and varies with the degree of water intercalation between clay sheets. The latter region is referred to as the *hk* band region, which is independent of interlayer hydration and is generally similar for all

smectite clays. The basal reflection is the region we are concerned with, since it indicates the degree of osmotic swelling of clay particles. The vacuum-dried powder Cloisite® $Na^+$ displayed a reference 2θ value of ~ 5.65°, corresponding to an average d-spacing value of ~ 15.6 Å.

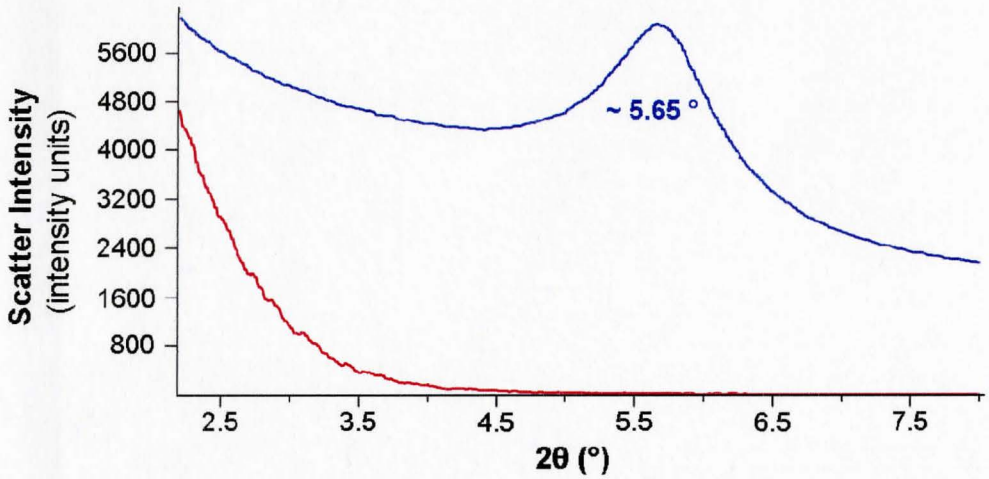


**Fig. 2.7.** X-ray diffraction curve of powder pristine Cloisite® $Na^+$ (—) and 10.0 wt % Cloisite® $Na^+$ dispersed in water (—)

Subsequently, the 10.0 wt % aqueous Cloisite® $Na^+$ solution was mounted and tested under the same conditions. The resulting 2θ spectrum did not reveal any basal spacings (Fig. 2.7.) and simply displayed the characteristic *hk* bands expected for montmorillonite clay. The absence of any Bragg reflections indicates that the interlamellar void is larger than the X-ray beam can detect, or that, alternatively, we are dealing with tactoids randomly oriented in suspension. Therefore, we cannot discern much about the degree of delamination, save that a change in clay particle morphology occurs upon dispersion in water.

Characterization of clay solutions by diffraction is limited to differentiating between intercalated and delaminated systems, and can not accurately describe the extent of particle delamination/exfoliation.[135] In fact, disordered or poorly ordered clay stacking can also cause the disappearance of the basal reflection peak, even if layers remain stacked within tactoids.[136] As the degree of disorder increases in the sample, XRD becomes a less definitive technique. Therefore, a method independent of the order of clay, TEM, becomes a complimentary tool for describing the state of exfoliation in aqueous clay dispersions.

**2.2.1.1.3 Transmission electron microscopy (TEM)**

Fundamentally, the basis of TEM involves the elastic scattering of an electron beam by the negative electronic potentials of atoms in a sample. The magnitude of this scatter is directly proportional to the atomic number (Z), with atoms of high *Z*-values displaying areas of dark contrast in TEM images. As a result, montmorillonite clay containing heavy elements such as silicon and aluminum will produce high contrast images when embedded in C, N, and O - based polymers.[137] Therefore, TEM can be used to determine the extent of clay delamination. The main disadvantage with TEM, however, lies in the small area analyzed per sample, and in the low likelihood of observing clay sheets edge-on. To some extent however, this issue can be overcome by studying several slices of the same sample.[138]

The information obtained by XRD for the aqueous Cloisite® $Na^+$ sample serves as a basis for the analysis of images produced by TEM. Consequently, it is expected that the resulting micrographs will display highly delaminated clay, preferentially consisting

of individual platelets and small tactoids. A comparative TEM analysis was performed on three distinct samples: a clean, sample-free polymer-coated grid (background), a non-agitated 1.0 wt % aqueous Cloisite® $Na^+$ solution, and the 1.0 wt % aqueous Cloisite® $Na^+$ solution with 10 minutes of ultrasonication. From the resulting images (Fig. 2.8.), it is apparent that the ultrasonicated clay solution is more delaminated than the non-agitated sample, which primarily consists of large aggregates.

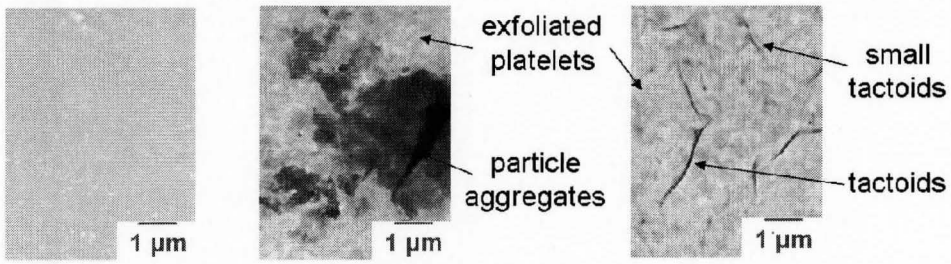


**Fig. 2.8.** TEM images of the formvar coated grid with **(a)** no sample, **(b)** the non-agitated clay solution, and **(c)** the ultrasonicated clay solution

In fact, the large regions of individual clay sheets and the minimal amount of small tactoids displayed in the ultrasonicated sample confirm the presence of exfoliated clay particles, rather than large clay aggregates.

The degree of clay particle delamination in an ultrasonicated 1.0 wt % aqueous Cloisite® $Na^+$ solution was characterized via three complimentary techniques: light scattering, x-ray diffraction, and transmission electron microscopy. Combining the qualitative descriptions obtained from each method allowed us to qualitatively characterize the ultrasonicated clay dispersion as exfoliated.

### 2.2.1.2 Characterization of polyurea-clay composite microcapsules

Incorporation of clay into the proposed microcapsule synthesis occurs by substituting the continuous aqueous phase for an exfoliated 1.0 wt % aqueous Cloisite® $Na^+$ solution. It is well established that small amphiphilic solid particles tend to self-assemble at liquid-liquid interfaces to reduce the interfacial energy between two immiscible liquids.[139] Therefore, the delaminated clay particles in the continuous phase of the interfacial polymerization may be able to stabilize the dispersed organic phase droplets without the use of additional emulsion stabilizers. Such a system, where particles such as clay platelets are used instead of surfactants to stabilize an emulsion, is commonly referred to as a "Pickering emulsion".[140,141] There are several examples describing the use of inorganic clay sheets to form Pickering emulsions for polymerizations,[142,143,144] as well as water-in-oil counterparts.[145] For example, Voorn et al.[146] investigated the stabilization of aqueous monomers by organically modified clay sheets dispersed in cyclohexane. This inverse Pickering emulsion resulted in the formation of polydisperse composite latex particles.

During interfacial polycondensation to form polyurea microcapsules, it is hence possible that the nano-scale clay sheets would stabilize the dispersed isocyanates and further remain at the emulsion interfaces upon amine addition to the aqueous phase. This would allow the coating of clay onto polyurea capsules *in situ*. Therefore, polyurea microcapsules were synthesized by interfacial polymerization with a 1.0 wt % Cloisite $Na^+$ aqueous solution as the continuous phase. The resulting microcapsules and the

distribution of clay in the polymer membrane were characterized via optical microscopy and TEM.

**2.2.1.2.1 Optical microscopy**

The polyurea microcapsules formed with clay present in the aqueous phase were non-spherical (Fig. 2.9.(a)), and accompanied by polyurea wall fragments. This suggested that the Cloisite® $Na^+$ was ineffective at stabilizing the organic phase droplets. Accordingly, a second emulsion stabilizer was added in attempts to facilitate the formation of stable, spherical microcapsules.

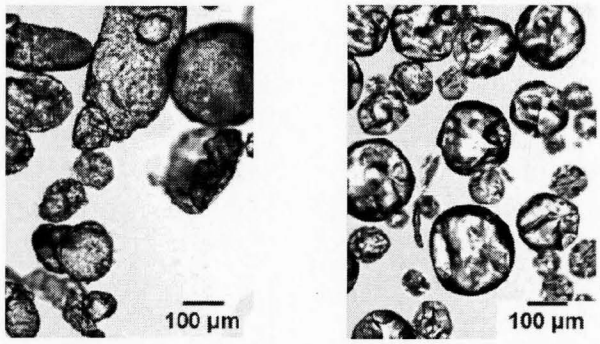


**(a)** **(b)**

**Fig. 2.9.** Optical microscope images of polyurea-clay composite microcapsules synthesized **(a)** without PVA and **(b)** with PVA

Poly(vinyl alcohol) (PVA) is a commonly used emulsion stabilizer for aqueous solutions. The amphiphilic nature of PVA enables it to assemble at oil-water interfaces and reduce the interfacial tension of the emulsion, hence stabilizing the dispersed oil droplets. The PVA (1 wt %) was added directly to the aqueous phase containing DETA, rather than the Cloisite® $Na^+$ dispersion, and the resulting microcapsules were observed

under the optical microscope (Fig. 2.9.(b)). The polyurea capsules formed from aqueous PVA clay dispersion were more spherical, and showed fewer wall fragments. It must be noted however, that the size of the microcapsules was much larger than that of conventional capsules ($\leq$ 100 μm). Although the composite capsule synthesis appeared successful, the nano-scale clay platelets on the capsules could not be resolved with conventional microscopy, but required TEM of thin capsule cross-sections.

**2.2.1.2.2 TEM**

The high electron density of the silica/aluminum clay sheets result in high contrast TEM images of clay in presence of polyurea and epoxy. The PVA-free microcapsules showed polyurea walls of about 100 nm in thickness, with an uneven distribution of clay aggregates on the outer surface (Fig. 2.10.(a)). The capsules formed with PVA showed 1 micron thick polyurea walls with an even distribution of clay on the outer surface (Fig. 2.10.(b)).

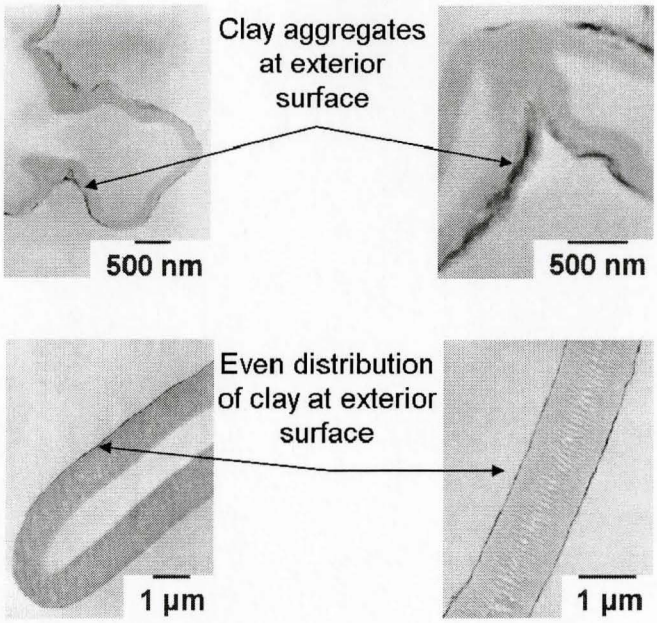


**Fig. 2.10.** TEM images of polyurea-clay composite microcapsules synthesized **(a)** without PVA and **(b)** with PVA

Similar results were obtained upon substitution of IPDI for poly[(phenyl isocyanate)-co-formaldehyde] (PMPPI), an isocyanate of higher functionality and reactivity that effectively improves capsule morphology and strength (images not shown). With both isocyanates, PVA is shown to enhance emulsion stability and increase the thickness of the polyurea wall, as well as provide an even distribution of clay on the exterior capsule surface.

It is believed that PVA stabilizes the emulsion interfaces and hence the dispersed organic phase, leading to spherical microcapsules. Most of the clay will complex with PVA in the continuous phase, resulting in only a thin layer of clay depositing on the capsules. This layer likely also complexes with the added emulsion stabilizer, as it is has

been suggested[147,148] that PVA hydrogen bonds irreversibly to clay sheets through OH – O bonds between single chains and the clay surface oxygens, respectively.[149] Although the viscosity of the aqueous phase containing PVA and clay did not change during polymerization, complexation between both species may have occurred at the emulsion interfaces.[150] Conversely, the PVA-free composite system generates a strict Pickering emulsion in which a layer of clay serves to stabilize the emulsion. This presumably dense layer of clay may also hinder the in-diffusion of amine into the organic phase, resulting in thinner polyurea walls formed.

The characterization of composite capsules synthesized with PVA suggests that the mechanism of clay incorporation during polymerization occurs via the external layering of clay onto the PVA-functionalized emulsion droplets. In the absence of PVA, the Pickering emulsion results in nonspherical polyurea microcapsules with unevenly distributed clay aggregates at the external capsule surface. In conclusion, clay incorporation from the aqueous phase during polymerization suffers from low colloidal stability and irregular clay deposition in absence of PVA. In the presence of PVA, clay is successful at stabilizing the dispersed organic phase, but may interfere with polyurea wall formation by interacting with the added stabilizer.

#### 2.2.1.3 Fluorescent labeling of Cloisite® $Na^+$ with rhodamine

While clay distribution can be revealed by TEM, sample preparation is a lengthy process. Consequently, fluorescent labeling of clay was explored as a simpler way to observe the distribution of clay in the capsule walls. The most straightforward method of labeling clay sheets with a fluorescent chromophore is to replace the native sodium of

Cloisite® $Na^+$ with a cationic fluorophore, both in the intergallery spacings, and on the platelet surfaces. The extent of exchange at the surface varies with each type of smectite clay, and is described as the cationic exchange capacity (CEC), with Cloisite® $Na^+$ having a CEC of 92.6 meq/100 g clay. The large size of cationic fluorophores facilitates the displacement of smaller $Na^+$ ions, given the preference of clay minerals for larger over smaller cations.[151] The labeling of clay by cation exchange mechanisms has been extensively studied.[152,153] Younessi et al.[154] labeled an organically modified clay with Safranine O, a quaternary ammonium chromophore, as part of a study on delamination in various solvents. In the case of montmorillonite clays in aqueous dispersions, rhodamine dyes are more commonly used.[155] In the present work, a degree of labeling corresponding to < 1.0 mol % of the CEC was attempted, in order to minimize changes to the chemistry of the clay surface.

**2.2.1.3.1 Fluorescent labeling of clay with rhodamine 6G (R6G)**

The first fluorescent probe tested was rhodamine 6G (R6G), a xanthene-based molecule containing a tertiary ammonium cation available for exchange with the sodium ions of Cloisite® $Na^+$ (Fig. 2.11.(a)). Experimentally, the concentration of R6G added to a 1.0 wt % Cloisite® $Na^+$ solution was 1.0 mol % of the CEC of the pristine clay. Identification of the degree of fluorophore adsorption onto the clay surface was monitored by the shift of UV-vis absorbance and fluorescence emission peaks. As the R6G molecules are adsorbed onto the clay surface, their local environment becomes more hydrophobic[156] and leads to a red-shift of both absorbance and emission maxima.[157] Upon binding to clay, the R6G peak maxima have been reported to shift from ~ 525 nm to ~

545 nm and from ~ 550 nm to ~ 569 nm, for absorbance and emission peaks, respectively. [158] The presence of any free dye remaining in solution would give rise to shoulders at lower wavelengths that correspond to the unbound chromophore.

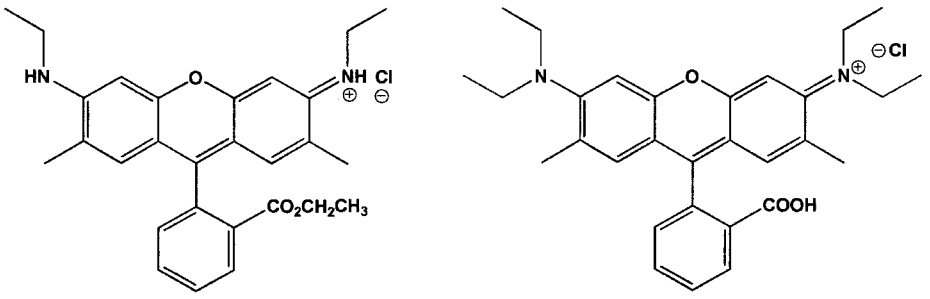


**(a)** **(b)**

**Fig. 2.11.** The chemical structures of the fluorescent labels **(a)** rhodamine 6G (R6G) and **(b)** rhodamine B (RhB)

Experimentally, the absorbance and emission spectra displayed substantial red-shifting of the free R6G peak, with the peak maxima reaching 548 nm and 571 nm respectively (Fig. 2.12.); close to the expected values. The absence of a shoulder at 551 in the fluorescence emission spectrum indicates complete adsorption of R6G onto the clay surface.

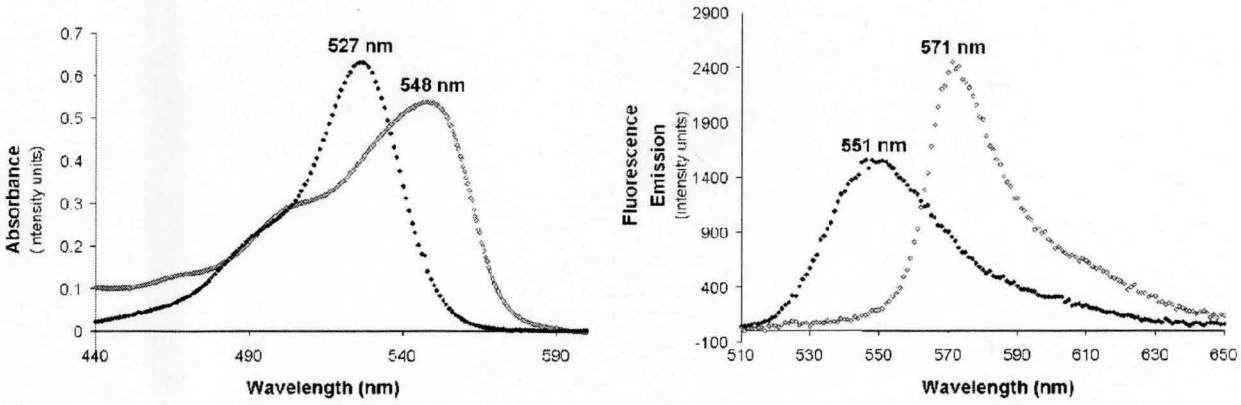


**(a)** **(b)**

**Fig. 2.12.** The **(a)** UV-vis absorbance and **(b)** fluorimeter fluorescence emission spectra of free R6G (♦) and R6G-labeled Cloisite® $Na^+$ (◊)

It must be noted that the absorbance spectra reveal a small shoulder at shorter wavelengths for the free and adsorbed dye, at ~ 490 nm and ~ 500 nm respectively. This blue shift is referred to as the metachromatic effect, attributed to the interaction between the electron π-system of the dye and the electron lone pair of oxygen atoms at the clay surface.[159] In rhodamine dyes, however, the *o*-carboxyphenyl group that lies perpendicular to the xanthene plane sterically hinders this electronic interaction. Therefore, the blue-shifting of absorbance peaks due to metachromasy is attributed to dye aggregation, and representative of rhodamine dimerization.[160,161]

Additional TEM imaging of the labeled clay dispersion verified that addition of R6G at 1 mol % the CEC of Cloisite® $Na^+$ did not have a significant effect on the extent of delamination of clay in water. Therefore, the incorporation of the labeled clay from the aqueous phase during polyurea microcapsule formation seemed promising, and was subsequently tested. It was found that the UV-vis and fluorimeter spectra of the aqueous

phase containing R6G-labeled clay, PVA and DETA tested prior to polymerization revealed the presence of unbound rhodamine (Fig. 2.13.).

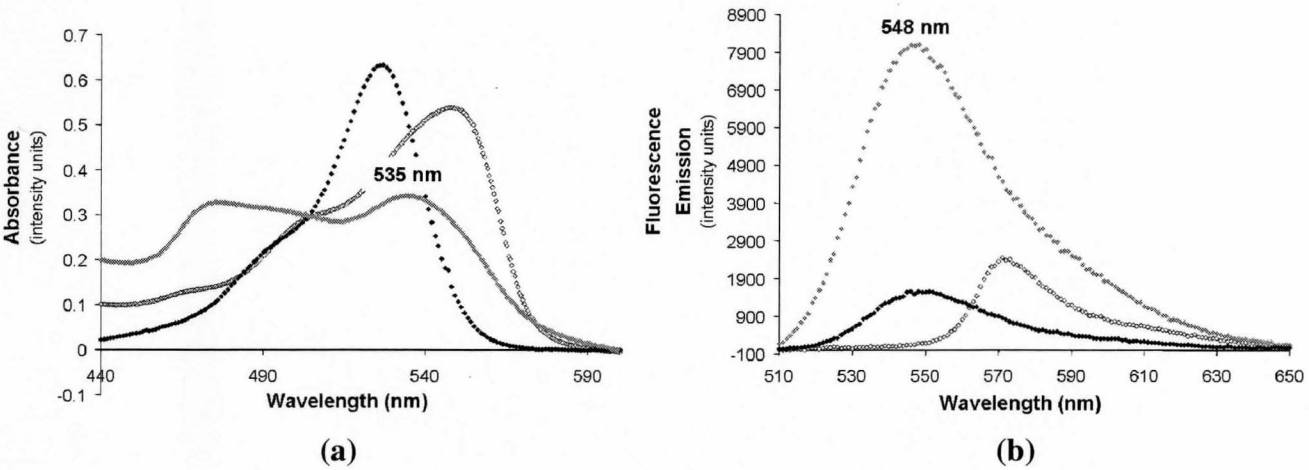


**Fig. 2.13.** The **(a)** UV-vis absorbance and **(b)** fluorimeter fluorescence emission spectra of dissociated R6G in the aqueous phase (♦), free R6G (♦) and R6G-labeled Cloisite® $Na^+$ (◊)

It was hypothetized that the amine, DETA, might cause either deprotonation and extraction, or direct displacement, of RG6. Therefore an alternate fluorescent label containing a quaternary ammonium cation, rhodamine B, was tested for binding to clay under present conditions.

**2.2.1.3.2 Fluorescent labeling of clay with rhodamine B (RhB)**

Rhodamine B (RhB) is a xanthene-based fluorophore with a quaternary ammonium group (Fig. 2.11.(b)), which would prevent neutralization and dissociation of uncharged RhB from the clay surface. Aloisi et al.[162] reported the absorbance and emission maxima of free rhodamine B at 550 nm and 578 nm respectively. Dimerization also occurs with RhB, leading to a small shoulder at ~ 513 nm. Adsorption of rhodamine

B at 1 mol % the CEC of Cloisite® $Na^+$ gave similar red shifts as observed for rhodamine 6G, indicating quantitative binding to clay (Fig. 2.14.).

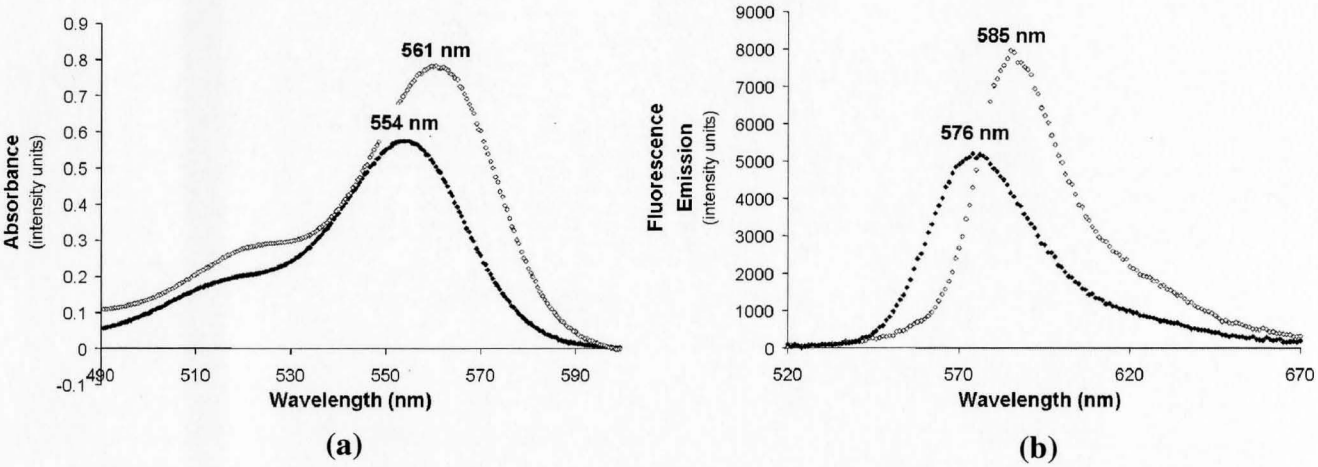


**Fig. 2.14.** The **(a)** UV-vis absorbance and **(b)** fluorimeter fluorescence emission spectra of free RhB (♦) and RhB-labeled Cloisite® $Na^+$ (◊)

However, dispersion of the RhB-labeled clay into the aqueous phase prior to polymerization resulted again in complete dissociation of the label, as seen by the blue-shifting back to original wavelength values (Fig. 2.15.).

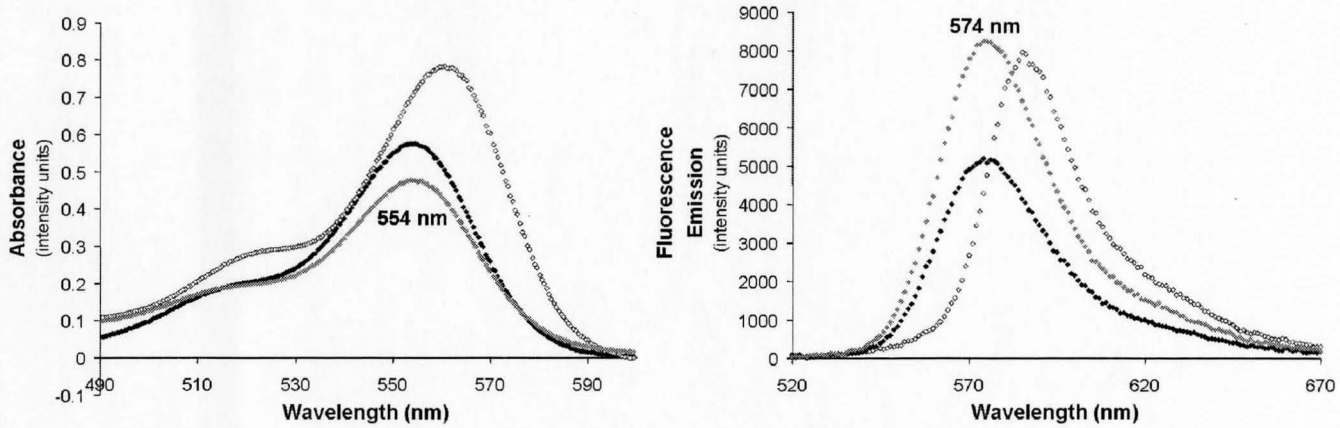


**Fig. 2.15.** The **(a)** UV-vis absorbance and **(b)** fluorimeter fluorescence emission spectra of dissociated RhB in the aqueous phase (♦), free RhB (♦) and RhB-labeled Cloisite® $Na^+$ (◊)

This evidence suggested that a second factor was responsible for the displacement of RhB from the clay surface. Therefore, a sample of the aqueous RhB labeled clay was combined with a 1.0 wt % solution of PVA, in the absence of DETA. UV-Vis and fluorescence measurements showed complete dissociation of rhodamine from clay. Literature search revealed that organo-ammonium cations electrostatically bound to clay platelets have been known to be replaced by hydrogen bonding molecules such as PVA.[163] Subsequently, the potential for permanent intercalation of RhB into the clay galleries with extended mixing time[164] was also explored. However, even with mixing of RhB and Cloisite® $Na^+$ over several weeks, PVA addition immediately displaced rhodamine B from the clay, confirming that permanent binding had not occurred.

Therefore, both the basic conditions imparted by DETA and the presence of PVA in the aqueous solution interfere with the fluorescent labeling of natural montmorillonite clay. Given the importance of both species in the present process of interfacial polymerization, the fluorescent labeling of montmorillonite clay was not pursued any further.

### 2.2.2 Incorporation of organically-modified clay from the dispersed organic phase (Fig. 2.1. (b))

Incorporation of clay into the organic phase during polymerization was not extensively explored due to the potential difficulties involved with the characterization and identification of clay dispersions in organic solvents. The incorporation of organically modified clays during polymerization lacked the simplicity of Cloisite® $Na^+$ delamination in the aqueous phase. Furthermore, the mechanism of clay incorporation by interfacial polycondensation suggested the homogeneous dispersion of delaminated clay sheets throughout the polymer membrane, rather than trapped at the interface. Consequently, only little of the organo-clay would be forming a release controlling interfacial layer, while most would instead be randomly captured within the polyurea wall, possibly enhancing strength but not release control. Therefore, this section only briefly describes preliminary investigations into clay particle delamination in organic solvents, with a single attempt at synthesizing polyurea-clay composite microcapsules.

### 2.2.2.1 Characterization of clay delamination

Currently, several pre-modified montmorillonite clays are commercially available for direct laboratory use, each with different quaternary ammonium cations electrostatically bound to the platelet surface. These clays derive from the cation exchange of $Na^+$ at the surface of pristine montmorillonite clay platelets, which is commonly performed in aqueous solutions. In its natural form, the surface of sodium montmorillonite is hydrophilic, resulting in clay particles that swell and delaminate in aqueous solutions. Upon cation exchange with organo-ammonium ions, the nature of the clay surface becomes partially organophilic and restricts osmotic swelling. Therefore, an ideal dispersing solvent for each type of organically modified clay was necessary prior to polyurea system incorporation. Preliminary identification of effective dispersing solvents was specific to each type of clay and involved the balance between hydrophobic substituents and inherent hydrophilic character. Furthermore, investigations into solvents immiscible with water were ideal candidates for potential application in interfacial polyurea capsule formation. Experimentally, preliminary comparative analyses of the dispersed clay solutions were performed by optical microscopy, with the aqueous Cloisite® $Na^+$ dispersion set as the standard for delamination. The three types of organically-modified clay investigated were Cloisite® 30B, Cloisite® 10A and Cloisite® 15A (Fig. 2.16.).

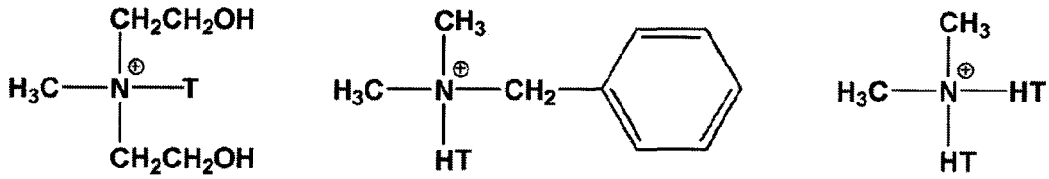


**Cloisite® 30B** **Cloisite® 10A** **Cloisite® 15A**

**Fig. 2.16.** Structures of the interlayer cations of three commercially available organically-modified clays. **T** = tallow (~ 65 % C18; ~ 30 % C16; ~ 5 % C14); **HT** = hydrogenated tallow

#### 2.2.2.1.1 Cloisite® 30B

The ammonium cation possesses two hydroxyethyl groups, one methyl group and a long-chain tallow ($\geq C_{14}$) substituent, and has a surface energy (SE) of 34.5 mN/m.[165] Thus, good dispersions of this amphiphilic clay would require polar organophilic solvents, with high surface energy. Dimethylformamide (DMF; SE = ~ 35.8 mN/m) gave good clay dispersions, but is fully miscible with water and hence unable to form an oil-in-water emulsions. Methyl benzoate (SE = ~ 37.2 mN/m) and ethyl benzoate (SE = ~ 34.8 mN/m) generated good clay dispersions, in addition to forming stable oil-in-water emulsions. Propylene carbonate (SE = ~ 41.9 mN/m) dispersed Cloisite® 30B even better than the other solvents, while still forming a marginally stable emulsion in water.

#### 2.2.2.1.2 Cloisite® 10A

The ammonium cations possess a benzyl group, two methyl groups and a long-chain hydrogenated tallow substituent. The presence of aromatics and long chain hydrocarbons introduces an organophilic character to the clay surface, ideal for dispersion in organic solvents. Consequently, a solvent such as xylene would be expected

to be a good dispersing solvent. Experimentally however, Cloisite® 10A partially settled out of solution upon dispersing in xylene. Given the success with high surface energy solvents, propylene carbonate and a propylene carbonate/xylene (50/50) mixture were investigated. Both solvents displayed great improvements over neat dispersions in xylene, with the latter solution proving to be more effective due to lower solvent polarity.

#### 2.2.2.1.3 Cloisite® 15A

The ammonium cations possess two methyl groups and two long-chain hydrogenated tallow substituents. The organophilic character of the Cloisite® 15A surface renders organic, nonpolar solvents ideal for clay dispersion. Moderate dispersion was realized in cyclohexane, with xylene resulting in a solution with a high extent of clay delamination and exfoliation.

### 2.2.2.2 Characterization of polyurea-clay composite microcapsules

A 1.0 wt % dispersion of Cloisite® 30B in ethyl benzoate was determined to be the best candidate for incorporating clay into the polyurea walls from the organic phase. Cloisite® 30B dispersed very well in ethyl benzoate, and the resulting dispersion gave stable emulsions. As importantly, the two hydroxyethyl groups on this cation would be able to react with isocyanates in the organic phase during preparation and set-up, with the resulting urethane linkages ensuring good bonding between clay and the forming polyurea. Consequently, wall formation in the organic phase may involve the covalent incorporation of clay in the polyurea wall during polymerization (Fig. 2.17.).

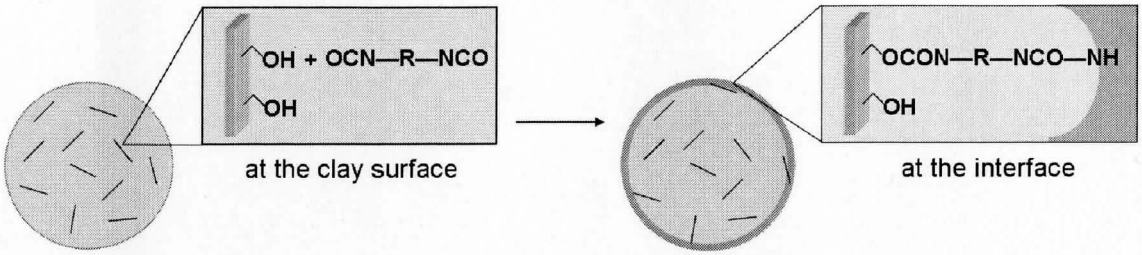


**Fig. 2.17.** Schematic representation of the method of clay incorporation from the organic phase to form a composite polyurea wall

Experimentally, microcapsule formation involved the dispersion of the clay-isocyanate phase into the continuous aqueous phase containing a reactive amine and PVA. The resulting spherical microcapsules were unusually small (diameter 10 – 25 μm), with thin polyurea walls that generally collapsed upon dehydration (Fig. 2.18). It is possible that the amphiphilic nature of the clay platelets causes them to assemble at the oil-water interface. There, the clay may be acting as a strong emulsion stabilizer in conjunction with aqueous PVA, and cause the formation of unusually small microcapsules. Furthermore, the clay layer formed at the emulsion interface might hinder the in-diffusion of the amine, resulting in a much thinner and weaker capsule wall.

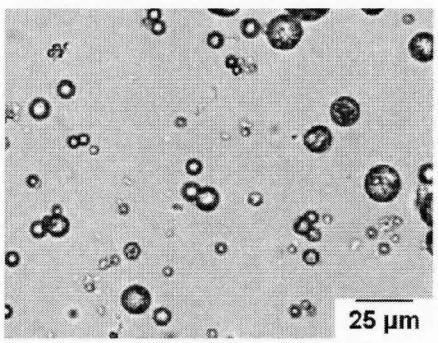


**Fig. 2.18.** Optical microscope image of polyurea-clay composite microcapsules synthesized with Cloisite® 30B in the dispersed organic phase

Analysis of TEM images confirmed the formation of thin capsule walls of 20-40 nm (Fig. 2.19.).

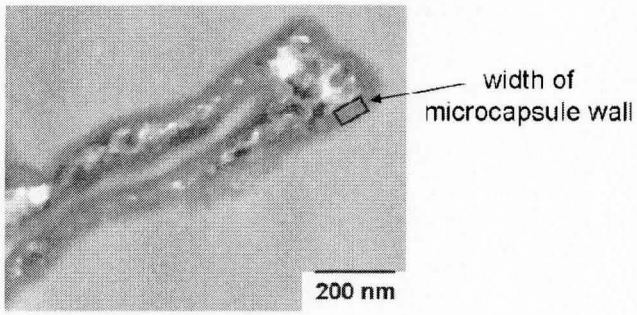


**Fig. 2.19.** Transmission electron microscope image of the cross-section of a polyurea microcapsule formed with Cloisite® 30B dispersed in the organic phase

Preliminary TEM analysis did not reveal the presence of clay on or within the polyurea membrane. It is plausible that this is simply due to the thin polyurea wall, and the limited resolution of the TEM used. Nevertheless, the incorporation of organically-modified clay into the organic phase during interfacial polymerization would have required significant optimization, and was abandoned at this stage.

## 2.3 Conclusions

The incorporation of clay into polyurea microcapsules during interfacial polymerization was attempted by two routes:

1. the dispersion of Cloisite® $Na^+$ in water as the continuous aqueous phase
2. the dispersion of Cloisite® 30B in ethyl benzoate as the dispersed organic phase

Both approaches required a fundamental understanding of clay chemistry, as well as solvent compatibility, extent of delamination and methods of characterization.

Light scattering, XRD, and TEM indicated that ultrasonication of a 1.0 wt % aqueous Cloisite® $Na^+$ dispersion for 10 minutes resulted in a reasonable degree of exfoliation. Although aqueous clay platelets can stabilize emulsions through the Pickering effect, here they were unable by themselves to stabilize the present organic phase to a degree sufficient for formation of spherical polyurea capsules. Furthermore, the clay distribution at the resulting composite microcapsule surface was uneven, and involved clay aggregates. Therefore, an additional stabilizer, poly(vinyl alcohol) (PVA), was added to the aqueous phase to improve the morphology of the capsules. The formation of composite polyurea microcapsules was successful, with homogeneous distribution of clay concentrated as a thin layer at the exterior shell surface. It was demonstrated, however, that the introduction of clay platelets during polymerization interfered with capsule formation, while subsequently complexing with reagents, such as PVA, in the aqueous phase. Furthermore, PVA complexation with clay interfered with fluorescent labeling of clay.

The second route was limited to preliminary experiments designed to test several commercially available organically-modified clays for incorporation into the organic phase during polyurea microcapsule formation. After screening several systems, a dispersion of 1.0 wt % hydroxyl-functional Cloisite® 30B in ethyl benzoate was used as the organic phase. The interfacial polymerization resulted in small, weak polyurea microcapsules. The clay distribution in the thin polymer membrane could not be resolved

via TEM, and therefore the method of composite capsule formation could not be established. This method was not extensively studied due to the need to match the organic phase to the needs of the active ingredient, polyurea and clay, likely leading to significant restrictions in the choice of organic phase materials.

Although both methods showed serious shortcomings, the experiments were useful for exploring new methods of composite formation. In both cases, clay appears to be at least partially located at the capsule surface, indicating that interactions between the clay and the external polyurea shell exist. Consequently, the next chapter focuses on clay incorporation by layer-by-layer electrostatic coating onto polyurea microcapsules post-polymerization. It is anticipated that the post-polymerization method will prevent clay interference in the actual wall formation, and allow modification of release from the resulting composite capsules.

## 3.0 Montmorillonite Clay Incorporation Post-Polymerization

The incorporation of montmorillonite clay sheets into polymer films can result in nanocomposites with improved barrier properties[166] due to the high aspect ratio of the inorganic additive of up to 1000:1. The randomly oriented clay sheets are individually impermeable, and create a tortuous path for the diffusant through the polymer membrane. Consequently, much research effort has focused on reducing permeability by incorporation of delaminated clay into different polymers by a variety of methods.[167, 168] For example, Yano et al.[169] described a 50 % decrease in the permeability with regards to small molecules such as $O_2$, $H_2O$ and He after incorporating 2.0 wt % montmorillonite clay into polyimide films. In addition to the significant reductions in permeability achieved at low clay loadings, incorporation of the inorganic additive provides a means of controlling barrier properties separate from the nature of the matrix itself. This may prove beneficial in controlling the permeability of polyurea microcapsule systems, in which minor changes to capsular and wall parameters can lead to unpredictable and undesirable release rate profiles.

Introduced by Decher in 1991,[170,171] LbL sequential assembly of polyelectrolytes is driven by charge neutralization and resaturation upon adsorption of charged materials on oppositely charged surfaces, resulting in an alternating surface charge.[172] The main incentives for applying LbL to coat spherical polyurea microcapsules with clay lie in the simplicity of deposition and in its independence of the nature, size and topology of the substrate. Furthermore, the opposite charges of native polyurea microcapsule surfaces and the delaminated clay sheets render this system ideal for the application of LbL

electrostatic assembly. Specifically, the external surfaces of polyurea capsules possess an overall positive charge, owing to protonated amines. The capsules are therefore weakly charged, enabling the direct layering of negatively charged clay sheets through electrostatic bonding. This deposition results in charge reversal to enable subsequent adsorption of polycations, setting the stage for another potential cycle of clay binding, in a classic LbL fashion (Fig. 3.1.).

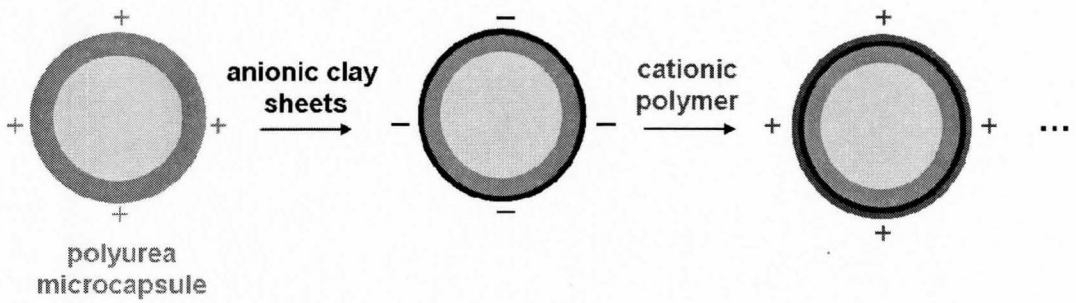


**Fig. 3.1.** Schematic of the layer-by-layer assembly at the microcapsule surface

Research on the application of layer-by-layer deposition to polymer-clay systems is quite extensive,[173,174] with specific investigations concentrating on barrier and transport properties for optical and electrochemical applications.[175,176] Clay incorporation onto the polyurea capsule surface via LbL may prove beneficial at controlling the barrier properties of the membrane, by a method separate from the nature of the wall itself. This method of LbL assembly of montmorillonite clay onto the capsule surface is shown schematically in Fig. 3.2.

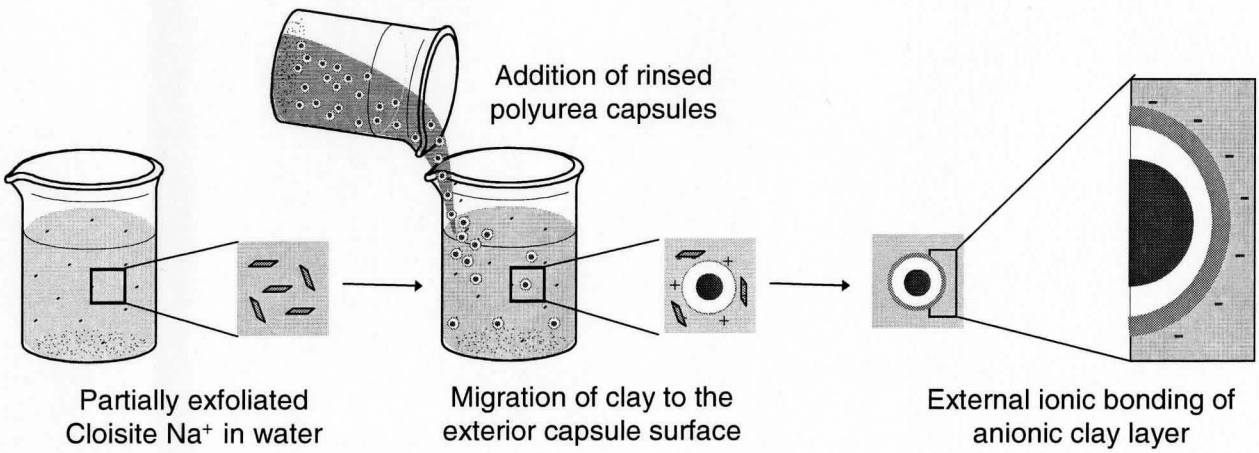


**Fig. 3.2** Post-polymerization deposition of Cloisite® $Na^+$ onto the microcapsule surface

The layer-by-layer assembly of montmorillonite clay sheets and a polycation binder should allow for post-polymerization reduction of release rates, controlled by the clay layer density and numbers of layers, independent of the capsule membrane.

Initial investigations include selecting co-monomers, reaction parameters and encapsulated fills to give strong capsules that enable release-rate testing on a diffusive reservoir system, rather than by rupture release. Subsequently, layer-by-layer assembly of clay sheets onto the polyurea microcapsule surface was studied, with characterization by optical microscopy, TEM and thermogravimetric analysis (TGA). The effect of adsorption time, clay loading, and pH on clay deposition was additionally explored. This involved use of fluorescently labeled polycations, characterized via UV-Vis absorbance. Finally, release from native and clay-coated capsules was studied by temperature-accelerated gravimetric analysis, and by proton nuclear magnetic resonance ($^1$H-NMR).

## 3.1 Experimental

### 3.1.1 Materials

**Cloisite® $Na^+$,** cation exchange capacity (CEC) of 92.6 meq/100 g clay (from supplier), $d_{001}$ layer spacing of 11.7 Å, Southern Clay Products, Texas, USA.

Polymethylene polyphenyl isocyanate (PMPPI, $M_n$ 340), 4,4′-methylenebis(phenyl isocyanate) (MDI, 98 %), poly(vinyl alcohol) (PVA, 80% hydrolyzed, M.W. 9000-10000), diethylenetriamine (DETA, 99 %), and tetraethylene pentamine (TEPA, technical grade), fluorescein isothiocyanate (FITC, 90%), 2,2'–azobis(2-methylpropionamidine) dihydrochloride (AAPH, 97 %), all purchased from Aldrich Chemical Company, Inc.

Cyclohexane, 99.0 %, N,N-dimethylformamide (DMF), 99.8 %, and tetrahydrofuran (THF), 99.0 %, purchased from Caledon Laboratory Chemicals.

Xylene (o-, m-, p-isomers, contains up to 25 % ethyl benzene, 99.9 %), and *n*-butyl acetate (reagent grade), purchased from Fisher Scientific.

Deuterated dimethyl sulfoxide (DMSO-d6, 99.9 %) purchased from Cambridge Isotope Laboratories, Inc.

3-(amino propyl)-methacrylamide (APM, ≥ 98 %) purchased from Polysciences, Inc.

### 3.1.2 Instruments

**Fisher Isotemp Oven**, Fisher Scientific, junior model/forced draft, with a temperature range from 40 ° to 200 °C.

**Sheldon Forced Air Oven**, VWR Scientific Products, Model 1321F, 50/60 Hz, with a temperature range from 40 ° to 200 °C and temperature uniformity of ± 3.5 ° @ 100 °C.

**Rugged Rotator**, GLAS-COL, 50/60 Hz, 2-83 rpm capacity, equipped with a friction drive test tube head.

**pH meter,** Corning 440 electronic pH meter with side-arm, 50/60 Hz, pH range from -1.99 to 16, mV ± 1999 with LCD display.

**Safe Pressure Reactor,** Büchiglasuster polyclave reactor equipped with a Cyclone 075 80W stirrer drive, a propeller type mixer, and a Büchi Miniclave Drive 100 mL glass reactor.

**Ultrasonicator,** Branson Sonifier 150 Digital, 60 Hz, sonication level set to 7 (~ 15 watt rms).

**Optical Microscope,** Olympus BH-2, equipped with a Kodak DC 120 Zoom Digital Camera for taking optical microscope pictures.

**TEM,** Transmission Electron Microscope, JEOL 1230 equipped with a 4 megapixel AMT digital camera. All aqueous clay solutions were deposited onto 100 mesh, formvar (polyvinyl formal) coated copper TEM grids and left to dry prior to analysis. All microcapsules for TEM analysis were swollen in tetrahydrofuran to extract residual solvents and unreacted isocyanates. The extracted capsules were dried under vacuum at 70 °C, embedded in Spurr epoxy resin, and ultramicrotomed to about 100 nm thickness.

**UV-Vis Absorbance,** Varian Cary 50 Bio UV-Visible Spectrophotometer equipped with a Xenon lamp. The data was processed with Varian Cary WinUV software.

**Thermogravimetric Analysis (TGA),** Netzsch STA-409 PC/PG with 'Lnxx' measuring head, DTA/TGA, measured 10-30 mg of sample in air at a scan speed of 5 °C/minute from 25 °C to 700 - 900 °C. Data processed with Proteous analysis software.

**1D Nuclear Magnetic Resonance (NMR),** Bruker AV200, 200 MHz, equipped with a dual $^{1}H/^{13}C$ probe. Data analyzed by XWIN-NMR 3.5 and plotted with XWIN-PLOT 3.5.

### 3.1.3 Procedures

#### 3.1.3.1 Preparation of Cloisite® $Na^{+}$ dispersions

Commercial sodium montmorillonite clay (Cloisite® $Na^{+}$) was dried in a vacuum oven at 70 °C for a minimum of 24 hours to remove excess moisture. A 20 mL aqueous dispersion of 1.0 weight % (wt %) dried Cloisite® $Na^{+}$ was prepared by ultrasonicating the dispersion for 10 minutes in a 50 mL polypropylene conical tube. The solution warmed to 70 °C during sonication, and was left to cool to room temperature prior to use.

#### 3.1.3.2 Preparation of polyurea microcapsules by interfacial polycondensation

The multifunctional isocyanate (MDI or PMPPI, 1.0 g) was added to xylene to make up 10 mL of organic phase. The aqueous phase consisted of 1.0 wt % PVA dissolved in distilled water. The aqueous phase (30 mL) was placed into a 100 mL reaction vessel fitted with 3-bladed overhead stirrer set to 800 rpm. The organic phase (10 mL) was added to the reaction vessel through an inlet at the top of the reactor, and dispersed for 15 minutes under stirring at room temperature. Finally, the difunctional amine (DETA, 1.5 g), dissolved in another 5 mL of aqueous phase, was added to the reactor to start the isocyanate – amine polycondensation at the interfaces. The reaction vessel was submerged into a water bath heated to 70 °C, and left to react overnight under stirring at 600 rpm. The resulting polyurea microcapsules were washed three times with distilled water in a separatory funnel, and stored as an aqueous slurry of capsules.

### 3.1.3.3 Coating of microcapsules with clay

A representative dispersion of polyurea capsules (~ 180 mg in 5 mL) was introduced into 20 mL of a partially exfoliated 1 wt % aqueous Cloisite® $Na^+$ clay solution. The solution was placed on the rugged rotator and rotated for 15 minutes at an average speed of rotation of ~ 28 rpm. The clay-coated capsules were washed three times with distilled water to remove residual unbound clay.

### 3.1.3.4 Gravimetric analysis

Aluminum weighing pans of two inches diameter were etched with 10 wt % aqueous sodium carbonate at room temperature for 1 hour to ensure proper wetting by aqueous samples. The pans were rinsed with distilled water, and loaded with a predetermined amount (~ 180 mg of filled capsules) of the capsule slurry. The slurry in the aluminum weighing dishes was dried in air until constant weight and to ensure the bulk of the water had evaporated, leaving behind a near mono-layer of filled capsules. The pans were then placed in the convection oven at 80 °C, and weighed twice daily on an analytical balance until fill release was complete.

Small, circular pieces of etched aluminum pan were placed, one each, in 10 5-mL glass vials. One drop of capsule slurry was placed onto each piece of aluminum, dried as described above, and placed inside its uncapped glass vial in the convection oven alongside the regular aluminum pans. The vials were removed throughout the gravimetric analysis, and 1 mL of deuterated dimethylsulfoxide (DMSO-d6) was added to allow for 4 days of extraction of internal contents. The DMSO solution was then filtered through a

small column of glass wool in a glass pipette to remove microcapsule shells, and analyzed by $^{1}$H-NMR.

### 3.1.3.5 Synthesis of poly ([3-(amino propyl)]-methacrylamide), PAPM

The PAPM sample was provided by Jafar Mazumder.[177] As the synthesis is described in a manuscript to be submitted, the procedure is repeated here. APM (5.24 g, 29.3 mmol) and 2,2'–azobis(2-methylpropionamidine) dihydrochloride (AAPH; 0.159 g, 0.59 mmol, 2 mol% relative to monomer) were dissolved in 50 mL deionized water in a 60 mL high-density polyethylene bottle. The solution was bubbled with nitrogen for several minutes before the bottle was sealed and heated in an UVP HB-1000 Hybridizer at 60 °C for 24 h with rotation at 15 rpm to provide mixing. PAPM was purified by dialysis using cellulose tubing (12 kDa MW cut-off, Spectrum Laboratories, USA) against deionized water and then isolated by freeze-drying. Yield: 4.29 g (82 %).

The weight-average molecular weight was determined to be 320 000 ± 60 000 g/mol by standard viscometry measurements with an Ubelohde viscometer.[178]

### 3.1.3.6 Labeling of PAPM with fluorescein isothiocyanate, FITC (PAPM-FITC)

PAPM (0.5 g; 2.8 mmol) was dissolved in 50 mL deionized water in a 250 mL glass beaker, and the pH was adjusted to ~ 8.0 by the addition of 0.1 M NaOH. Fluorescein isothiocyanate (FITC, 0.010 g, 0.026 mmol) was dissolved in 1 mL DMF and added to the polymer solution under constant stirring. The mixture was stirred for 1 hour at room temperature, followed by the adjustment of the pH back down to 5.6 by the addition of 0.1 M HCl. The FITC-labelled polymer was purified by dialysis in cellulose tubing (12 kDa MW cut-off, Spectrum Laboratories, USA) against deionized water,

followed by freeze-drying. Final label content was determined by UV/Vis spectroscopy to be 0.06 mol % of the total monomer units.

#### 3.1.3.7 Coating clay-coated microcapsules with PAPM-FITC

A dispersion of polyurea capsules (0.5 mL, ~ 90 mg capsules, surface area 90 $cm^2$) was introduced into 5 mL of a 0.1 mg/mL aqueous solution of PAPM/FITC. The solution was placed on the rugged rotator for 15 minutes at an average speed of rotation of ~ 28 rpm. The (PAPM-FITC)-coated capsules were washed three times with distilled water to remove residual unbound polymer.

## 3.2 Results and Discussion

### 3.2.1 Selection of the appropriate model polyurea capsule system

The role of the polyurea microcapsule wall in controlled release pesticide delivery systems is to isolate and protect the fill during storage, while enabling its release in a controlled fashion upon application.[179] The mechanism of release depends on the design of the microcapsule wall, and can include: membrane erosion, retrograde chemical reactions, and diffusion through a rate-controlling membrane.[180] The polyurea microcapsules described here are designed to exhibit diffusive release from a reservoir. Strong capsule walls are important for subsequent layer-by-layer coatings, since the shell must withstand the stresses of clay and polymer loadings, especially during drying. Empirical optimization of wall strength and permeability is essential to maintain controlled diffusive release of composite capsules, and to prevent catastrophic release by capsule rupture. Therefore, the capsule wall strength and permeability were varied in

search of a polyurea microcapsule system exhibiting diffusive release of internal materials in a reasonable amount of time.

### 3.2.1.1 Microcapsule strength

The tuning of microcapsule strength by varying capsular and wall parameters requires careful consideration of such parameters as: crosslink density, polymer crystallinity, microcapsule size, wall thickness, and morphology. These parameters are often linked, as demonstrated by Degennaro et al.[181] in his description of microcapsules with increased crosslink density. While the highly crosslinked capsules demonstrated improved mechanical strength, they also displayed an increase in release rates due to enhanced membrane porosity. In the present work, the mechanical strength of model polyurea microcapsules was optimized to produce a reference capsule. This standard capsule was subsequently modified with clay to explore adjusting the permeability of the polyurea wall.

Previous research suggested 4,4′-methylenebis(phenyl isocyanate) (MDI), as the ideal isocyanate to react with diethylene triamine (DETA) to form strong, spherical polyurea microcapsules. In contrast to commercial PMPPI, the commercial MDI is a nearly pure solid material that dissolves in organic solvents to form polyurea that does not auto-fluoresce. This allows for the identification of fluorescently-labeled polyelectrolytes at the capsule surface by fluorescence microscopy. However, while MDI/DETA capsules were found to be spherical, they had very thin shells of such low strength that the majority broke during washing. In hopes of increasing MDI capsule strength by enhancing the crosslink density, DETA was replaced with an amine of higher

functionality, tetraethylene pentamine (TEPA). This, however, did not lead to enhanced capsule strength. As well, a higher isocyanate loading was investigated in hopes of increasing strength by enhancing monomer conversion to form thicker capsule walls. Unfortunately, this proved unsuccessful, as no capsules formed under these conditions.

Although auto-fluorescent, poly[(phenyl isocyanate)-*co*-formaldehyde] (PMPPI)-based polyurea capsules were synthesized next, for their enhanced shell wall strength and morphology retention during cleaning. The advantages to increasing the isocyanate functionality of the co-monomer greatly outweigh any potential problems arising from the auto-fluorescence due to impurities. The resulting PMPPI-capsules displayed strong, spherical, and dense polyurea walls, which were characterized by optical microscopy and TEM (Fig. 3.3.).

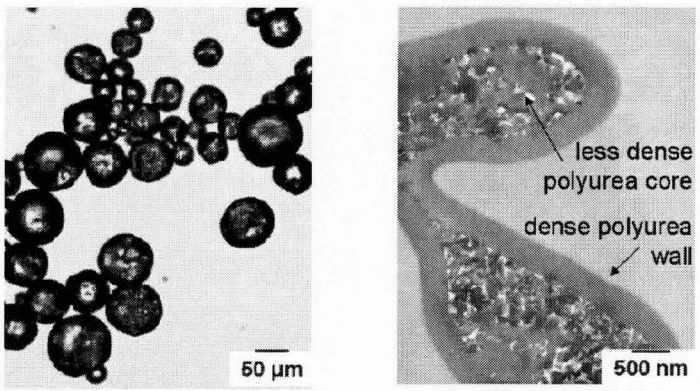


**(a)** **(b)**

**Fig. 3.3. (a)** Optical microscope and **(b)** TEM cross-sectional images of PMPPI-based polyurea microcapsules

The average diameter of the microcapsules was determined to be 52 ± 3 μm, based on the manual measurement of ~ 100 capsule diameters using optical microscopy. Furthermore, the resulting monomer to polymer conversion was 66.0 ± 0.2 %, based on a 1:1 stoichiometric monomer ratio. Therefore, PMPPI was used as the organic phase wall former, with DETA as the reactive amine.

### 3.2.1.2 Microcapsule permeability

The two main methods of fill release from polyurea microcapsules are diffusive loss through the shell wall and release due to shell rupture caused by internal or external stresses. External stresses include physical stress applied to the microcapsules during drying, contact with insects, or by chemical dissolution of the shell, or components of the shell.[182] Rupture release is sometimes measured thermogravimetrically,[183] with rupture occurring due to the steady build up of internal pressure with increasing temperature. In diffusive systems, however, a zero-order release of internal materials is desired. Release of active ingredients from microcapsules has been monitored by gas phase chromatography (GPC) and by pH change.[184] For example, Hiresh et al.[185] measured the decrease in pH upon release of an acidic insecticide, diazinon, from microcapsules into an aqueous disinfectant solution.

As the present research is primarily concerned with diffusive release of volatile fills, gravimetric analysis was used to record release of model fills such a xylene. The rate-limiting step of release in this case is diffusion through the capsule wall, followed by rapid evaporation from the capsule surface. This parallels field conditions, where the foliage or soil acts as a 'sink' for pesticides, even those of low volatility, and hence the

pesticide exists at a very low concentration at the outer surface of the microcapsule.[186] Plotting the normalized mass loss due to fill release versus time elapsed enables the comparison of diffusion rates through capsule walls between different types of capsules and under various external conditions.

#### 3.2.1.2.1 Temperature accelerated release

In the present systems, xylene is used as the model active ingredient. Initial gravimetric release experiments showed very slow release at room temperature (Fig. 3.4.). In fact, measuring release rates of xylene from PMPPI/DETA capsules at room temperature proved to be impractical due to the low permeability of the polymer walls. Accordingly, release at elevated temperatures was explored in order to accelerate diffusive release.[187] The diffusion coefficient of the membrane is related to temperature by the following Arrhenius-type equation:

$$D = D_0 \exp\left(\frac{-E_D}{RT}\right) \qquad (2)$$

where $D$ is Fick's law diffusion coefficient, $E_D$ is the apparent activation energy for diffusion, $R$ is the gas constant and $T$ is the temperature.

Given the good thermal stability of polyurea, it is assumed that moderate increases in the release temperature would change release rates mainly through faster diffusion, and not through fundamental changes in membrane structure. Although large increases in temperature are not typically part of the crop environment, an accelerated release test should still enable the analysis of the barrier properties of clay. Consequently,

gravimetric analysis of the PMPPI-based microcapsules was carried out in a conventional drying oven at 65 °C, and at 75 °C.

The resulting mass loss profiles confirmed the acceleration of release with increasing temperatures (Fig. 3.4.), with the capsules at 75 °C releasing in near linear fashion. In theory, release from mono-dispersed reservoir-type capsules should continue until only the polyurea, stabilizer and unreacted isocyanates remain, together responsible for about 10 % of the total initial capsule weight. In practice, one would expect an earlier leveling-off of the release rate as smaller capsules would empty sooner than larger capsules.

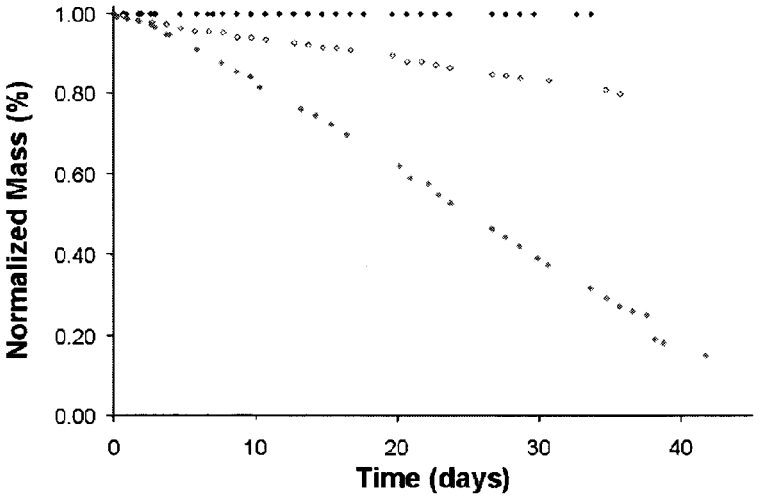


**Fig. 3.4.** The gravimetric release rate profile of PMPPI/DETA polyurea microcapsules at room temperature (♦), 65 °C (◊), and 75 °C (♦)

In order to ensure release occurred by diffusion, rather than through the rupture of individual capsules from the slow build-up of external stresses, a sample of capsules was monitored on a glass slide via optical microscopy over time, while being stored at

elevated temperatures. The capsules appeared to deflate over the course of the release study, and ruptured only when manually probed; confirming internal solvents were still present for release. This verifies that release occurred by diffusive means. For practical reasons, the release rate profile of xylene at 75 °C was still considered too slow for the purpose of this study. Therefore, other means to increase the release rate were explored.

**3.2.1.2.2 Internal co-solvent accelerated release**

The nature of the organic solvent encapsulated in the polyurea shell can directly affect the formation and permeability of the polymer wall, as well as the release rate. Xylene, a poor solvent for polyurea, causes the forming polymer to precipitate during wall formation to form a tight shell. This also limits the further in-diffusion of amines from the aqueous phase, and hence can lead to incomplete isocyanate conversion and thin walls. Therefore, mixtures of good and poor solvents are sometimes used to increase wall permeability during encapsulation.[188] Selection of an appropriate co-solvent is primarily based on the Hildebrand solubility parameter, or more specifically, the 3D Hansen solubility parameters that define it. Overall, these parameters describe the swellability of a polymer in a given solvent based on three terms: dispersive ($\delta_d$), hydrogen bonding ($\delta_h$), and dipolar interactions ($\delta_p$).[189] Given the significant amount of hydrogen bonding present between polyurea chains, a good solvent with a high H-bonding term would swell the polymer by interfering with polymer-polymer interactions. Butyl acetate was chosen as an appropriate co-solvent to be added to the organic core to increase wall permeability, given its high polarity ($\delta_p$ = 3.7 $MPa^{1/2}$) and H-bonding interactions ($\delta_h$ = 6.3 $MPa^{1/2}$) as compared to xylene ($\delta_p$ = 1.0 $MPa^{1/2}$; $\delta_h$ = 2.0 $MPa^{1/2}$).[190] Butyl acetate has a similar

boiling point and density to xylene, but may prove to swell the polyurea shell and thereby accelerate the release of all fill components.

To explore the effects of butyl acetate as a co-solvent, polyurea microcapsules were prepared with various volume ratios of butyl acetate to xylene. Addition of 50 % butyl acetate by volume to the organic phase resulted in the formation of sticky, swollen capsule walls that instantly released their fill upon drying. Capsules formed with only 10 % butyl acetate, however, exhibited moderately accelerated release as anticipated. These capsules were spherical with a number average diameter of 50 ± 2 μm, as measured by optical microscopy (Fig. 3.5. (a)). The isocyanate conversion increased from 66 to 74 % upon substitution of 10 % butyl acetate, attributed to improved in-diffusion of amines during polymerization. TEM showed a typical polyurea microcapsule structure, with similar wall thicknesses and less dense inner polyurea cores, compared to the 100 % xylene capsules (Fig. 3.5. (b)).

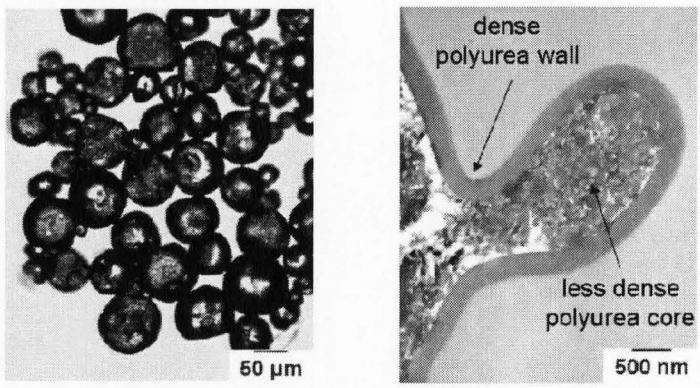


**Fig. 3.5. (a)** Optical microscope and **(b)** TEM cross-sectional images of PMPPI/DETA polyurea microcapsules prepared with a 10:90 butyl acetate:xylene organic phase

Gravimetric analysis at 75 °C showed a 50 % higher release rate compared to the xylene-only capsules, with complete release after 20 days (Fig. 3.6.). Optical microscopy confirmed the absence of ruptured capsules, confirming release by diffusion.

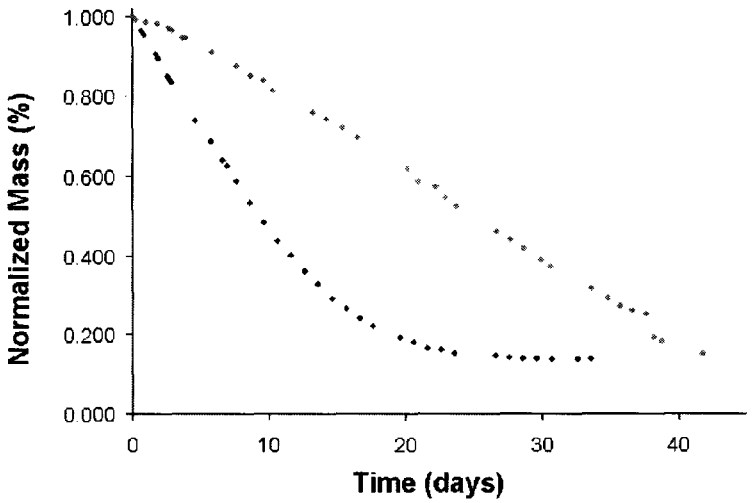


**Fig. 3.6.** Gravimetric release profile at 75 °C of PMPPI/DETA microcapsules prepared with 100 % xylene (♦) and 10:90 butyl acetate:xylene (♦) organic phases

In parallel, capsules containing 15 % and 20 % butyl acetate in the organic phase were prepared to further increase the rate of diffusive release through the polyurea membrane. The resulting release profiles displayed similar initial release rates to the 10 % butyl acetate capsules, followed by a slightly more significant drop after 7.0 days (Fig. 3.7.).

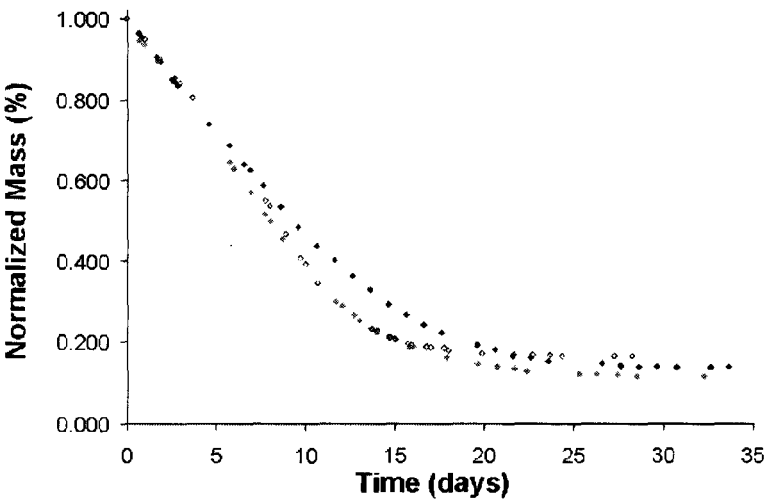


**Fig. 3.7.** Gravimetric release rate profile at 75°C of PMPPI/DETA microcapsules prepared with 10 % (♦), 15 % (◊) and 20 % (♦) butyl acetate in the organic phase

Progressive analysis of these microcapsules via optical microscopy throughout release confirmed the presence of several empty, hollow polyurea shells prior to complete release. This is indicative of the premature diffusion of internal materials through the walls of several of the capsules, possibly due to the formation of weak or thin walls. The uneven permeability among the 15 % and 20 % butyl acetate capsules thus rendered these systems inappropriate for controlled release, and subsequent release rate studies on clay coated capsules were limited to a 10 % butyl acetate fill at 75 °C.

### 3.2.2 Coating microcapsules with montmorillonite clay

The method investigated for polyurea composite capsules synthesis involved the layer-by-layer (LbL) electrostatic binding of clay platelets to the external capsule surface post-polymerization. The external surface of polyurea capsules possesses an overall positive charge due to protonated amine residues from both DETA and hydrolyzed

isocyanate, enabling the attraction of negatively charged clay sheets for ionic bonding to the external surface. Upon dehydration, the clay coating would form a tortuous path for encapsulate diffusion through the microcapsule wall, resulting in decreased rates of release.

### 3.2.2.1 Characterization of composite microcapsules

An 5 mL aliquot of the capsule suspension was added to 20 ml of a 1.0 wt % dispersion of Cloisite® $Na^+$ in water which had been sonicated for 10 minutes. The mixture was placed on the "rugged rotor" and rotated at 28 rpm for 15 minutes. Given that the saturation of a cationic surface with clay has been shown to occur in as little as 5-6 minutes,[191] the 15-minute immersion time is believed to be sufficient.

#### 3.2.2.1.1 Optical microscopy and TEM

The coated, washed microcapsules were found to have retained their spherical shape and their diameter of 50 ± 2 μm, both in the aqueous slurry, and upon drying on an aluminum dish. TEM (Fig. 3.8.) of 100 nm thick sections of clay-coated microcapsules embedded in Spurr epoxy showed a 15 ± 1 nm homogeneous layer of clay at the exterior surface. This confirms the successful LbL deposition of clay sheets on the polyurea microcapsule, at an approximate loading of 0.12 ± 0.03 g clay/g polyurea, as determined from calculated volumes of the polymer shell and the clay layer. This loading was based on average layer thicknesses of 350 and 15 nm respectively and on average densities of polyurea and clay of 1.0 and 2.9 g /cm3 accordingly. Based on the temperature-accelerated gravimetric analysis, it was determined that water in the microcapsule slurry accounted for 75 % of the original sample mass, while the polyurea shell accounted for

13 % of the dehydrated capsule mass. Based on these gravimetric measurements, together with the original experimental loading of clay (1.23 g clay/g polyurea), it was determined that the clay loading efficiency of the aqueous 1.0 wt % Cloisite® $Na^+$ solution was ~ 10 ± 3 %, indicating a surplus of clay sheets in solution.

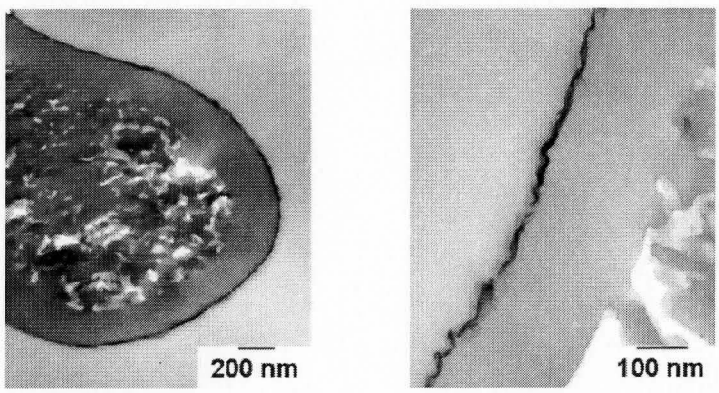


**Fig. 3.8.** TEM cross-sectional images of clay-coated PMPPI/DETA polyurea microcapsules with a 15-minute immersion time

Interestingly, the TEM images display a layer of clay at the capsule surface, rather than a monolayer of single inorganic sheets. The thickness of the clay layer suggested that platelets were stacked on top of each other, but repeated stacking and alignment could not be resolved. This result contradicts standard LbL principles which claim that the adsorption of multiple clay platelets is inhibited by the Coulombic repulsion between anionic sheets.[192] However, the stacking of clay platelets at the substrate surface during LbL deposition is common,[193,194] and indicative of the reorientation of clay sheets on the film surface to give the most stable arrangement. Specifically, stacking results from both van der Waals and dipole-dipole interactions between sheets, where areas of partial

positive charge (metal ions, Al, Si) alternate with areas of partial negative charge (oxygen). The crystallinity of the aluminosilicate sheet surface results in overlapping structures where the platelets orient themselves parallel to each other to maximize the dipole-dipole interaction between regularly alternating spots. Therefore, attractive forces between clay platelets occur at short distances (1-3 nm) to form random stacks, while long-range electrostatic repulsion of negatively charged sheets occurs at greater distances in the classic fashion of LbL.[195] Therefore, the TEM images displayed stacked clay platelets at the polyurea microcapsule surface, with their flexible nature enabling them to follow the topology of the surface.

**3.2.2.1.2 Thermogravimetric analysis (TGA)**

Cloisite® $Na^+$ shows less than 10 % mass loss at temperatures up to 800 °C, attributed to loss of different types of adsorbed water (Fig. 3.9.).[196] Given this high thermal stability, the total clay content in a clay/polymer composite can be determined by thermogravimetric analysis (TGA) from the mass remaining after heating in air above 700 °C.[197] TGA results of pristine Cloisite® $Na^+$, uncoated PMPPI/DETA capsules and clay-coated PMPPI/DETA capsules (MMT-PMPPI/DETA) are shown in Fig. 3.9. The uncoated capsules exhibited an expected mass loss due to residual solvent from 0 °C to ~ 325 °C, followed by the quantitative loss of polyurea from ~ 325 °C to ~ 650 °C. The clay-coated capsules displayed a similar mass loss profile, but with a residual mass of ~ 4 ± 1 % attributed to silicate persisting up to 800 °C. Correcting for the ~ 5 % volatiles present in pristine Cloisite® $Na^+$, as indicated by its TGA curve, the initial clay loading of the capsules can be estimated as 4.2 ± 1 %.

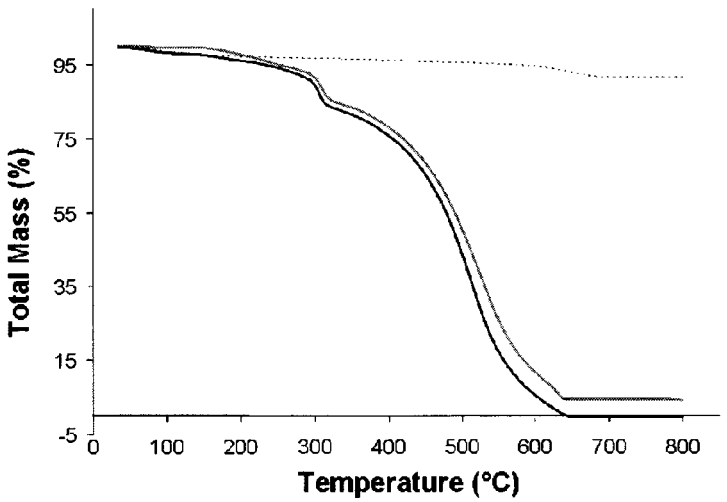


**Fig. 3.9.** Thermogravimetric analysis of pristine Cloisite® $Na^+$ (---), PMPPI/DETA (—) and MMT-PMPPI/DETA polyurea microcapsules (—)

The TGA profile indicated that the composition of the clay-coated microcapsules was ~ 81 ± 1 mass % polyurea, and ~ 4.2 ± 1 mass % clay, from which the loading of clay per gram polyurea was calculated to be ~ 0.05 ± 0.01 g clay. Based on these TGA measurements, together with the original experimental loading of clay (1.23 g clay/g polyurea), it was determined that the clay loading efficiency of the aqueous 1.0 wt % Cloisite® $Na^+$ solution was ~ 4 ± 1 %. Therefore, analysis by TEM and TGA indicate utilization of between 4 ± 1 % and 10 ± 3 % of the available clay, possibly allowing for a reduction of the clay to capsule ratio during coating.

The number average surface area ($SA_n$) and volume ($V_n$) of the microcapsules was determined from the original diameter measurements manually obtained via optical microscopy. The resulting values were used in conjunction with TGA mass ratios, and the aforementioned polyurea and clay densities to determine an average clay loading of

$(6.3 \pm 0.7) \times 10^{-6}$ g clay/cm$^2$. Furthermore, the external neat clay layer thickness, as based on $SA_n$ and the total sample mass, was calculated to be ~ 22 ± 2 nm. These values, along with the described method of analysis, were set as the reference for further comparison of LbL clay deposition onto microcapsules of varying experimental conditions.

### 3.2.2.2 Optimization of clay deposition

Although adsorption is primarily driven by ionic interactions, the amount of clay adsorbed may vary considerably, depending on the deposition conditions.[198] In fact, the extent of clay adsorption can depend on such factors as concentration and agitation of the solutions.[199] Experimentally, tuning of the conditions of clay deposition involved variations in two key parameters: the immersion time and the concentration of clay dispersions.

#### 3.2.2.2.1 Concentration of clay in solution

The loading efficiency of the 1.0 wt % Cloisite® $Na^+$ solution was calculated to be ~ 10 ± 3 % and ~ 4 ± 1 %, based on TEM and TGA measurements respectively. In both cases, it appears that we have an excess of clay in solution. Still, though clay is inexpensive compared to many active ingredients, it is of fundamental interest to study the effect of clay concentration on surface coverage. Therefore, polyurea microcapsules were coated as before, but using 0.5 wt % and 0.1 wt % Cloisite® $Na^+$ dispersions, respectively. The coated microcapsules were investigated via TGA, and the resulting mass loss profiles and accompanying data are shown in Figure 3.10. and Table 3.1., respectively.

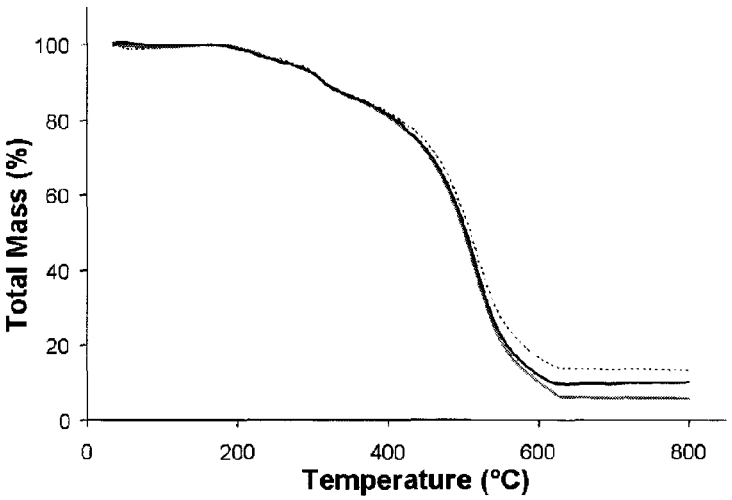


**Fig. 3.10.** Thermogravimetric analysis of MMT-PMPPI/DETA polyurea microcapsules immersed in a 1.0 wt % (—), 0.5 wt % (—), and 0.1 wt % (---) aqueous Cloisite® $Na^+$ solution

| Weight % Clay | TGA Residual Mass (%) | Clay Loading (g clay/cm$^2$ filled capsules) | Layer Thickness (nm) |
|---|---|---|---|
| 1.0 | 10 ± 1 | (1.6 ± 0.2) x $10^{-5}$ | 55 ± 7 |
| 0.5 | 5 ± 1 | (0.8 ± 0.2) x $10^{-5}$ | 29 ± 7 |
| 0.1 | 12 ± 1 | (2.1 ± 0.3) x $10^{-5}$ | 72 ± 10 |

**Table 3.1.** Comparison of approximate clay loadings and clay layer thicknesses based on the TGA mass loss profiles at various clay concentrations

It appeared as though reducing the concentration of clay to 0.5 wt % resulted in the adsorption of half the amount of clay (Table 3.1.), while further decreasing the clay concentration to 0.1 wt % led to the highest loading of clay at the capsule surface. A high clay loading at a low solution concentration seemed unusual, and therefore TEM imaging was performed to qualitatively determine the distribution of clay at the capsule surface.

Firstly, the TEM images of the 0.5 wt % clay solution displayed a thin, homogenous layer of clay at the capsule surface, similar to the reference 1.0 wt % loading solution (Fig. 3.11.).

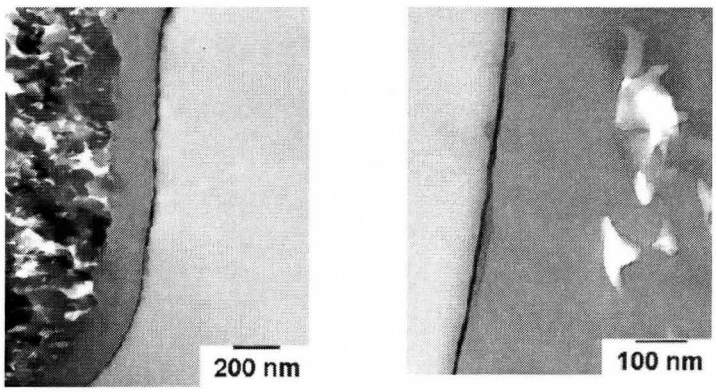


**Fig. 3.11.** TEM cross-sectional images of MMT-PMPPI/DETA polyurea microcapsules immersed in a 0.5 wt % clay solution

Therefore, based on characterization via TGA and TEM, we were able to determine that halving the clay concentration resulted in half the amount of clay adsorbing homogeneously to the microcapsule surface. Given that we are concerned with maximizing the thickness of the external clay coating, the 1.0 wt % solution was the preferred concentration for further analysis. A further increase in concentration to 2.0 wt % was not attempted, however, due to the significant increase in viscosity of the aqueous clay solution above a concentration of 1.0 wt %.

Secondly, the TEM images of the 0.1 wt % clay solution displayed a heterogeneous distribution of clay aggregates loosely bound to the microcapsule surface, alongside patches of clay flocculation (Fig. 3.12.).

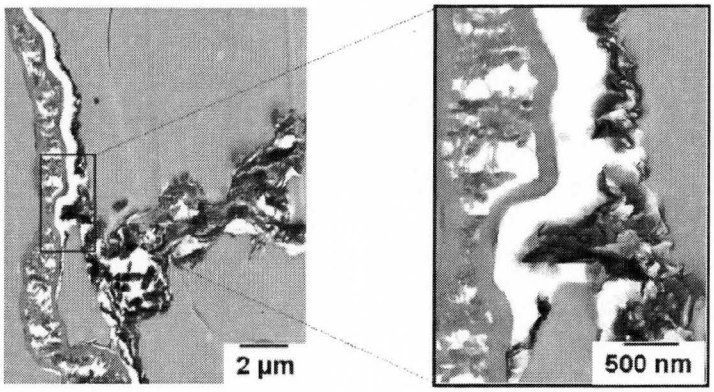


**Fig. 3.12.** TEM cross-sectional images of MMT-PMPPI/DETA polyurea microcapsules immersed in a 0.1 wt % clay solution

The TEM images showed a large amount of irregular clay aggregates at the capsule surface, indicating that the 0.1 wt % clay dispersion, as used, was unsuitable for forming release controlling clay barrier layers.

**3.2.2.2.1.1 Effect of pH**

The significant flocculation observed by TEM for the 0.1 wt % clay solution (Fig. 3.12.) indicated that a secondary factor was responsible for the inhomogeneous coating of capsules. The cross-sectional images suggest the most common type of clay flocculation, referred to as the house-of-cards model, where clay minerals are held together by edge(+)/face(-) contacts.[200] In this type of network, the platelet edges possess a partial positive charge and form cohesive junction points with the anionic surface of other platelets at several locations of low or high specific charge densities.[201] The result is a three-dimensional volume of hydrated clay aggregates, dominated by the chemistry at the broken bond surface. Given that the broken edges consist of alumina and silica, the occurrence of positive edges to form a card-house structure is certainly pH-dependent. In

fact, the changes in solution viscosity upon flocculation of a 2.2 wt % aqueous montmorillonite clay dispersion with varying pH was determined by Permien et al (Fig. 3.13).[202]

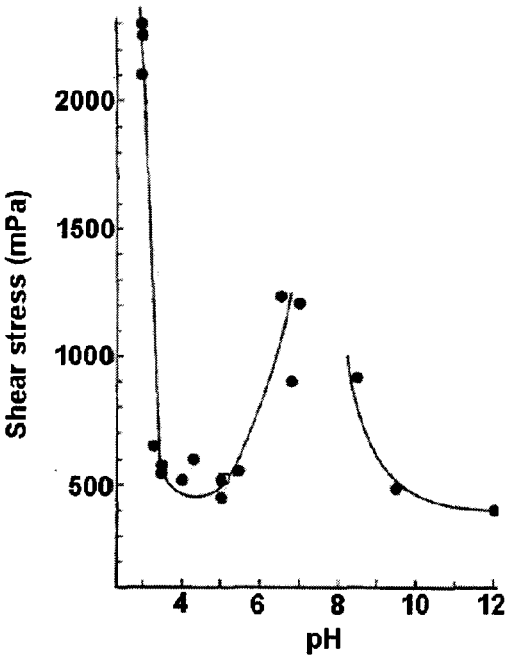


**Fig. 3.13.** Dependence of the shear stress on the dispersion pH for a sodium montmorillonite dispersion[203]

The silica groups at the broken edges ionize above a pH of 2.0, while the ionization of aluminol begins below a pH of 9.2.[204] Consequently, as the pH decreases below 9.2, the number of negative charges at the edges is reduced and an increasing number of edge(+)/face(-) associations occur at sites of positive charge.[205] The point of zero charge (PZT) for the edge surface is assumed to lie between a pH of 7.3 and 7.7,[206, 207] below which an initial sharp minimum is found. This minimum, around pH ~ 4, corresponds to the complete breakdown of initial edge/face contacts in a highly acidic

environment due to positive charges originating from silica. Therefore, the occurrence of card-house aggregates in a less concentrated aqueous clay dispersion may be due to the lower pH.

The basal surface of clay is dominated by siloxane groups, resulting in the progressive increase in basicity of aqueous dispersions with increased clay loadings. Consequently, unless buffered, less concentrated dispersions are expected to possess a lower solution pH, resulting in the potential for card-house flocculation. Therefore, the pH of the previously described solutions of varying clay concentrations was measured prior to coating, as well as upon microcapsule addition (Table 3.2.). Given the addition of a neutral microcapsule slurry, it is expected that the pH would slightly decrease for the sample solution.

| Weight % Clay | pH of Clay Solution | pH of Sample Solution |
|---|---|---|
| 1.0 | 9.7 ± 0.1 | 9.6 ± 0.1 |
| 0.5 | 9.4 ± 0.1 | 9.4 ± 0.1 |
| **0.1** | **8.3 ± 0.1** | **8.0 ± 0.1** |

**Table 3.2.** Measured pH values of the aqueous clay solutions and the PMPPI/DETA polyurea microcapsule sample solutions at various clay concentrations

The resulting pH values indicated that the 0.1 wt % solution was below the point of ionization of alumina (9.2), and approaching the PZT of the clay platelet surface. Consequently, card-house aggregation had occurred due to the low pH value of the sample solution, confirming the flocculation initially observed under TEM (Fig. 3.12.). Upon increasing the pH of the 0.1 wt % Cloisite® $Na^+$ sample solution to ~ 9.8 ± 0.1 through the addition of 0.1 M NaOH prior to capsule coating, the resulting cross-

sectional TEM images displayed a more homogeneous distribution of clay at the capsule surface (Fig. 3.14.).

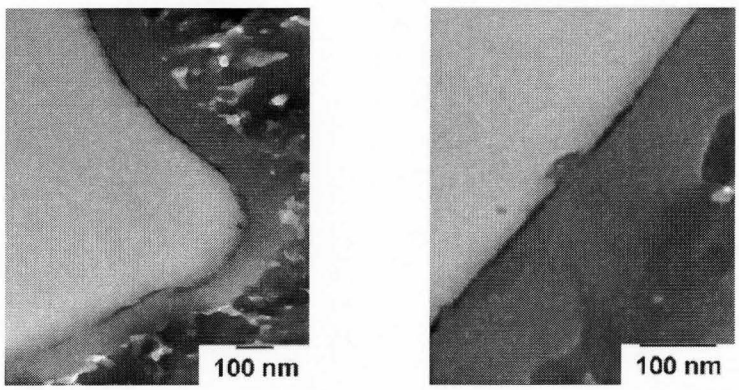


**Fig. 3.14.** TEM cross-sectional images of MMT-PMPPI/DETA polyurea microcapsules immersed in a 0.1 wt % clay solution at a pH of 9.8

However, given the low loading of clay in solution, the external clay coating was unable to completely coat the surfaces of the microcapsules and only patches of the thin clay coating were observed. TGA resulted in a clay loading of 5 %, about 70 % lower than the original 0.1 wt % clay solution, indicating a significant reduction in clay aggregation. Although TGA and TEM imaging indicated the absence of clay aggregates at the microcapsule surface upon coating with a 0.1 wt % Cloisite® $Na^+$ solution at increased pH, the uneven distribution of clay rendered this system inapplicable for further barrier property analysis.

**3.2.2.2.2 Immersion time**

The immersion time of polyurea microcapsules in aqueous clay solutions is crucial,[208] particularly in systems where the clay particles are highly delaminated. With extended immersion times, larger charged species have more time to approach the

substrate for adsorption. Given that we are aiming to maximize clay adsorption to the polyurea surface, the 15-minute immersion time was extended to 1 hour and 48 hours for subsequent analysis via TEM and TGA. The resulting TGA mass loss profiles and accompanying data analysis are shown in Figure 3.15. and Table 3.3.

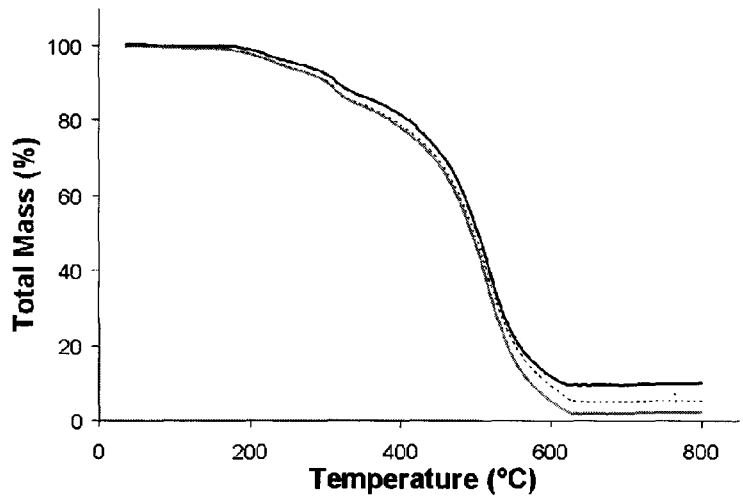


**Fig. 3.15.** Thermogravimetric analysis of MMT-PMPPI/DETA polyurea microcapsules immersed in a 1.0 wt % clay solution for 15 minutes (—), 1 hour (—), and 48 hours (---)

| Immersion Time (mins) | TGA Residual Mass (%) | Clay Loading (g clay/cm$^2$ filled capsules) | Layer Thickness (nm) |
|---|---|---|---|
| 15 | 10 ± 1 | (1.6 ± 0.2) x $10^{-5}$ | 55 ± 7 |
| 60 | 2 ± 1 | (0.3 ± 0.2) x $10^{-5}$ | 10 ± 7 |
| 2880 | 5 ± 1 | (0.8 ± 0.2) x $10^{-5}$ | 27 ± 7 |

**Table 3.3.** Comparison of approximate clay loadings and clay layer thicknesses based on the TGA mass loss profiles at various immersion times

The TGA mass loss profiles suggest that maximum clay loading onto the microcapsule surface occurs after 15 minutes of immersion in the aqueous clay solution. Accordingly,

the TEM images of the three microcapsule samples were compared, and all three displayed a similar homogeneous, even distribution of clay at the external capsule surface (Fig. 3.16.).

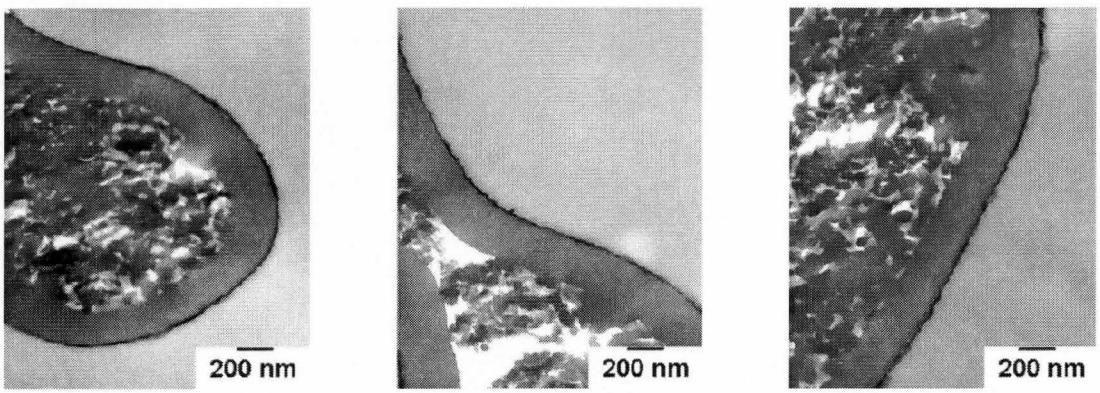


**Fig. 3.16.** TEM images of MMT-PMPPI/DETA polyurea microcapsules coated with 1.0 wt % Cloisite® $Na^+$ at **(a)** 15 minute, **(b)** 1 hour, and **(c)** 48 hour immersion times

The TGA and TEM results indicate that immersion of the microcapsules into the clay solution for 15 minutes sufficed to maximize clay adsorption. Given more time, the clay platelets appear to dissociate from the capsule wall, potentially owing to the increased amount of applied agitation. Therefore, the ideal conditions for LbL microcapsule coating with clay resulted from 15 minutes immersion in a 1.0 wt % aqueous Cloisite® $Na^+$ solution.

### 3.2.3 Gravimetric analysis of clay-coated polyurea microcapsules

The primary objective in investigating polyurea microcapsule release was to determine methods to reduce and control diffusion of internal materials through the shell wall. It is expected that the addition of an external layer of montmorillonite clay onto the

polyurea microcapsule will reduce the permeability of the polyurea membrane, by a means separate from the nature of the capsule itself. Following the optimization of a model PMPPI/DETA polyurea microcapsule containing 90:10 xylene:butyl acetate, the development of a temperature-accelerated release test, and the optimization of a LbL clay-coating procedure, a gravimetric study into barrier properties of the added clay layer was carried out at 75 °C.

Preliminary analyses involved the use of a standard gravity convection oven for the accelerated release of internal materials. The mass loss of one sample each of uncoated and clay-coated polyurea microcapsules was measured over a period of several weeks, and the resulting release profile is shown in Fig. 3.17.

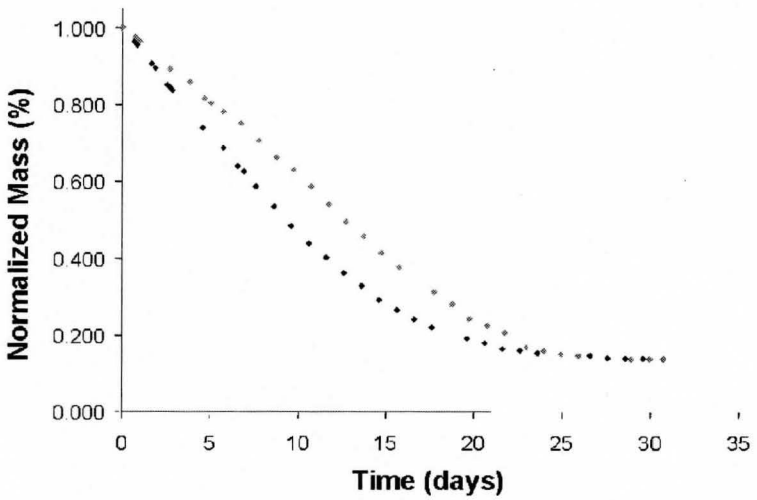


**Fig. 3.17.** The gravimetric release rate profile at 75 °C of PMPPI/DETA (♦) and MMT-PMPPI/DETA (♦) polyurea microcapsules

The uncoated polyurea microcapsules release 50 % of their fill within about 9 days, while the clay-coated capsules release 50 % within 12 days, indicating a circa 25 % decrease in

the release rate due to coating the microcapsules with one layer of montmorillonite clay. Next, the experiment was repeated using triplicate samples and an oven with fan-forced air circulation to ensure temperature homogeneity (Fig. 3.18.).

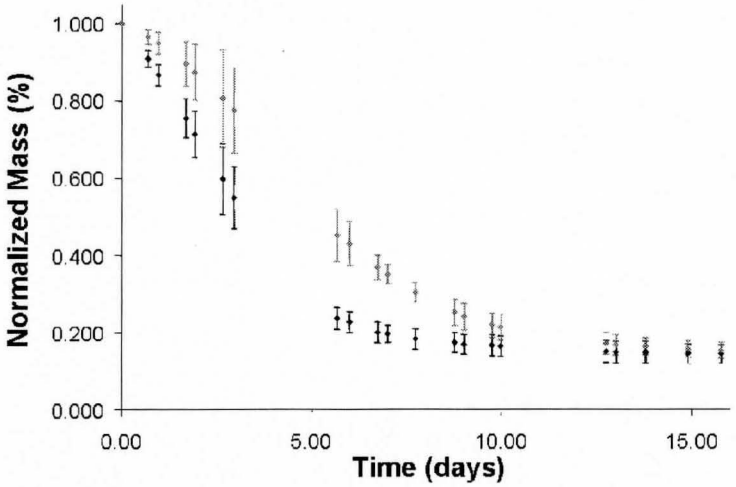


**Fig. 3.18.** The gravimetric release rate profile at ~ 80 °C in a convection oven of PMPPI/DETA (♦) and MMT-PMPPI/DETA (♦) polyurea microcapsules

However, the temperature setting in this oven proved difficult to control, and therefore an average experimental temperature of 75 ± 7 °C was maintained, resulting in further accelerated release. While the uncoated polyurea microcapsules realized a 50 % fill loss in ~ 3.5 days, the same percentage fill loss in the clay-coated capsules occurred at t ~ 5.5 days. This suggests ~ 40 % decrease in the overall average rate of release in composite microcapsules, owing to the external clay layer barrier. Therefore, we were able to significantly reduce the permeability of a model polyurea microcapsule membrane by the LbL addition of montmorillonite clay onto the external capsule surface.

### 3.2.3.1 Mechanism of encapsulate release

It is well known that the release of internal materials from a reservoir through the polyurea membrane occurs via Fickian diffusion, or zero-order release.[209] Consequently, the gravimetric release rate profile of the remaining sample mass (Fig. 3.18.) should display a linear relationship between the average mass remaining and time, assuming the capsules maintain their surface area during release. The measured release profiles were not entirely linear, and appeared to exhibit three regions of release. The three regions, as displayed in Figure 3.19., have been attributed to the following systematic effects:

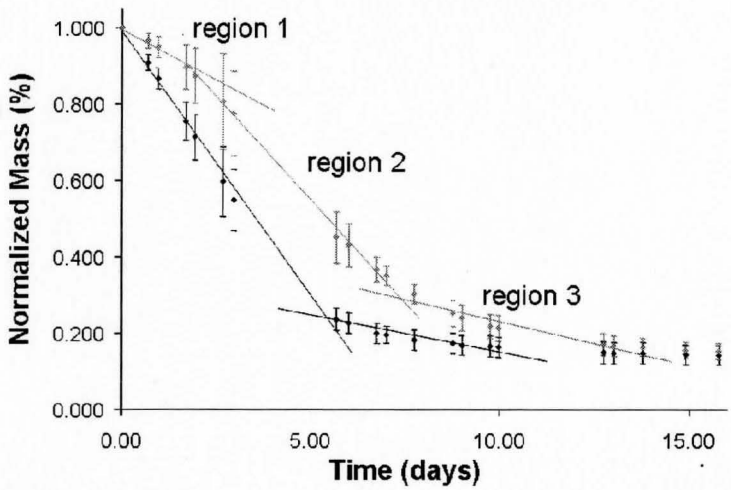


**Fig. 3.19.** The regions of release in the gravimetric release rate profile at ~ 80 °C of PMPPI/DETA (♦) and MMT-PMPPI/DETA (♦) polyurea microcapsules

**Region 1:** Appears only in the clay-coated system as an area of significantly hindered release. This is due to the barrier formed by the external clay coating, which may develop defects, or cracks in the wall, upon the slow contraction of the

capsule with release. These defects result in the higher linear release of the encapsulate, as shown by the linear relationship in region 2.

**Region 2:** Similar in both systems, this linear region corresponds to zero-order diffusive release of the fill from the microcapsules.

**Region 3:** Similar in both systems, this region of slow release occurs due to the polydispersity of microcapsule sizes. In this region, it is presumed that only the larger capsules still contain internal materials for continuous release. At the end of this release region, capsules are empty. The normalized mass of the empty clay-coated capsules is higher than the uncoated sample, due to the additional mass imparted by the clay layer.

Finally, based on the breakdown of the various regions of release, it is apparent that the first region is solely attributed to the barrier effects of the clay coating on the microcapsules. It is possible that the clay coating loses integrity, or cracks, upon loss of some of the fill and the resulting deformation of the capsule. Ideally, optimization of the clay-coated system would involve a barrier coating that remains intact upon capsule deformation in order to prolong the slower release displayed in region 1. Consequently, the layering of a polycation 'glue' onto the clay-coated microcapsule will be investigated as a method to prevent defect formation, as well as enable charge reversal for further layering with clay.

### 3.2.3.2 Monitoring of individual encapsulate release from PMPPI/DETA polyurea microcapsules

The model fill used in this study was a 90:10 mixture of xylene:butyl acetate. During the gravimetric release test in the convection oven, the composition of the fill remaining was analyzed by $^1$H-NMR to measure the relative release rates of the two fill components. This involved the extraction of residual encapsulated materials using deuterated dimethyl sulfoxide (DMSO-d6), followed by $^1$H-NMR analysis. Integration of the $^1$H-NMR spectrum of the 10 % butyl acetate microcapsule sample extracted at t = 0 (immediately following dehydration) indicated that at this point the capsules still contained butyl acetate and xylene in the original ratio (Fig. 3.20.).

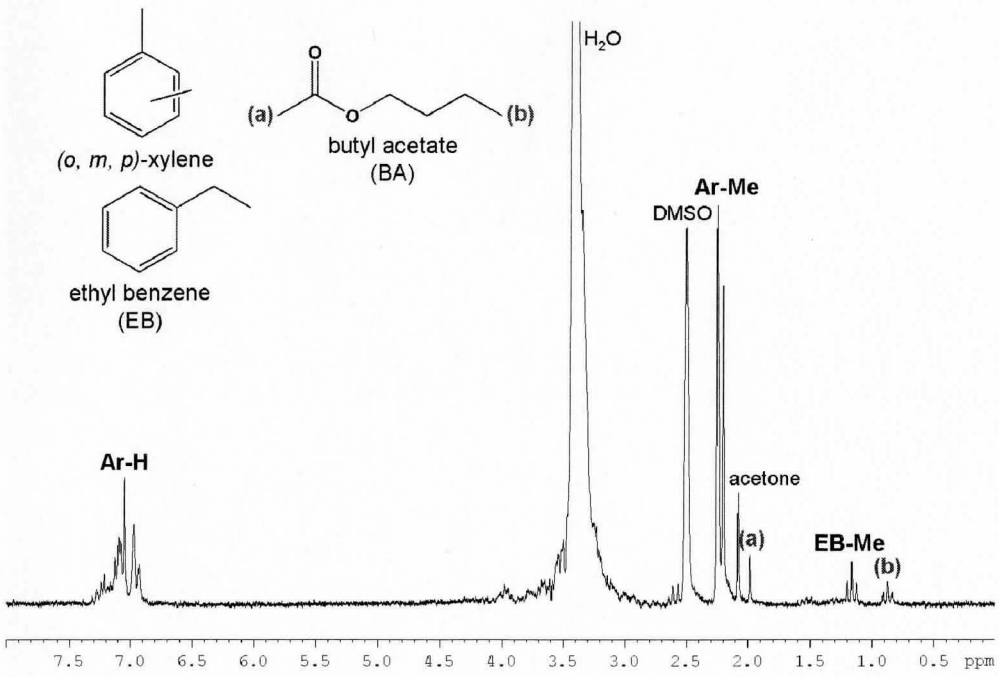


**Fig. 3.20.** $^{1}$H-NMR spectrum of the microcapsule extract at t = 0. Characteristic xylene peaks (containing ethyl benzene) = 1.18 (t), 2.21 (s), 2.24 (q), 7.05 (s), 3.99 (t); butyl acetate = 0.89 (t), 1.32 (m), 1.54 (m), 1.99 (s), 3.99 (t).[210]

Specifically, integration of the aromatic (**Ar-H**) and the methyl group (**Ar-Me**) hydrogen peaks of xylene in relation to the acetate Me peak (**(a)**) resulted in a relative mole % composition of 90.9 % versus 9.1 %, respectively. The close match with the actual mole % composition of the organic phase (90.6 % xylene; 9.4 % butyl acetate) suggests that little fill was lost during encapsulation, and that $^{1}$H-NMR can be used to monitor release of the internal materials.

Weighed samples of microcapsules were removed from the convection oven during gravimetric analysis after 1, 2, 6, and 7 days of heating at ~ 80 °C, and extracted into 1 ml DMSO. The extracts were filtered through a small column of glass wool in a

glass pipette to remove microcapsule shells. The extracted amounts of xylene and butyl acetate were quantified by integration of the $^1$H-NMR peaks corresponding to Ar-H and acetate-Me, using the $^1$H-NMR DMSO peak at ~ 2.5 ppm (s) as the calibration standard. A plot describing the decrease in xylene and butyl acetate over time is shown in Figure 3.21. It must be noted, however, that the specific integration value at t = 0 days is a rough estimate, given that a portion of the deuterated extract was lost during handling due to the breaking of the NMR tube. It was assumed that 25 % (0.25 mL) of the original sample extract was retained for analysis, and the integration value was based on a 5-fold increase in the total volume of DMSO (1.25 mL sample).

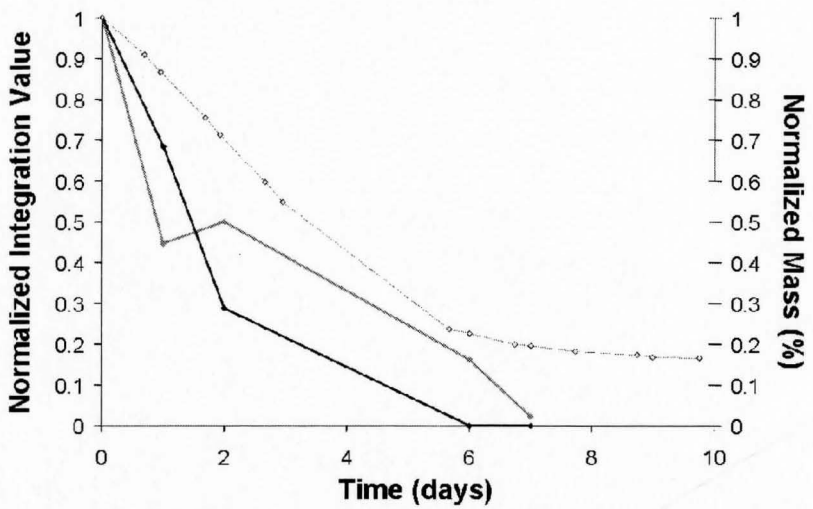


**Fig. 3.21.** Normalized amounts of xylene (♦, —) and butyl acetate (♦, —) plotted alongside the corresponding normalized mass loss of PMPPI/DETA polyurea microcapsules (◊, —) over several days of gravimetric analysis

The xylene weight loss curve seems to show a slight increase on day 2, which may be attributed to error in measurement. The data indicated that 50 % of the butyl acetate is

released after about 2 days, while the less polar xylene shows a 50 % release after about 5 days. Butyl acetate, with its higher polarity and H-bonding capabilities, is considered a better solvent for polyurea than xylene and can swell the polyurea wall for faster release. As xylene makes up the major part of the microcapsule fill, its release profile most closely matches the overlying gravimetric PMPPI/DETA polyurea microcapsule weight loss profile. Specifically, the plateau of complete solvent release in the gravimetric plot matches up well with the depletion of xylene shown by $^{1}$H-NMR analysis.

### 3.2.4 Layer-by-layer assembly of polyelectrolytes

The formation of a composite polyurea microcapsule by LbL electrostatic deposition of montmorillonite clay was shown to decrease release rates by about a factor of two, presumably by the creation of a tortuous diffusion path. The advantage of this method of barrier control over conventional polyurea membrane modifications[211,212] is that it can be applied to a variety of capsule systems post-polymerization.

Although release rates decreased after clay-coating, this approach to release control was not without flaw. Gravimetric analyses suggested the formation of defects, or cracks, in the clay coating, possibly due to shell contraction during drying or early fill release. Specifically, these fractures are expected to occur at sites of overlapping clay sheets.[213] Consequently, it may prove beneficial to electrostatically adsorb a polycation onto the clay coating, in order to hold the platelets in place, absorb contraction stresses, and prepare the surface for additional clay layering.

The electrostatic deposition of polycations onto a clay-coated surface results in charge reversal of the substrate in preparation for further clay layering, likely allowing

for a further reduction in release rates for a given type of polyurea capsule. LbL assembly of polyelectrolytes and clay to impart barrier properties has already been demonstrated for polymer composite systems. [214,215,216,217,218] Experimentally, the coating mechanism involves the use of a polycation that possesses positive charges along the polymer chains, rather than simply at chain ends, for multiple ionic bonding to negative surfaces. The large amount of oppositely charged chains has been shown to help smooth over defects in the previous clay layer,[219] and provide a highly charged cationic surface for subsequent adsorption of a second clay layer.[220] Consequently, LbL can provide a means to control encapsulate release by the addition of multiple external clay layers, for potential pesticide delivery applications. Therefore, the deposition of delaminated anionic montmorillonite clay with matching acrylic polycations was investigated to create such outer coatings using a layer-by-layer approach.

### 3.2.4.1 Polycation adsorption onto clay-coated capsules

The LbL assembly at the clay-coated microcapsule surface will involve the adsorption of a weak polycation, PAPM (Fig. 3.22.), onto the anionic substrate. Even though adsorption is primarily driven by ionic interactions, the amount of material adsorbed may vary considerably, depending on the deposition conditions.[221] Polyelectrolyte adsorption depends on the molecular weight of the polymer, ionic strength of the solution, and in the case of weak polyelectrolytes such as PAPM, on the degree of ionization. In weak polycation solutions, low degrees of ionization obtained at higher pH values usually lead to the deposition of a thick layer of polycation in a loop-and-tail conformation. At lower pH values, the degree of ionization increases and the

polycation can bind to multiple sites at the anionic surface, resulting in a significantly thinner layer of polycation. In the present work, we initially use PAPM coating solutions as formed, without adjusting their pH (pH ~ 6.2 ± 0.1).

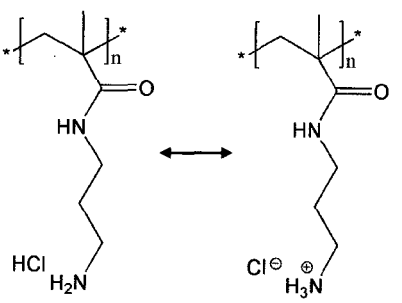


**Fig. 3.22.** The polycation for LbL assembly, poly(aminopropyl methacrylamide) (PAPM)

Identification of the polycation was facilitated by the fluorescent labeling of PAPM with fluorescein isothiocyanate (FITC). Experimentally, an excess of the polycation was added to a clay-coated microcapsule sample, and lightly agitated on the rugged rotor for 15 minutes. The PAPM-FITC coated microcapsules were rinsed of unbound polymer and observed under the fluorescent filter of the optical microscope (Fig. 3.23. (c)).

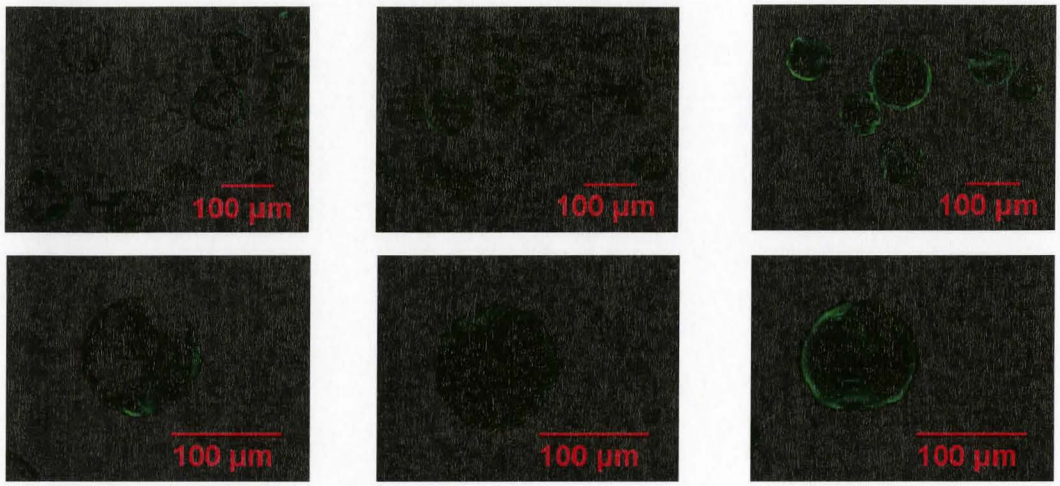


**Fig. 3.23.** Fluorescence microscopy images of **(a)** native PMPPI/DETA, **(b)** PAPM-coated PMPPI/DETA, and **(c)** PAPM-coated MMT-PMPPI/DETA polyurea microcapsules

In order to explore the effect of the clay coating on polycation binding, a second set of native polyurea capsules were exposed directly to a solution of the polycation, without prior clay coating. Analogous fluorescent microscopy images are shown in Fig. 3.23. (b). The native polyurea capsules are inherently positively charged, and electrostatically repel binding of PAPM-FITC, resulting in lower fluorescence. Conversely, the clay-coated capsules with a negative surface charge displayed an increase in fluorescence due to the electrostatic bonding of FITC-labeled PAPM. The increase in intensity was not significant, however, and the PMPPI-based polyurea microcapsules auto-fluoresce themselves. This indicates that some of the emission observed in Fig. 3.23. (a) and presumably (b) is due to PMPPI auto-fluorescence. Hence, the quantitative

analysis of adsorbed polycation was carried out by UV-Vis spectroscopy of the PAPM-FITC solutions before and after coating (residuals analysis).

The supernatant from polyurea microcapsule exposure to the PAPM-FITC solution was removed and filtered through a glass wool column for UV-Vis absorbance testing. Given the extinction coefficient of the fluorescently labeled polymer ($\epsilon = 3.09 \pm 0.05$ $mL \cdot mg^{-1} \cdot cm^{-1}$), the concentration of polycation in the supernatant was determined using the Beer-Lambert equation:

$$A = \varepsilon \cdot l \cdot c \qquad (3)$$

where $A$ is the absorbance at the absorbance maximum, $\varepsilon$ is the extinction coefficient, $l$ is the cell path length, and $c$ is the concentration of absorbing species in solution.

Therefore, the UV-Vis absorbance of the supernatant was measured for the PAPM-coated polyurea composite capsules, as well as the clay-free control microcapsules (Fig. 3.24.).

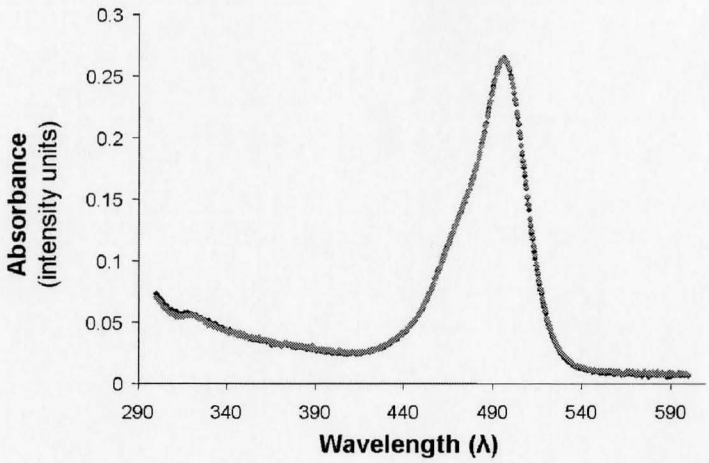


**Fig. 3.24.** UV-Vis absorbance spectrum of the supernatant of the PAPM-immersed PMPPI/DETA (♦) and MMT-PMPPI/DETA (♦) polyurea microcapsules

The close match between the two curves indicates that the both capsules absorb very little, or a similar amount of polycation.

As previously mentioned, many factors affect the LbL deposition of weak polyelectrolytes onto charged surfaces, including solution pH and ionic strength. Prior to clay coating, the initial positively charged polyurea capsule surface itself can be considered a weak polyelectrolyte substrate for LbL assembly. The unreacted primary amines from polyurea at the capsule surface have pKa values of about 9.2 and 10.0, respectively, indicating the need for low to neutral pH values in order to maximize the charge of the cationic substrate. The current clay coating was carried out at a pH of approximately 9.6 ± 1 (Table 3.2.), which corresponds to a low degree of protonation of surface amines and hence low cationic charge density during clay deposition. Therefore, the pH of the microcapsule dispersion was decreased in order to maximize clay

adsorption to the substrate, and ensure further adsorption of PAPM to the highly charged clay surface.

As previously discussed (section 3.2.2.2.1.1), clay platelets flocculate at certain pH values, which can cause inhomogeneous adsorption of clay aggregates to the microcapsule surface. Consequently, prior to altering the pH of the capsule dispersion, the effect of lowering the pH of the 1.0 wt % aqueous clay dispersion was investigated. Lowering the pH from ~9.7 ± 0.1 to ~ 7.4 ± 0.1 resulted in an increase in viscosity, with complete gelation occurring at ~ 5.0 ± 0.1. This corresponds well with literature, which describes the flocculation of aqueous clay suspensions below a pH of 7.0.[222] Therefore, the lowest potential pH range for the clay coating of polyurea microcapsules of maximized charge density lies around 7.1 - 7.5 ± 0.1.

The pH of the clay solution was lowered to approximately 7.8 ± 0.1 prior to addition of microcapsules, at which point the pH dropped further to ~ 7.4 ± 0.1. The resulting clay-coated microcapsules were observed by TEM (Fig. 3.25.), in order to compare the thickness of the clay layer to that of earlier capsules coated at a pH of 9.7.

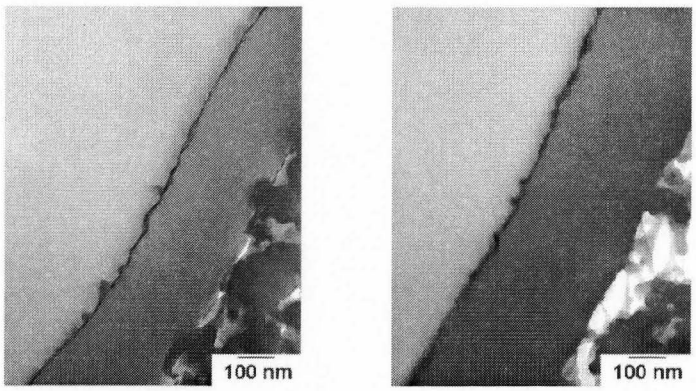


**(a)** **(b)**

**Fig. 3.25.** TEM cross-sectional images of MMT-PMPPI/DETA polyurea microcapsules synthesized under a solution pH of **(a)** 9.6 ± 0.1 and **(b)** 7.4 ± 0.1

The TEM images do not indicate a significant increase in the thickness of the clay layer upon adsorption to the microcapsules at a lower solution pH. Further quantification by TGA confirmed that the amount of clay remained the same for both samples, regardless of the initial clay solution pH.

Subsequently, the polyurea microcapsules coated with clay at the lower solution pH of 7.4 ± 0.1 were immersed in the PAPM-FITC solution at pH ~ 6.2 ± 0.1, in order to determine if the polycation would adsorb to the surface. Upon observation under the fluorescent filter of the optical microscope (Fig. 3.26.), no noticeable increase in fluorescence intensity was observed.

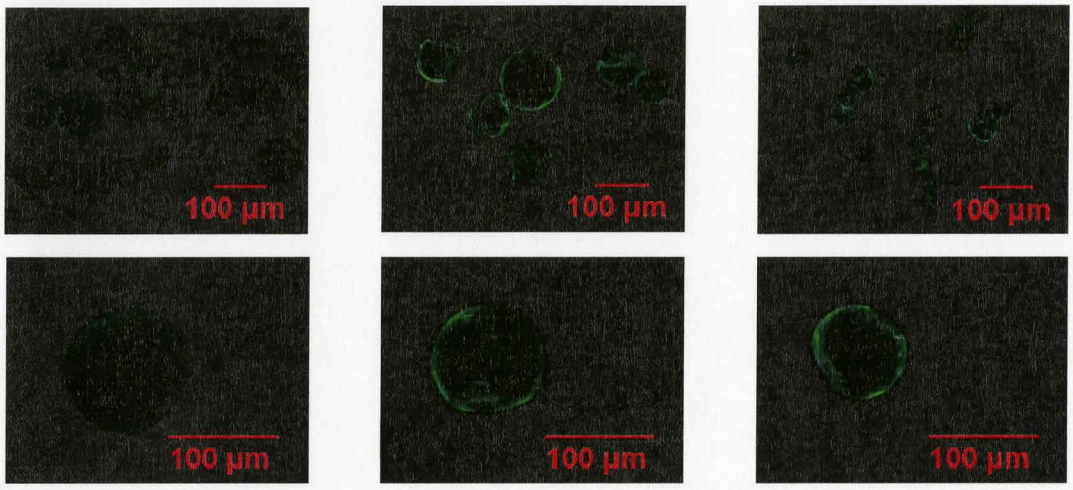


**Fig. 3.26.** Optical microscope images under the fluorescent filter of the PAPM-coated **(a)** PMPPI/DETA, **(b)** MMT-PMPPI/DETA, and **(c)** lower solution pH MMT-PMPPI/DETA polyurea microcapsules

Although the characterization thus far indicated no noticeable change in charge density at the microcapsule surface upon clay-coating at a lower solution pH, a UV/Vis residuals analysis of the PAPM-FITC supernatant was performed (Fig. 3.27.). The resulting spectra showed a decrease in absorbance compared to the coatings at higher pH values, indicating that adsorption of some polycation had occurred.

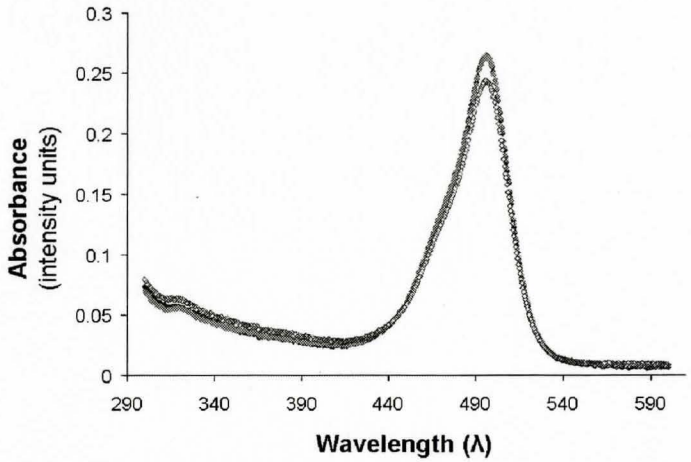


**Fig. 3.27.** UV-Vis absorbance spectrum of the supernatant of the PAPM-immersed PMPPI/DETA (♦), MMT-PMPPI/DETA (♦), and MMT-PMPPI/DETA at low pH (◊) polyurea microcapsules

The data indicate that about 8 % of PAPM-FITC was adsorbed to the surface of the clay-coated polyurea microcapsule, corresponding to about 0.00008 mg PAPM/mg filled capsules, or 0.00008 mg PAPM/cm$^2$.

### 3.3. Conclusions

The incorporation of clay onto polyurea microcapsules post-polymerization was performed by the layer-by-layer assembly of anionic clay platelets onto the cationic substrate. Application of this method required a fundamental understanding of polyurea microcapsule formulations, in order to determine a model system for further LbL assembly and gravimetric analysis. Therefore the empirical optimization of wall strength and permeability was investigated in order to determine an ideal model polyurea microcapsule system for the diffusive release of internal materials in a reasonable amount

of time. Firstly, the fine-tuning of wall strength involved variations in capsular and wall parameters, such as crosslink density and wall thickness. Once optimized, the permeability of the PMPPI-based microcapsules was increased by adding a polar, hydrogen bonding co-solvent (butyl acetate), and by carrying out the release measurements at elevated temperatures. Characterization of the model polyurea microcapsule system by optical microscopy, TEM and TGA confirmed diffusive release, rather than rupture release, of 90:10 xylene:butyl acetate-filled polyurea microcapsules at 75 °C. The PMPPI/DETA microcapsules were then exposed to a 1.0 wt % Cloisite® $Na^+$ solution for 15 minutes. Analysis by TEM and TGA indicated coating with a homogeneous clay layer corresponding to 4.2 ± 1 % relative to the polyurea. The exposure concentration and time was confirmed to be optimal for the current capsules.

The release rate profiles displayed an approximate 40 % decrease in permeability upon clay coating. $^1$HNMR testing confirmed diffusive release, with butyl acetate escaping from the capsules about twice as fast as xylene. Consideration of the release rate profiles suggests that the diffusion through the clay-capsule coating may involve fractures formed by the contraction of the microcapsules during release. Once formed, the defects allowed for the zero-order release of the encapsulate, in a similar fashion to the uncoated polyurea capsule control. Therefore, the LbL deposition of a cationic polymer onto the clay surface was investigated, in order to hold the platelets in place and reverse the charge at the capsule surface for subsequent clay layering.

Finally, preliminary investigations of the coating of composite polyurea microcapsules with a fluorescently-labeled weak polycation, PAPM-FITC, were carried

out. Initial analysis via fluorescent optical microscopy showed weak absorption of the polycation, at levels too low to be detected by residuals analysis of the supernatant by UV/Vis. At this point it was realized that the initial clay layer had been deposited at a high pH of 9.6 ± 0.1, potentially limiting the deposition of clay and the charge reversal to an anionic surface. Subsequent deposition of clay at pH 7.5 ± 0.1, the threshold for clay flocculation in aqueous solutions, led to a comparable deposition of clay. Residuals analyses revealed adsorption of 0.00008 mg PAPM-FITC per $cm^2$, about 8.4 % of the coating solution. However, fluorescent microscopy images did not reflect this enhanced deposition of PAPM-FITC. Therefore, while deposition of PAPM-FITC was confirmed by residual analysis, more experiments are needed to resolve some of the contradictions in the observations. This would allow for the preparation of polycation coated microcapsules for further gravimetric analysis, followed by a second clay deposition. Overall, the approach is promising and may lead to the ability to modify release from polyurea microcapsules for agricultural applications.

## 4.0 Future Work

Future work in the area of clay-coated polyurea microcapsules may involve fundamental research into the charge density of the polyurea shell in order to maximize clay adsorption to the capsule surface. Quantification of charge at the substrate by mobility measurements (i.e. electrophoresis) may prove beneficial at understanding the factors that effect layer-by-layer assembly of the charged colloids from aqueous solutions. The rate of release should be measured as function of the pH at which the capsules were coated with clay. In terms of the mechanism of release from the clay-coated capsules, surface imaging by an environmental scanning electron microscope (ESEM) may qualitatively confirm the formation of fractures in the external coating.

The LbL deposition of a polycation onto the clay-coated capsule should be continued towards the final goal of controlling the permeability of the polyurea microcapsule by multiple clay coatings. Little is understood regarding the parameters that control adsorption of the polycation, such as solution concentration, immersion time, strength of the polyelectrolyte, etc. Preliminary work may concentrate on optimizing the adsorption of the polycation layer to ensure that any subsequent clay layering occurs homogeneously and at a maximized clay loading. Consequently, the relationship between alternating layer thicknesses of polycation and clay, and the diffusive release rate of active materials from the polyurea core may be established. Once optimized, the post-polymerization LbL addition of polycations and clay may be applied to polyurea microcapsules containing agriculturally active materials.

Additional future work may include the incorporation of polyanions into the LbL assembly that lightly crosslink with underlying polycations. This would enable the formation of a permanent shell at the clay-coated capsule surface to hold clay sheets in place during encapsulate release. The coating of the capsule with various inorganic colloids similar to clay, such as silica, may also prove to be an interesting area of investigation. Finally, additional research may involve the functionalization of layering polymers to promote adhesion between the microcapsule and the host plant.

## REFERENCES


[1] Tsuji, K. In *Microspheres Microcapsules & Liposomes (MML), Volume 1: Preparation & Chemical Applications*; Arshady, R., Ed.; Citus Books: London, UK, 1999: pp. 349-355.
[2] Cardarelli, N. F. *Controlled Release Pesticides Formulations*; CRC Press, Inc.: Cleveland, Ohio, 1976.
[3] Lewis, D. H., and Cowsar, D.R. In *Controlled Release Pesticides*; Scher, H. B., Ed.; ACS Symposium Series 53: USA, 1977: pp. 1-16.
[4] Shirley, I. M., Scher, H. B., Perrin, R. M., Wege, P. J., Rodson, M., Chen, J.-L., and Rehmke, A. W. *Pest. Manag. Sci.* **2001**, *57*, 129-132.
[5] Tsuji, K, *J. Microencapsulation* **2001**, *18*, 137-147.
[6] Tsuji, K, *J. Microencapsulation* **2001**, *18*, 137-147
[7] Lewis, D. H., and Cowsar, D.R. In *Controlled Release Pesticides*; Scher, H. B., Ed.; ACS Symposium Series 53: USA, 1977: pp. 1-16.
[8] Shasha, B. S., Doane, W. M., and Russell, C. R. *J. Polym. Sci. Pol. Lett. Ed.* **1976**, *14*, 417-420.
[9] Mathiowitz, E., Raziel, A., Cohen, M. D., and Fischer, E. *J. Appl. Polym. Sci.* **1981**, *26*, 809-822.
[10] Van Koppenhagen, J. E., Scher, H. B., Lee, K.-S., Shirley, I. M., Wade, P., and Follows, R., U.S. Patent 6,544,540 B2, (2003).
[11] DeGennaro, M. D., Thompson, B. B., and Luzzi, L.A. In *Controlled Release Polymeric Formulations*; Paul, D. R., and Harris, F. W., Eds.; ACS Symposium Series 33: Washington, D.C., 1976: pp. 195-207.
[12] Lowell Jr., J. R., and Culver W. H. In *Controlled Release Pesticides*; Scher, H. B., Ed.; ACS Symposium Series 53: USA, 1977: pp. 145-151.
[13] Scher, H. B. In *Controlled Release Pesticides*; Scher, H. B., Ed.; ACS Symposium Series 53: USA, 1977: pp. 126-144.
[14] Kydonieus, A. F., Smith, I. K., and Beroza, M. In *Controlled Release Polymeric Formulations*; Paul, D. R., and Harris, F. W., Eds.; ACS Symposium Series 33: Washington, D.C., 1976: pp. 283-294.
[15] Fanger, G. O. In *Microencapsulation Processes and Applications*; Vandegaer, J. E., Ed., Plenum Press: New York, 1974: pp. 1-19.
[16] Lewis, D. H., and Cowsar, D. R. In *Controlled Release Pesticides*; Scher, H. B., Ed.; ACS Symposium Series 53: USA, 1977: pp.1-16.
[17] Arshady, R. In *Microspheres Microcapsules & Liposomes (MML), Volume 1: Preparation & Chemical Applications*; Arshady, R., Ed.; Citus Books: London, UK, 1999: pp.280-285.
[18] Green B. K., and Schleicher, L., US Patent 2,217,507, (1955).
[19] Tsuji, K, *J. Microencapsulation* **2001**, *18*, 137-147.
[20] Desavigny, C. B., U.S. Patent 3,959,464, (1976).
[21] Kondo, T., Ueda, O., Fukakusa, Y., Moriwaki, M., and Fuziwara, H., U.S. Patent 5,002,768, (1991).
[22] Beestman, G. B., and Deming, J. M., U.S. Patent 4,280,833, (1981).
[23] Shukla, P. G., Sivaram, S., and Rajagopalan, N., U.S. Patent 5,962,003, (1999).
[24] Ericsson, R. J., Downing, H. E., Marsh, R. E., and Howard, W. E. *J. Wildl. Manage.* **1971**, *35*, 573-576.
[25] Jackson, W. B. *Use of microencapsulation to enhance rodenticide acceptance.* Paper presented at Controlled Release Pesticide Symposium, University of Akron, Sept. 16-18, 1974.
[26] Baker, R. W., U.S. Patent 4,670,250, (1987).
[27] Carothers, W. H., U.S. Patent 2,130,523, (1938).
[28] Beaman, G., Morgan, P. W., Koller, C. R., Wittbecker, E. L., and Magat, E. E. *J. Polym. Sci.* **1959**, *40*, 329-336.
[29] Katz, M. *J. Polym. Sci.* **1959**, *40*, 337-342.
[30] Wittbecker, E. L., and Morgan, P. W. *J. Polym. Sci.* **1959**, *40*, 289-297.
[31] Scher, H. B., Rodson, M., and Lee K.-S. *Pestic. Sci.* **1998**, *54*, 394-400.
[32] Mathiowitz, E., and Cohen, M. D., *J. Membrane Sci.* **1989**, *40*, 1-26.
[33] Mathiowitz, E., and Cohen, M. D., *J. Membrane Sci.* **1989**, *40*, 27-41.

[34] Morgan, P. W. *Condensation Polymers: By Interfacial and Solution Methods*, Interscience Publishers: New York, 1965.
[35] Scher, H. B. In *Controlled Release Pesticides*; Scher, H. B., Ed.; ACS Symposium Series 53: USA, 1977: pp. 126-144.
[36] Shirley, I. M., Scher, H. B., Perrin, R. M., Wege, P. J., Rodson, M., Chen, J.-L., and Rehmke, A. W. *Pest. Manag. Sci.* **2001**, *57*, 129-132.
[37] Cardarelli, N. F., and Walker, K. E., Report, Environmental Protection Agency/540/9-77/016, 1978. Referenced by Zweig, G. In *Controlled Release Pesticides*; Scher, H. B., Ed.; ACS Symposium Series 53: USA, 1977: pp. 37-53.
[38] Zweig, G., In *Controlled Release Pesticides*; Scher, H. B., Ed.; ACS Symposium Series 53: USA, 1977: pp. 37-53.
[39] Sjogren, R. D., U.S. Patent 4,971,796, (1990).
[40] Fanger, G. O. In *Microencapsulation Processes and Applications*; Vandegaer, J. E., Ed., Plenum Press: New York, 1974: pp. 1-19.
[41] Yadav, S. K., Khilar, K. C., and Suresh, A. K. *J. Membrane Sci.* **1997**, *125*, 213-218.
[42] Yadav, S. K., Khilar, K. C., and Suresh, A. K. *AIChE Journal* **1996**, *42*, 2616-2626.
[43] Dhumal, S. S., Wagh, S. J., and Suresh, A. K. *J. Membrane Sci.* **2008**, *325*, 758-771.
[44] Dappert, T., and Thies, C. *J. Membrane Sci.* **1979**, *4*, 99-113.
[45] Sirdesai, M., and Khilar, K. C. *Can. J. Chem. Eng.* **1988**, *66*, 509-513.
[46] Yadav, S. K., Khilar, K. C., and Suresh, A. K. *AIChE Journal* **1996**, *42*, 2616-2626.
[47] Scher, H. B., Rodson, M., and Lee K.-S. *Pestic. Sci.* **1998**, *54*, 394-400.
[48] Scher, H. B. In *Controlled Release Pesticides*; Scher, H. B., Ed.; ACS Symposium Series 53: USA, 1977: pp. 126-144.
[49] Shirley, I. M., Scher, H. B., Perrin, R. M., Wege, P. J., Rodson, M., Chen, J.-L., and Rehmke, A. W. *Pest. Manag. Sci.* **2001**, *57*, 129-132.
[50] Mathiowitz, E., and Cohen, M. D. *J. Membrane Sci.* **1989**, *40*, 27-41.
[51] Yariv, S., and Michaelian, K. H. In *Organo-Clay Complexes and Interactions*; Yariv, S., and Cross, H., Eds.; Marcel Dekker, Inc.: NY, USA, 2002: pp. 1-38.
[52] Yoonessi, M., Toghiani, H., Kingery, W. L., and Pittman Jr., C. U. *Macromolecules* **2004**, *37*, 2511-2518.
[53] Van Olphen, H. *An Introduction to Clay Colloid Chemistry, 2nd Edition*; Wiley: New York, 1977. Referenced by Lagaly, G. In: *Handbook of Clay Science*; Bergaya, F., Theng, B. K. G., and Lagaly, G., Eds.; Elsevier: Amsterdam, 2006: pp.141-245.
[54] Keren, R., Shainberg, I., and Klein, E. *Soil Sci. Soc. Am. J.* **1988**, *52*, 76-80.
[55] Zeta Potential: A Complete Course in 5 Minutes; Zeta-Meter Inc.: Staunton, Va. Available at www.zeta-meter.com/contact.html.
[56] Wiklander, L. In *Chemistry of the Soil, 2nd Edition*; Bear, F. E., Ed.; Reinhold Pub. Co.: N.Y., 1964: pp. 163-166.
[57] Grim, R. E. *Clay Minerology, 2nd Edition*; McGraw-Hill: New York, 1968. Van Olphen, H. *An Introduction to Clay Colloid Chemistry, 2nd Edition*; Wiley: New York, 1977. Referenced by Secor, R. B., and Radke, C. J. *J. Colloid Interface Sci.* **1985**, *103*, 237-244.
[58] Tateyama, H., Scales, P. J., Ooi, M., Nishimura, S., Rees, K., and Healy, T. W. *Langmuir* **1997**, *13*, 2440-2446.
[59] Ottewill, R. H. *J. Colloid Interface Sci.* **1977**, *58*, 357-373.
[60] Secor, R. B., and Radke, C. J. *J. Colloid Interface Sci.* **1985**, *103*, 237-244.
[61] Massam, J., and Pinnavaia, T. J. *Mater. Res. Soc. Symp. Proc.* **1998**, *520*, 223-232.
[62] Burnside, S. D., and Giannelis, E. P. *Chem. Mater.* **1995**, *7*, 1597-1600.
[63] Kawasumi, M., Hasegawa, N., Kato, M., Usuki, A., and Okada, A. *Macromolecules* **1997**, *30*, 6333-6338.
[64] Wang, Z., and Pinnavaia, T. J. *Chem. Mater.* **1998a**, *10*, 3769-3771.

[65] Giannelis, E. P. *Adv. Mater.* **1996**, *8*, 29-35.
[66] Lan, T., and Pinnavaia, T. J. *Chem. Mater.* **1994**, *6*, 2216-2219.
[67] Fukushima, Y., and Inagaki, S. *J. Inclusion Phenom.* **1987**, *5*, 473-482.
[68] LeBaron, P. C., Wang, Z., and Pinnavaia, T. J. *Appl. Clay Sci.* **1999**, *15*, 11-29.
[69] Yano, K., Usuki, A., Okada, A., Kurauchi, T., and Kamigaito, O. *J. Polym. Sci., Part A: Polym. Chem.* **1993**, *31*, 2493-2498.
[70] Yano, K., Usuki, A., and Okada, A. *J. Polym. Sci. A Polym. Chem.* **1997**, *35*, 2289-2294.
[71] Kojima, Y., Fukumori, K., Usuki, A., Okada, A., and Kurauchi, T. *J. Mater. Sci. Lett.* **1993c**, *12*, 889-890.
[72] Messersmith, P. B., and Giannelis, E. P. *J. Polym. Sci., Part A: Polym. Chem.* **1995**, *33*, 1047-1057.
[73] Kojima, Y., Fukumori, K., Usuki, A., Okada, A., and Kurauchi, T. *J. Mater. Sci. Lett.* **1993c**, *12*, 889-890. Referenced by LeBaron, P. C., Wang, Z., and Pinnavaia, T. J. *Appl. Clay Sci.* **1999**, *15*, 11-29.
[74] Lutkenhaus, J. L., Olivetti, E. A., Verploegen, E. A., Cord, B. M., Sadoway, D. R., and Hammond, P. T. *Langmuir* **2007**, *23*, 8515-8521.
[75] Lvov, Y., Ariga, K., Onda, M., Ichinose, I., and Kunitake, T. *Langmuir* **1997**, *23*, 6195-6203. Lvov, Y. M., Rusling, J. F., Thomsen, D. L., Papadimitrakopoulos, F., Kawakami, T., Kunitake, T. *Chem. Commun.* **1998**, 1229-1230. Referenced by Ariga, K., Lvov, Y., Ichinose, I., and Kunitake, T. *Appl. Clay Sci.* **1999**, *15*, 137-152.
[76] Caruso, F., Lichtenfeld, H., Giersig, M., Möhwald, H. *J. Am. Chem. Soc.* **1998**, *120*, 8523-8524.
[77] Fendler, J. H. In *Organic Thin Films and Surfaces: Directions for the Nineties*; Ulman, A., Ed.; Academic Press: New York, 1995: pp. 11-40.
[78] Moriguchi, I., Maeda, H., Teraoka, Y., Kagawa, S. *J. Am. Chem. Soc.* **1995**, *117*, 1139-1140.
[79] Pastoriza-Santos, I., Koktysh, D. S., Mamendov, A. A., Giersig, M., Kotov, N. A., and Liz-Marzán, L. M. *Langmuir* **2000**, *16*, 2731-2735.
[80] Ichinose, I., Tagawa, H., Mizuki, S., Lvov, Y., and Kunitake, T. *Langmuir* **1998**, *14*, 187-192.
[81] Yonezawa, T., Matsune, H., and Kunitake, T. *Chem. Mater.* **1999**, *11*, 33-35.
[82] Schmitt, J., Decher, G., Dressick, W. J., Brandow, S. L., Geer, R. E., Shashidhar, R., and Calvert, J. M. *Adv. Mater.* **1997**, *9*, 61.
[83] Ostrander, J. W., Mamedov, A. A., and Kotov, N. A. *J. Am. Chem. Soc.* **2001**, *123*, 1101-1110.
[84] Aliev, F. G., Correa-Duarte, M. A., Mamedov, A., Ostrander, J. W., Giersig, M., Liz-Marzán, L. M., and Kotov, N. A. *Adv. Mater.* **1999**, *11*, 1006-1010.
[85] Gao, M., Y., Richter, B., Kirstein, S., and Möhwald, H. *J. Phys. Chem. B* **1998**, *102*, 4096-4103.
[86] Kleinfeld, E. R., and Ferguson, G. S. *Chem. Mater.* **1996**, *8*, 1575-1578.
[87] Kotov, N. A., Dekany, I., and Fendler, J. H. *Adv. Mater.* **1996**, *8*, 637-641.
[88] Schmitt, J., Decher, G., Dressick, W. J., Brandow, S. L., Geer, R. E., Shashidhar, R., and Calvert, J. M. *Adv. Mater.* **1997**, *9*, 61-65.
[89] Kotov, N. A., Magonov, S., and Tropsha, E. *Chem. Mater.* **1998**, *10*, 886-895.
[90] Decher, G., and Hong J.-D. *Makromol. Chem. Macromol. Symp.* **1991**, *46*, 321-327.
[91] Decher, G., and Hong J.-D. *Ber. Bunsenges Phys. Chem.* **1991**, *95*, 1430-1434.
[92] Bernt, P., Kurihara, K., and Kunitake, T. *Langmuir* **1992**, *8*, 2486-2490. Referenced by: Ariga, K. In: *Handbook of Polyelectrolytes and Their Applications*; Tripathy, S. K., Kumar, J. and Nalwa, H. S., Eds.; American Scientific Publishers: California, USA, 2002: pp. 127-145.
[93] Decher, G. *Science* **1997**, *277*, 1232-1237.
[94] LeBaron, P. C., Wang, Z., and Pinnavaia, T. J. *Appl. Clay Sci.* **1999**, *15*, 11-29.
[95] Sasaki, T. In *Handbook of Polyelectrolytes and Their Applications*; Tripathy, S. K., Kumar, J. and Nalwa, H. S., Eds.; American Scientific Publishers: California, USA, 2002: pp. 241-262.
[96] Lu, C., and Mai, Y.-W. *Phys. Rev. Lett.* **2005**, *95*, 088303(1)-088303(4).
[97] Kleinfeld E. R., and Ferguson, G. S. *Science* **1994**, *265*, 370-373.
[98] Lvov, Y., Ariga, K., Ichinose, I., and Kunitake, T. *Langmuir* **1996**, *12*, 3038-3044.
[99] Kotov, N. A., Magonov, S., and Tropsha, E. *Chem. Mater.* **1998**, *10*, 886-895.

[100] Eckle, M., and Decher, G. *Nano Lett.* **2001**, *1*, 45-49.
[101] Lutkenhaus, J. L., Olivetti, E. A., Verploegen, E. A., Cord, B. M., Sadoway, D. R., and Hammond, P. T. *Langmuir* **2007**, *23*, 8515-8521.
[102] Lewis, D. H., and Cowsar, D.R. In *Controlled Release Pesticides*; Scher, H. B., Ed.; ACS Symposium Series 53: USA, 1977: pp. 1-16.
[103] Fanger, G. O. In *Microencapsulation Processes and Applications*; Vandegaer, J. E., Ed., Plenum Press: New York, 1974: pp. 1-19.
[104] Ariga, K., Lvov, Y., Ichinose, I., and Kunitake, T. *Appl. Clay Sci.* **1999**, *15*, 137-152.
[105] LeBaron, P. C., Wang, Z., and Pinnavaia, T. J. *Appl. Clay Sci.* **1999**, *15*, 11-29.
[106] Yano, K., Usuki, A., and Okada, A. *J. Polym. Sci. A Polym. Chem.* **1997**, *35*, 2289-2294.
[107] Kojima, Y., Fukumori, K., Usuki, A., Okada, A., and Kurauchi, T. *J. Mater. Sci. Lett.* **1993c**, *12*, 889-890.
[108] Messersmith, P. B., and Giannelis, E. P. *J. Polym. Sci., Part A: Polym. Chem.* **1995**, *33*, 1047-1057.
[109] Massam, J., and Pinnavaia, T. J. *Mater. Res. Soc. Symp. Proc.* **1998**, *520*, 223-232.
[110] Burnside, S. D., and Giannelis, E. P. *Chem. Mater.* **1995**, *7*, 1597-1600.
[111] Wang, Z., and Pinnavaia, T. J. *Chem. Mater.* **1998a**, *10*, 3769-3771.
[112] Giannelis, E. P. *Adv. Mater.* **1996**, *8*, 29-35.
[113] Lan, T., and Pinnavaia, T. J. *Chem. Mater.* **1994**, *6*, 2216-2219.
[114] Norrish, K. *Discuss. Faraday Soc.* **1954**, *18*, 120-134.
[115] Sasaki, T. In *Handbook of Polyelectrolytes and Their Applications*; Tripathy, S. K., Kumar, J. and Nalwa, H. S., Eds.; American Scientific Publishers: California, USA, 2002: pp. 241-262.
[116] Keren, R., Shainberg, I., and Klein, E., Soil Sci. Soc. Am. J. 1988, 52, 76-80.
[117] Ruiz-Hitzky, E., and Van Meerbeek, A., *Clay Mineral- and Organoclay-Polymer Nanocomposite.* In: F. Bergaya, B.K.G. Theng and G. Lagaly, Editors, *Handbook of Clay Science*, Elsevier, Amsterdam (2006), pp. 584–586.
[118] Sasaki, T. In *Handbook of Polyelectrolytes and Their Applications*; Tripathy, S. K., Kumar, J. and Nalwa, H. S., Eds.; American Scientific Publishers: California, USA, 2002: pp. 241-262.
[119] Morgan, A. B., and Gilman, J. W., *J. Am. Chem. Soc.* **2003**, 87, 1329-1338.
[120] Yoonessi, M., Toghiani, H., Kingery, W., and Pittman, Jr., C. U., *Macromolecules* **2004**, 37, 2511-2518.
[121] Morgan, A. B., Gilman, J. W., and Jackson, C. L., *Proc. Am. Chem. Soc. PMSE* **2000**, *82*, 270-271.
[122] Morgan, A. B., and Gilman, J. W., *J. Appl. Polym. Sci.* **2003**, 87, 1329-1338
[123] Norrish, K. *Discuss. Faraday Soc.* **1954**, *18*, 120-134.
[124] Yoonessi, M., Toghiani, H., Kingery, W., and Pittman, Jr., C. U., *Macromolecules* **2004**, *37*, 2511-2518.
[125] Choi, Y. S., Ham, H. T., and Chung, I. J. *Chem. Mater.* **2004**, *16*, 2522-2529.
[126] Koo, J. H., *Polymer Nanocomposites; Processing, Characterization, and Applications;* The McGraw-Hill Companies, Inc.: New York, 2006: pp. 9-48.
[127] Norrish, K. *Discuss. Faraday Soc.* **1954**, *18*, 120-134.
[128] Khatib, K., Bottero, J. Y., Pons, C. H., Uriot, J. P., and Anselme, C. *Clay Minerals* **1994**, *29*, 401-404.
[129] Fukushima, Y. *Clays and Clay Minerals* **1984**, *32*, 320-326.
[130] Tateyama, H., Scales, P. J., Ooi, M., Nishimura, S., Rees, K., and Healy, T. W., *Langmuir* **1997**, 13, 2440-2446.
[131] Bongiovanni, R., Mazza, D., Ronchetti, S., and Turcato, E. A. *J. Colloid Interface Sci.* **2006**, *296*, 515-519.
[132] Morgan, A. B., and Gilman, J. W., *J. Appl. Polym. Sci.* **2003**, 87, 1329-1338.
[133] Norrish, K. *Discuss. Faraday Soc.* **1954**, *18*, 120-134.
[134] Grim, R. E., *Clay Minerology, 2nd Edition;* McGraw-Hill Inc.: USA, 1968: pp. 126-164.
[135] Morgan, A. B., and Gilman, J. W., *J. Appl. Polym. Sci.* **2003**, 87, 1329-1338.
[136] Yoonessi, M., Toghiani, H., Kingery, W., and Pittman, Jr., C. U., *Macromolecules* **2004**, 37, 2511-2518.
[137] Elsass, F. In *Handbook of Polyelectrolytes and Their Applications*; Tripathy, S. K., Kumar, J. and Nalwa, H. S., Eds.; American Scientific Publishers: California, USA, 2002: pp. 939-963.

[138] Yoonessi, M., Toghiani, H., Kingery, W., and Pittman, Jr., C. U., *Macromolecules* **2004**, 37, 2511-2518.
[139] Voorn, D. J., Ming, W., and A. M. van Herk *Macromolecules* **2006**, *39*, 2137-2143.
[140] Wamsden, W. *Proc. R. Soc. London* **1903**, *72*, 156-164.
[141] Pickering, S. U. *J. Chem. Soc.* **1907**, *91*, 2001-2021.
[142] Cauvin, S., Colver, P. J., Bon, S. A. F. *Macromolecules* **2005**, *38*, 7887-7889.
[143] Lagaly, G., Reese, M., Abend, S. *Appl. Clay Sci.* **1999**, *14*, 83-103.
[144] Torres, L. G., Iturbe, R., Snowden, M. J., Chowdhry, B. Z., and Leharne, S. A. *Colloid Surf. A: Physicochem. Eng. Aspects* **2007**, *302*, 439-448.
[145] Binks, B. P., Clint, J. H., Whitby, C. P. *Langmuir* **2005**, *21*, 5307-5313.
[146] Voorn, D. J., Ming, W., and A. M. van Herk *Macromolecules* **2006**, *39*, 2137-2143.
[147] Emerson, W. W. *Nature* **1960**, *186*, 573-574.
[148] Geoghegan, M. J. *4th Int. Congr. Soil Sci.* **1950**, *1*, 198-201.
[149] Emerson, W. W., and Raupach, M. *Aust. J. Soil. Res.* **1964**, *2*, 46-55.
[150] Greenland, D. J. *J. Colloid Sci.* **1963**, *18*, 647-664.
[151] Bergaya, F., Lagaly, G., and Vayer, M. In *Handbook of Polyelectrolytes and Their Applications*; Tripathy, S. K., Kumar, J. and Nalwa, H. S., Eds.; American Scientific Publishers: California, USA, 2002: pp. 979-1001.
[152] López Arbeloa, F., Chaudhuri, R., López Arbeloa, T, and López Arbeloa, I. *J. Colloid Interface Sci.* **2002**, *246*, 281-287.
[153] Endo, T., Sato, T., and Shimada, M. *J. Phys. Chem. Solids* **1986**, *47*, 799-804.
[154] Yoonessi, M., Toghiani, H., Kingery, W., and Pittman, Jr., C. U., *Macromolecules* **2004**, 37, 2511-2518.
[155] López Arbeloa, F., López Arbeloa, T., and López Arbeloa, I. *Trends Chem. Phys.* **1996**, *4*, 191-213.
[156] Grauer, Z., Avnir, D., and Yariv, S. *Can. J. Chem.* **1984**, *62*, 1889-1894.
[157] Chu, G., and Xingkang, Z., *Acta Opt. Sinica* **1983**, *3*, 64-?
[158] Grauer, Z., Avnir, D., and Yariv, S. *Can. J. Chem.* **1984**, *62*, 1889-1894.
[159] Yariv, S., *Int. J. Trop. Agric.* **1988**, *6*, 1-19.
[160] Tapia Estévez, M. J., López Arbeloa, F., López Arbeloa, T., López Arbeloa, I., and Schoonheydt, R. A. *Clay Miner.* **1994**, *29*, 105-114.
[161] Tapia Estévez, M. J., López Arbeloa, F., López Arbeloa, T., and López Arbeloa, I. *J. Colloid Interface Sci.* **1994**, *162*, 412-417.
[162] Aloisi, G. G., Costantino, U., Latterini, L., Nocchetti, M., Camino, G., and Frache, A., *J. Phys. Chem. Solids* **2006**, 67, 909-914.
[163] Emerson, W. W. *Nature* **1957**, *180*, 48-49.
[164] Aloisi, G. G., Costantino, U., Latterini, L., Nocchetti, M., Camino, G., and Frache, A., *J. Phys. Chem. Solids* **2006**, 67, 909-914.
[165] Burgentzlé, D., Duchet, J., Gérard, J. F., Jupin, A., Fillon, B. *J. Colloid Interface Sci.* **2004**, *278*, 26-39.
[166] LeBaron, P. C., Wang, Z., and Pinnavaia, T. J. *Appl. Clay Sci.* **1999**, *15*, 11-29.
[167] Kojima, Y., Fukumori, K., Usuki, A., Okada, A., and Kurauchi, T. *J. Mater. Sci. Lett.* **1993c**, *12*, 889-890.
[168] Messersmith, P. B., and Giannelis, E. P. *J. Polym. Sci., Part A: Polym. Chem.* **1995**, *33*, 1047-1057.
[169] Yano, K., Usuki, A., and Okada, A. *J. Polym. Sci. A Polym. Chem.* **1997**, *35*, 2289-2294.
[170] Decher, G., and Hong J.-D. *Makromol. Chem. Macromol. Symp.* **1991**, *46*, 321-327.
[171] Decher, G., and Hong J.-D. *Ber. Bunsenges Phys. Chem.* **1991**, *95*, 1430-1434.
[172] Bernt, P., Kurihara, K., and Kunitake, T. *Langmuir* **1992**, *8*, 2486-2490. Referenced by: Ariga, K. In: *Handbook of Polyelectrolytes and Their Applications*; Tripathy, S. K., Kumar, J. and Nalwa, H. S., Eds.; American Scientific Publishers: California, USA, 2002: pp. 127-145.
[173] Kleinfeld E. R., and Ferguson, G. S. *Science* **1994**, *265*, 370-373.
[174] Lvov, Y., Ariga, K., Ichinose, I., and Kunitake, T. *Langmuir* **1996**, *12*, 3038-3044.
[175] Kotov, N. A., Magonov, S., and Tropsha, E. *Chem. Mater.* **1998**, *10*, 886-895.
[176] Eckle, M., and Decher, G. *Nano Lett.* **2001**, *1*, 45-49.

[177] Mazumder, M. A. J., Burker, N. A. D., Shen, F., Potter, M. A., and Stöver, H. D. H. *Manuscript to be submitted*
[178] Griebel, Th., Kulicke, W.-M., and Hashemzadeh, A. *Colloid Polym. Sci.* **1991**, *269*, 113-120.
[179] Scher, H. B. In *Controlled Release Pesticides*; Scher, H. B., Ed.; ACS Symposium Series 53: USA, 1977: pp. 126-144.
[180] Lewis, D. H., and Cowsar, D.R. In *Controlled Release Pesticides*; Scher, H. B., Ed.; ACS Symposium Series 53: USA, 1977: pp. 1-16.
[181] Degennaro, M., Thompson, B. B., and Luzzi, L. A. In *Controlled Release Polymeric Formulations*; Paul, D. R., and Harris, F. W., Eds.; ACS Symposium Series 33: Washington, D.C., 1976: pp. 195-207.
[182] Fanger, G. O., *Chemtech*, 397, (July, 1974).
[183] Mathiowitz, E., and Cohen, M. D., *J. Membrane Sci.* **1989**, *40*, 1-26.
[184] Yadav, S. K., Khilar, K. C., and Suresh, A. K. *J. Membrane Sci.* **1997**, *125*, 213-218.
[185] Hiresh, K., Payan, S., Carnelle, G., Brujes, L., and Legrand, J., *Powder Tech.* **2003**, 130, 324-330.
[186] Scher, S. B., Rodson, M., and Lee, K.-S., *Pestic. Sci.* **1998**, 54, 394-400.
[187] Rogers. C. E. In *Controlled Release Pesticides*; Scher, H. B., Ed.; ACS Symposium Series 53: USA, 1977: pp. 17-29.
[188] Scher, S. B., *Controlled Release Pesticides*, American Chemical Society, (1976).
[189] Brandrup, J., Immergut, E. H., and Grulke, E. A., Editors, *Polymer Handbook* (4th ed.), John Wiley & Sons, New York (1999), V11/675-683.
[190] Charles M. Hansen, *Hansen Solubility Parameters: A Users Handbook, 2nd Edition*; CRC Press: Boca Raton, Fla., 2007; pp. 45-110.
[191] Lvov, Y., Ariga, K., Ichinose, I., and Kunitake, T. *Langmuir* **1996**, *12,* 3038-3044.
[192] Kleinfeld E. R., and Ferguson, G. S. *Science* **1994**, *265*, 370-373.
[193] Lvov, Y., Ariga, K., Ichinose, I., and Kunitake, T. *Langmuir* **1996**, *12,* 3038-3044.
[194] Kotov, N. A., Haraszti, T., Turi, L., Zavala, G., Geer, R. E., Dékány, I., and Fendler, J. H. *J. Am. Chem. Soc.* **1997**, *119*, 6821-6832.
[195] Kotov, N. A., Haraszti, T., Turi, L., Zavala, G., Geer, R. E., Dékány, I., and Fendler, J. H. *J. Am. Chem. Soc.* **1997**, *119*, 6821-6832.
[196] Xie, W., Gao, Z., Pan, W.-P., Vaia, R., Hunter, D., and Singh, A., *Polym Mater Sci Eng* **2000**, 82, 284-285.
[197] Voorn, D. J., Ming, W., and A. M. van Herk *Macromolecules* **2006**, *39*, 2137-2143.
[198] Oliveira, Jr., O. N., He, J.-A., Zucolotto, V., Balasubramanian, S., Li, L., Nalwa, H. S., Kumar, J., and Tripathy, S. K. In *Handbook of Polyelectrolytes and Their Applications*; Tripathy, S. K., Kumar, J. and Nalwa, H. S., Eds.; American Scientific Publishers: California, USA, 2002: pp. 1-37.
[199] Decher, G. *Science* **1997**, *277*, 1232-1237.
[200] Lagaly, G. In: *Handbook of Clay Science*; Bergaya, F., Theng, B. K. G., and Lagaly, G., Eds.; Elsevier: Amsterdam, 2006: pp.141-245.
[201] Keren, R., Shainberg, I., and Klein, E. *Soil Sci. Soc. Am. J.* **1988**, *52*, 76-80.
[202] Permien, T., and Lagaly, G. *Clays and Clay Minerals* **1995**, *43*, 229-236.
[203] Permien, T., and Lagaly, G. *Clays and Clay Minerals* **1995**, *43*, 229-236.
[204] Yariv, S., and Michaelian, K. H. In *Organo-Clay Complexes and Interactions*; Yariv, S., and Cross, H., Eds.; Marcel Dekker, Inc.: NY, USA, 2002: pp. 1-38.
[205] Keren, R., Shainberg, I., and Klein, E. *Soil Sci. Soc. Am. J.* **1988**, *52*, 76-80.
[206] Gayer, K. H., Thompson, L. C., and Zajicek, O. T. *Can. J. Chem.* **1958**, *36*, 1268-1271.
[207] Parks, G. A. *Chem. Rev.* **1965**, *65*, 177-198.
[208] Oliveira, Jr., O. N., He, J.-A., Zucolotto, V., Balasubramanian, S., Li, L., Nalwa, H. S., Kumar, J., and Tripathy, S. K In *Handbook of Polyelectrolytes and Their Applications*; Tripathy, S. K., Kumar, J. and Nalwa, H. S., Eds.; American Scientific Publishers: California, USA, 2002: pp. 1-37.
[209] Lewis, D. H., and Cowsar, D.R. In *Controlled Release Pesticides*; Scher, H. B., Ed.; ACS Symposium Series 53: USA, 1977: pp. 1-16.

[210] Jones, I. C., Sharman, G. J., and Pidgeon, J. *Magn. Reson. Chem.* **2005**, *43*, 497-509.
[211] Yadav, S. K., Khilar, K. C., and Suresh, A. K. *J. Membrane Sci.* **1997**, *125*, 213-218.
[212] Scher, H. B., Rodson, M., and Lee K.-S. *Pestic. Sci.* **1998**, *54*, 394-400.
[213] Lvov, Y., Ariga, K., Ichinose, I., and Kunitake, T. *Langmuir* **1996**, *12*, 3038-3044.
[214] Kleinfeld E. R., and Ferguson, G. S. *Science* **1994**, *265*, 370-373.
[215] Lvov, Y., Ariga, K., Ichinose, I., and Kunitake, T. *Langmuir* **1996**, *12*, 3038-3044.
[216] Kotov, N. A., Magonov, S., and Tropsha, E. *Chem. Mater.* **1998**, *10*, 886-895.
[217] Eckle, M., and Decher, G. *Nano Lett.* **2001**, *1*, 45-49.
[218] Lutkenhaus, J. L., Olivetti, E. A., Verploegen, E. A., Cord, B. M., Sadoway, D. R., and Hammond, P. T. *Langmuir* **2007**, *23*, 8515-8521.
[219] Lvov, Y., Ariga, K., Ichinose, I., and Kunitake, T. *Langmuir* **1996**, *12*, 3038-3044.
[220] Decher, G. *Science* **1997**, *277*, 1232-1237.
[221] Oliveira, Jr., O. N., He, J.-A., Zucolotto, V., Balasubramanian, S., Li, L., Nalwa, H. S., Kumar, J., and Tripathy, S. K. In *Handbook of Polyelectrolytes and Their Applications*; Tripathy, S. K., Kumar, J. and Nalwa, H. S., Eds.; American Scientific Publishers: California, USA, 2002: pp. 1-37.
[222] Sasaki, T. In *Handbook of Polyelectrolytes and Their Applications*; Tripathy, S. K., Kumar, J. and Nalwa, H. S., Eds.; American Scientific Publishers: California, USA, 2002: pp. 1-37.